Advanced Detector Technologies 3/3

CERN Fermilab Hadron Collider Physics Summer School

Werner Riegler, CERN, werner.riegler@cern.ch

Sept 5th, 2019

How will LHC manage to deliver 3000fb^{-1} of pp Collisions

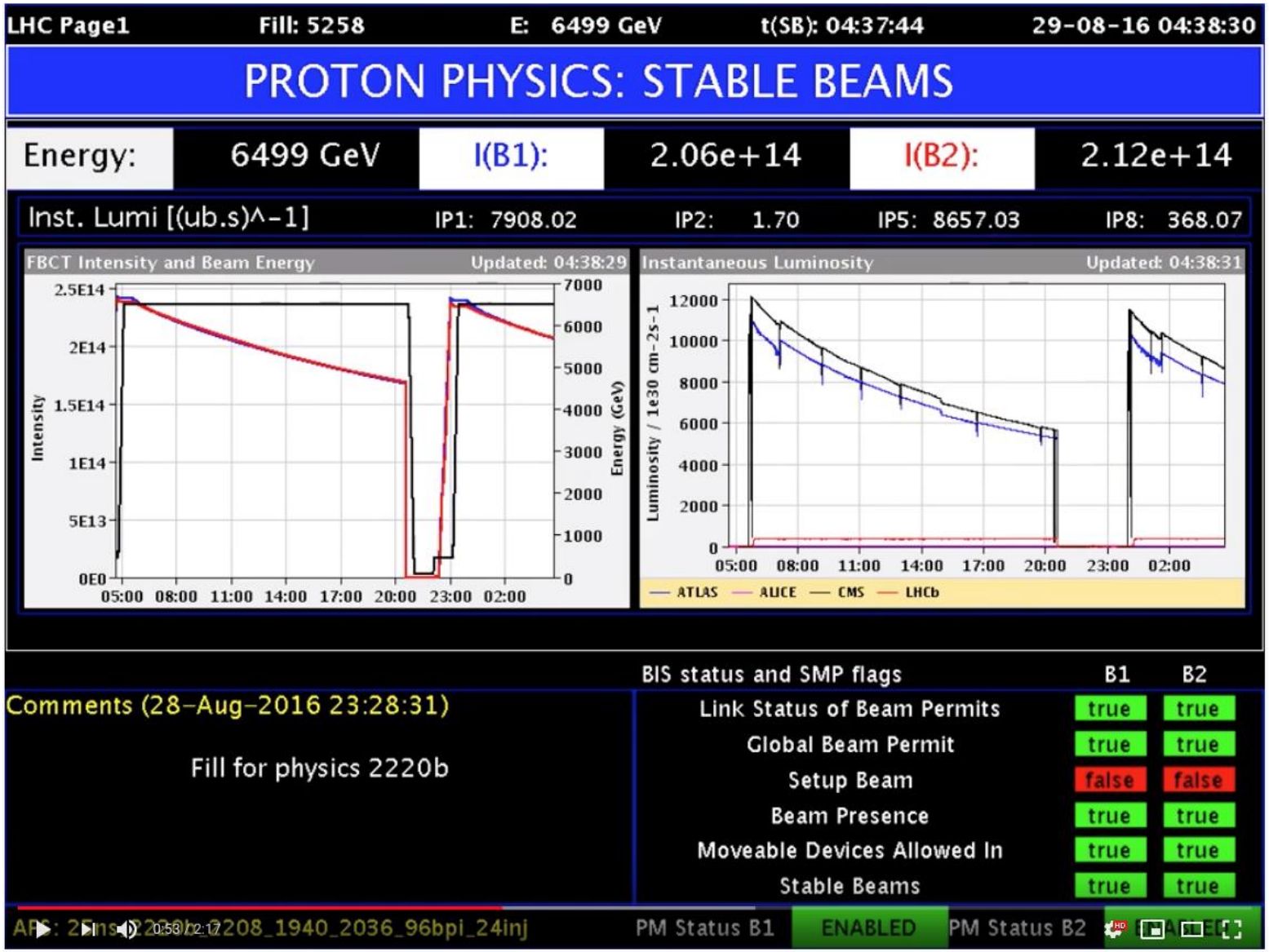
LHC Page1
Fill: 5258
E: 6499 GeV
t(SB): 04:37:44
29-08-16 04:38:30
PROTON PHYSICS: STABLE BEAMS
Energy:
6499 GeV
I(B1):
2.06e+14
I(B2):
2.12e+14
Inst. Lumi [(ub.s)^-1]
IP1: 7908.02
IP2: 1.70
IP5: 8657.03
IP8: 368.07
FBCT Intensity and Beam Energy
Updated: 04:38:29
Intensity
Energy (GeV)
Instantaneous Luminosity
Updated: 04:38:31
Luminosity / 1e30 cm-2s-1
ATLAS
ALICE
CMS
LHCb
BIS status and SMP flags
B1
B2
Comments (28-Aug-2016 23:28:31)
Fill for physics 2220b
Link Status of Beam Permits
Global Beam Permit
Setup Beam
Beam Presence
Moveable Devices Allowed In
Stable Beams
PM Status B1
ENABLED
PM Status B2

Pileup = Numer of pp interactions per bunchcrossing

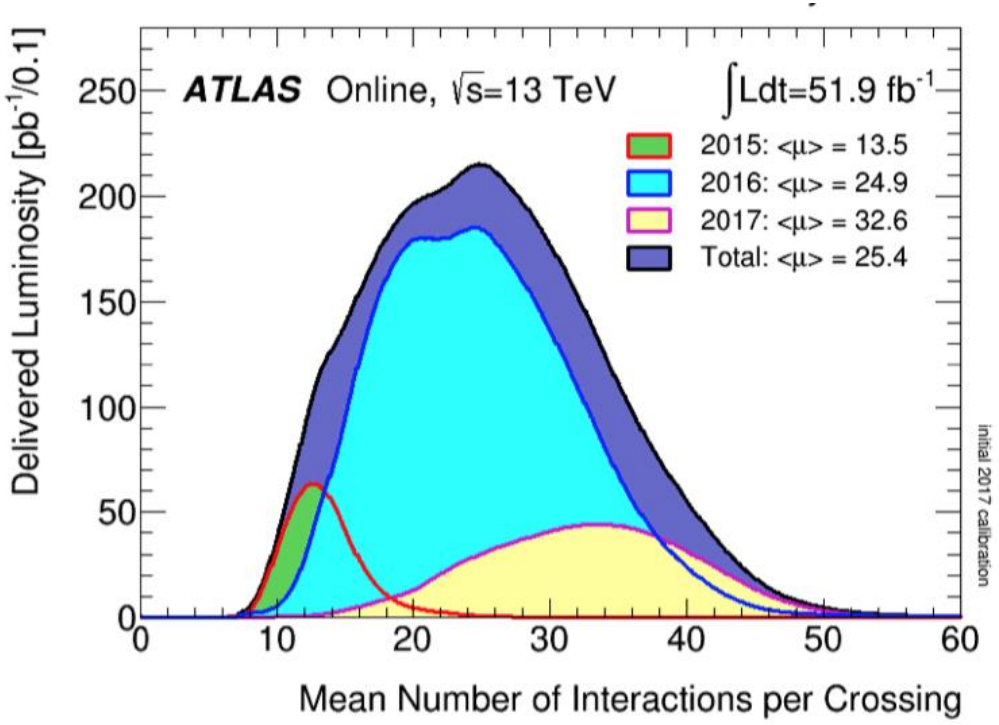

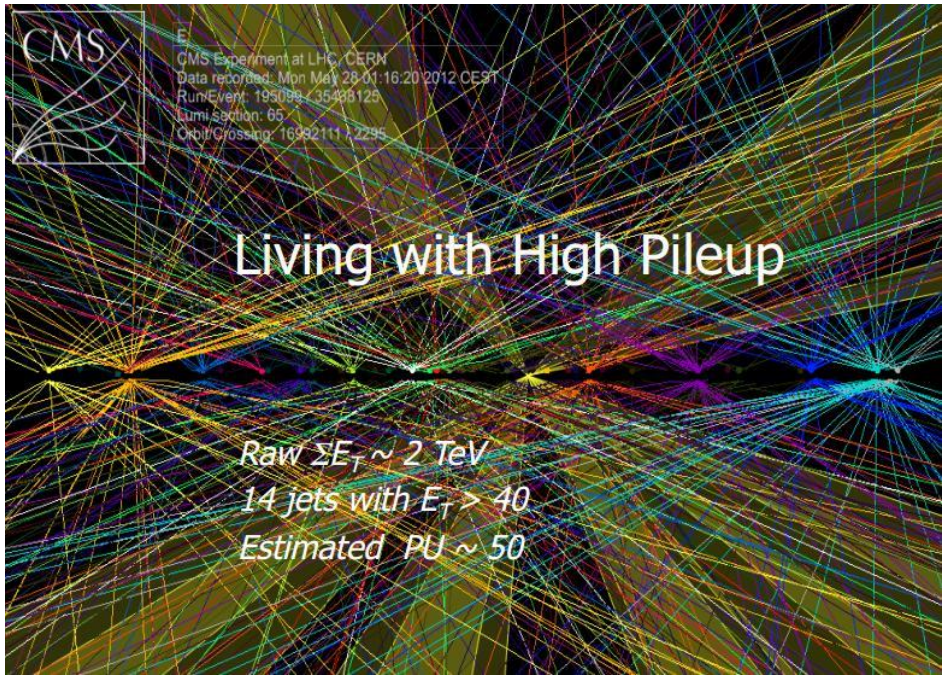

From nominal LHC (25ns) to HL-LHC: Number of bunches stays the same i.e. increase in Luminosity from 10^{34} to $5x10^{34}$ will increase the pile-up by a factor of 5.

Detectors have to be built to deal with a maximum average pileup per bunch-crossing of 140 or even 200 for the 'ultimate' HL-LHC luminosity of 7.5×10^{34} $cm^{-2}s^{-1}$

Luminosity levelling

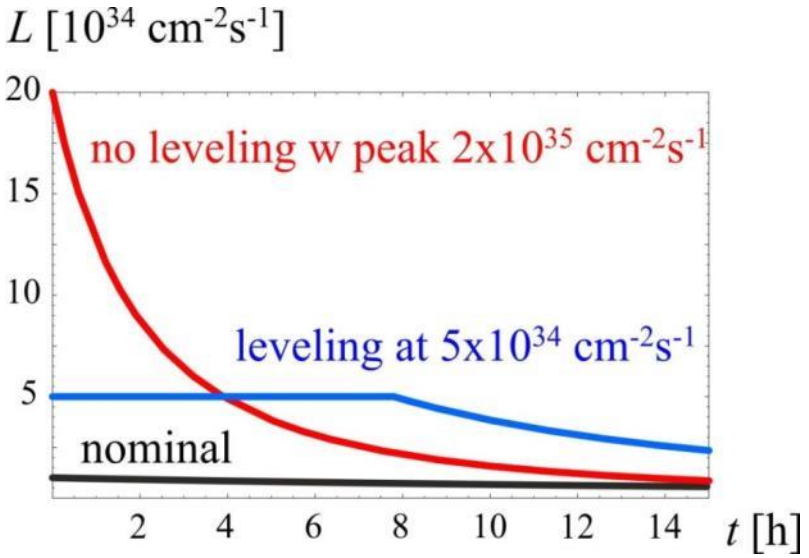

High peak luminosity

Minimize pile-up in experiments and provide "constant" luminosity

- Obtain about 3 - 4 fb^{-1}/day (40% stable beams)
- About 250 to 300 fb^{-1}/year

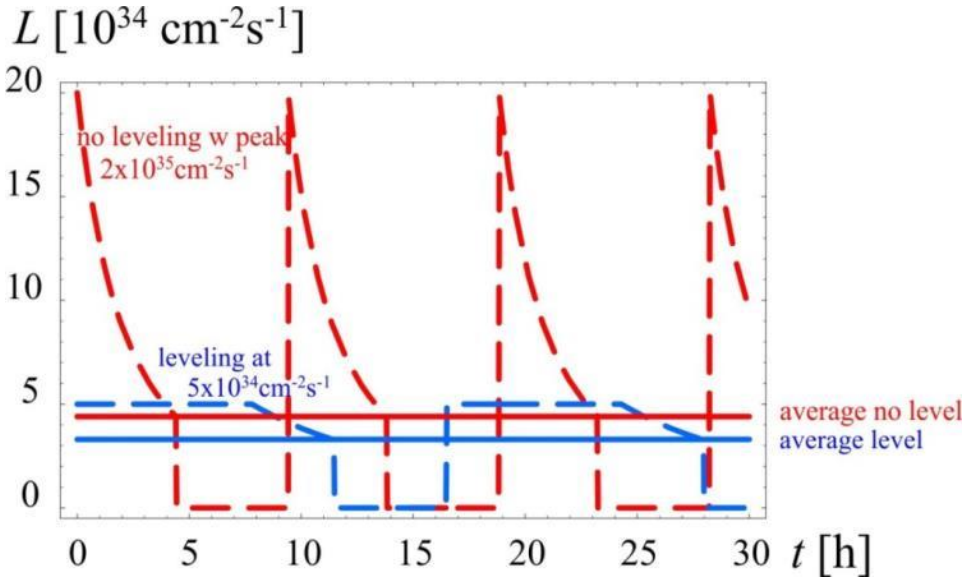

LHC luminosity evolution

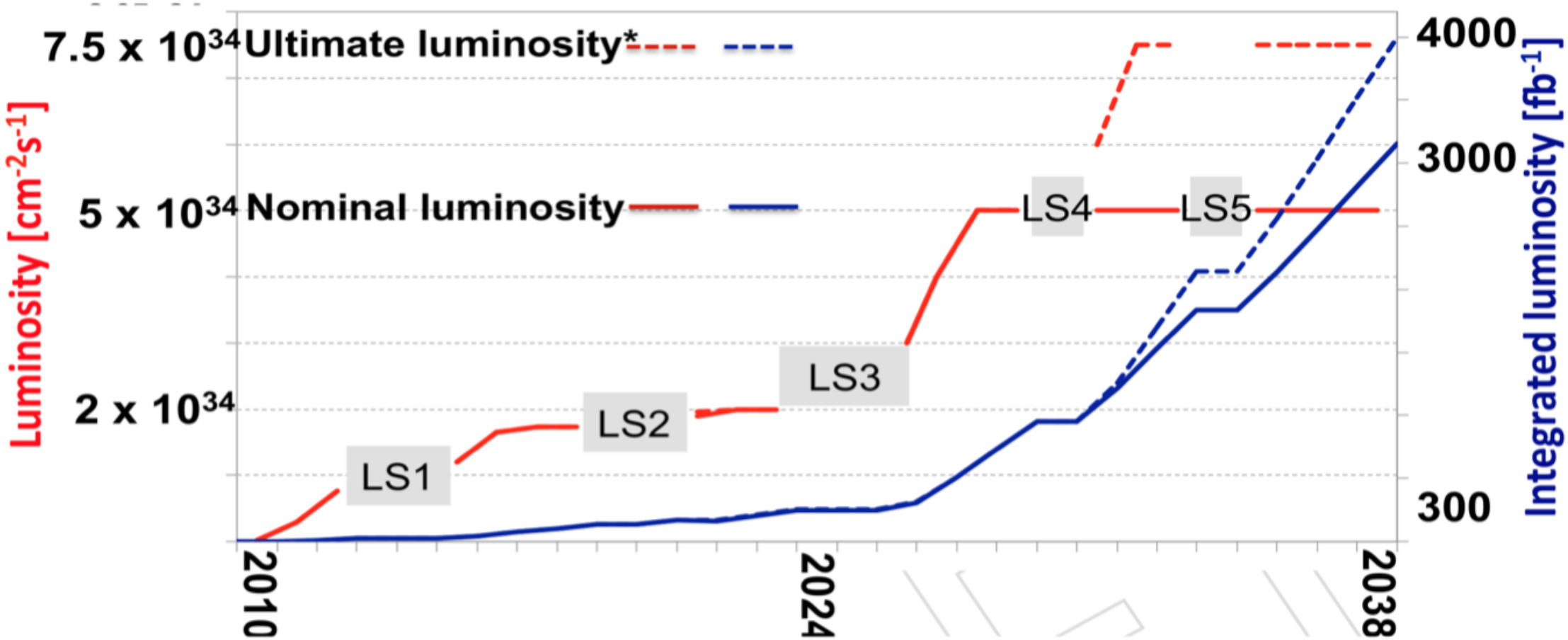

https://espace.cern.ch/HiLumi/PLC/default.aspx

$$L = \gamma \frac{f_{rev}\, n_b\, N_b^{\,2}}{4\pi \varepsilon_n \beta^*} R$$

Parameter	LHC nominal	HL-LHC 25ns	factor
N_b	1.15E+11	2.2E+11	1.9
n_b	2808	**2808**	
N_{tot}	3.2E+14	6.2E+14	
beam current [A]	0.58	**1.11**	
x-ing angle [µrad]	300	↔ 590	
beam separation [σ]	9.9	12.5	
β^* [m]	0.55	**0.15**	3.7 new focussing quadrupoles
ε_n [µm]	3.75	2.50	1.5
ε_L [eVs]	2.51	2.51	
energy spread	1.20E-04	1.20E-04	
bunch length [m]	7.50E-02	7.50E-02	
IBS horizontal [h]	80 -> 106	18.5	
IBS longitudinal [h]	61 -> 60	20.4	
Piwinski parameter	0.68	3.12	
Reduction factor 'R1*H1' at full crossing angle (no crabbing)	0.828	↔ 0.306	
Reduction factor 'H0' at zero crossing angle (full crabbing)	0.991	↔ **0.905**	crab cavities
beam-beam / IP without Crab Cavity	3.1E-03	3.3E-03	
beam-beam / IP with Crab cavity	3.8E-03	1.1E-02	
Peak Luminosity without levelling [$cm^{-2}\ s^{-1}$]	1.0E+34	7.4E+34	
Virtual Luminosity: Lpeak*H0/R1/H1 [$cm^{-2}\ s^{-1}$]	1.2E+34	**21.9E+34**	
Events / crossing without levelling	19 -> 28	210	
Levelled Luminosity [$cm^{-2}\ s^{-1}$]	-	5E+34	
Events / crossing (with leveling for HL-LHC)	*19 -> 28	140	
Leveling time [h] (assuming no emittance growth)	-	9.0	

Factor = 1.9^2 x 3.7 x 1.5 = 20

Pileup density, position

HL-LHC baseline and backup (25 ns): 250 fb^{-1}/y , μ_{tot}= 140 @5E34
(BB wire .or. crab w/o CK scheme)

"HL-LHC+" (25ns): 250 fb^{-1}/y , μ_{tot}= 140 @5E34
(BB wire .and. crabs with CK scheme)

"HL-LHC++" (25ns): 250 fb^{-1}/y , μ_{tot}= 140 @5E34
(BB wire .and. crabs with CK scheme .and. 800 MHz)

LHC2012 (50 ns): 25 fb^{-1}/y, μ_{tot}= 40 @7.5E33

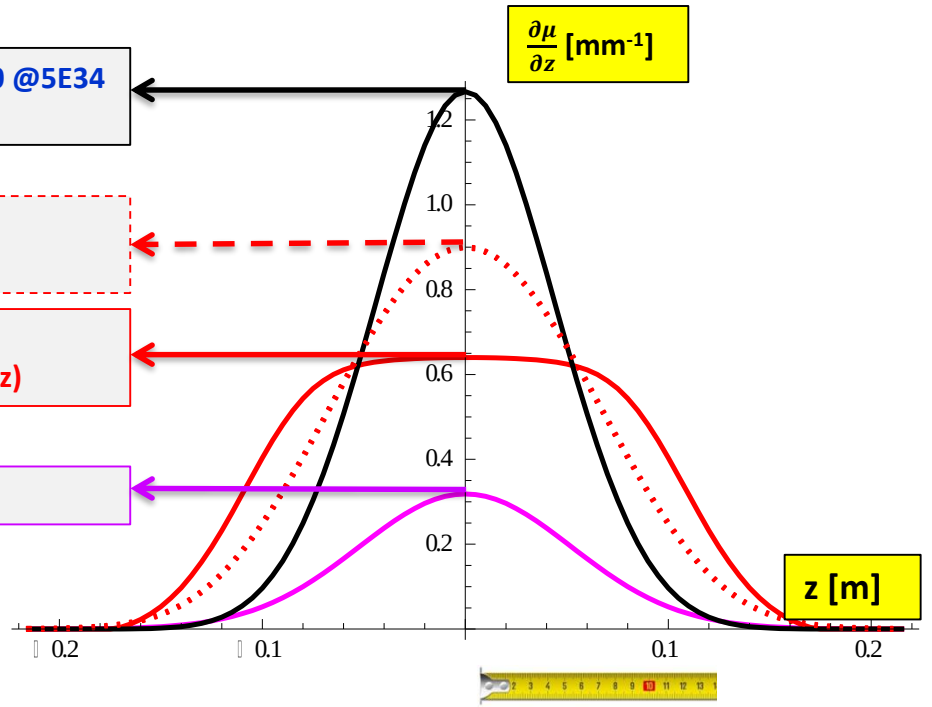

Possibly reduce pileup density from 1.25/mm to 0.6/mm.
→ However – shape changes with time.

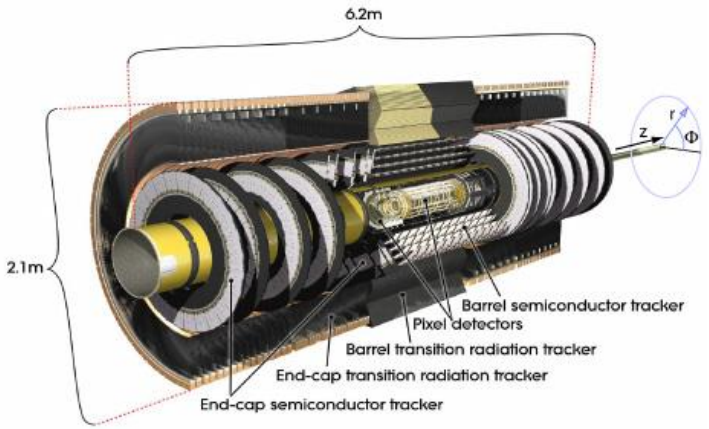

Pileup Density, time

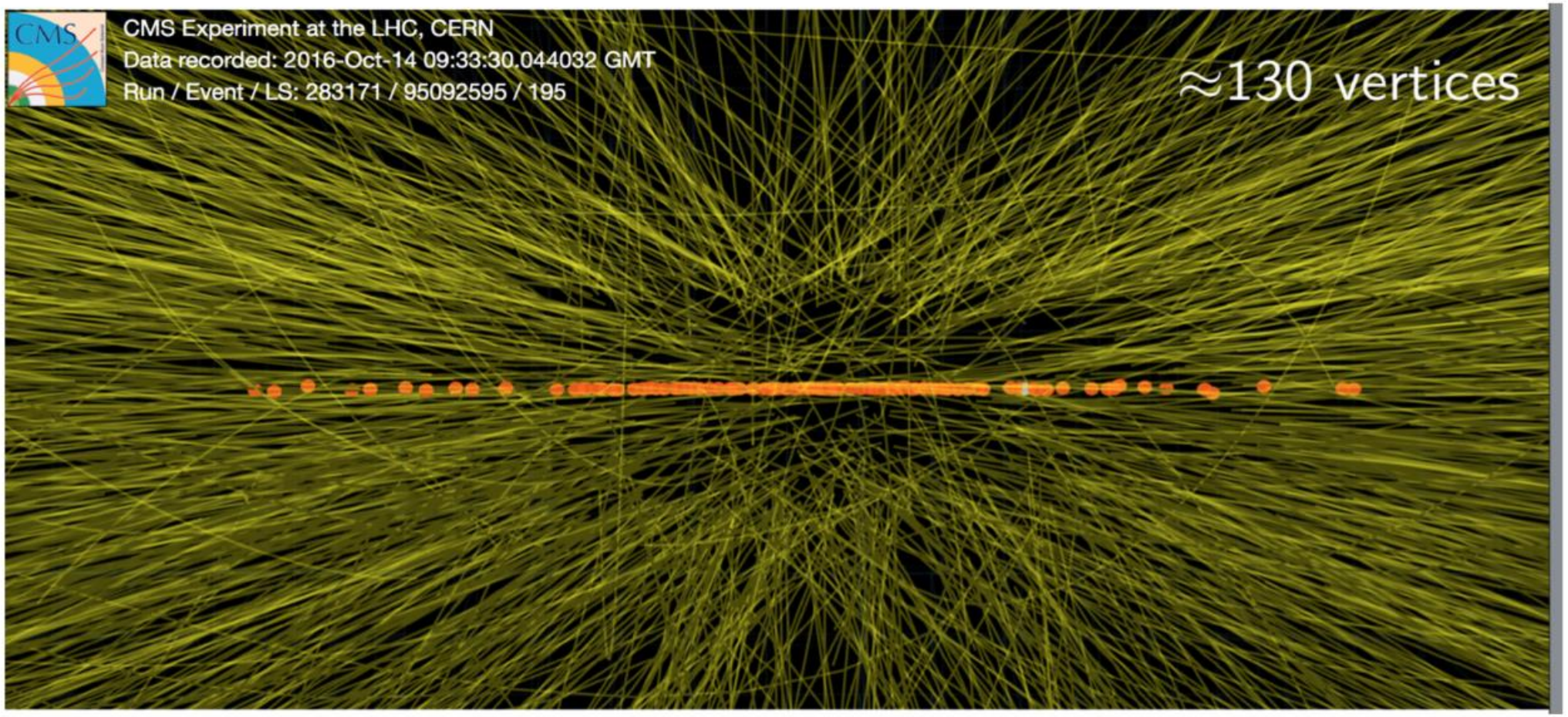

- Real-life event with HL-LHC-like pileup from special run in 2016 with individual high intensity bunches

Pileup density, time

Plan A @ σ_z =7.5 cm (Gaussian) → 0.34 PU/ps @ $<\mu_{tot}>$=140

Plan B variant @ σ_z =12.5 cm (Rectangular) →0.12 PU/ps @ $<\mu_{tot}>$=140

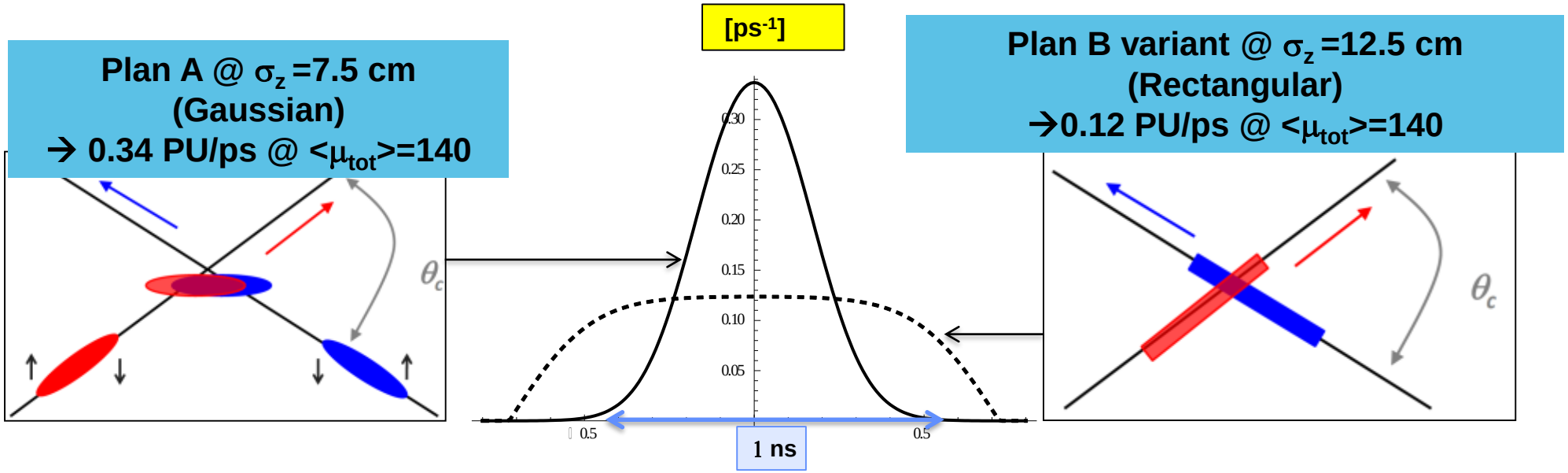

In the best case, still 1.2 pile-up every 10 ps

Measuring position and time of a track

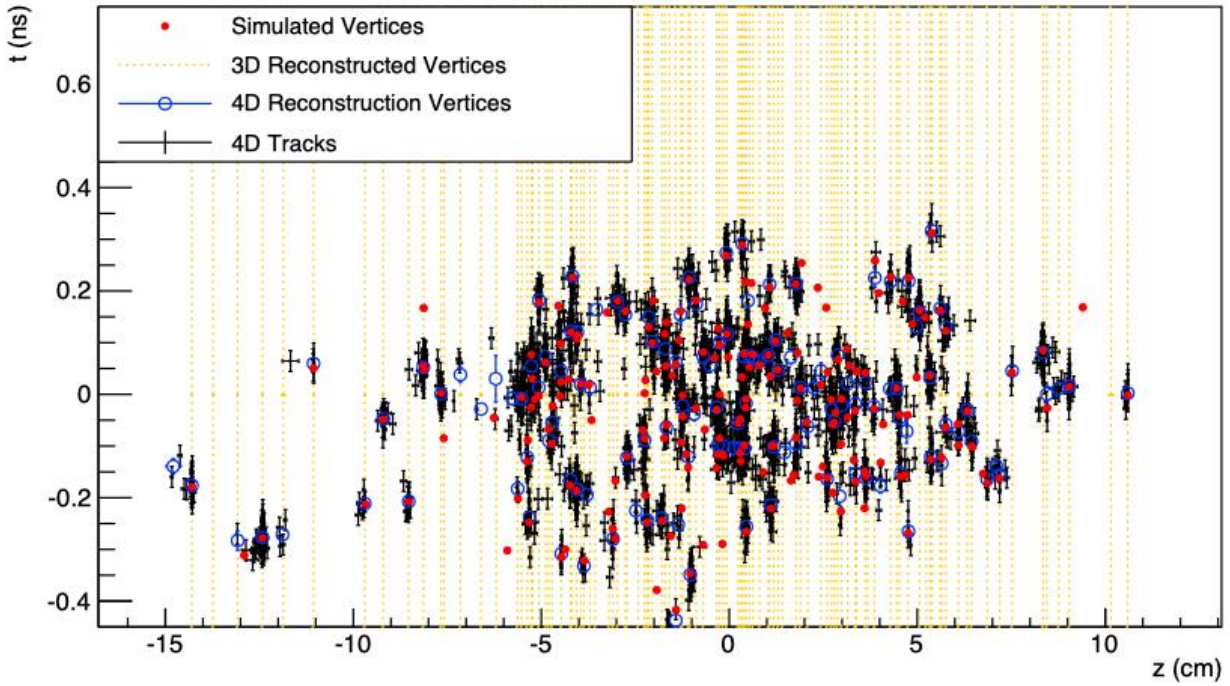

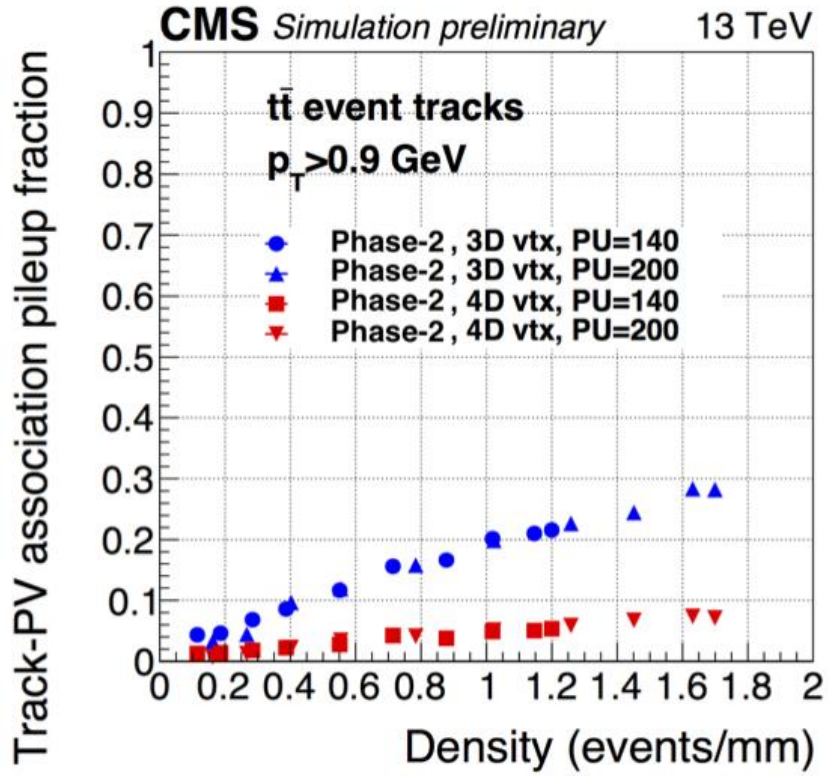

→ Allows more efficient separation of vertices

CMS timing layer

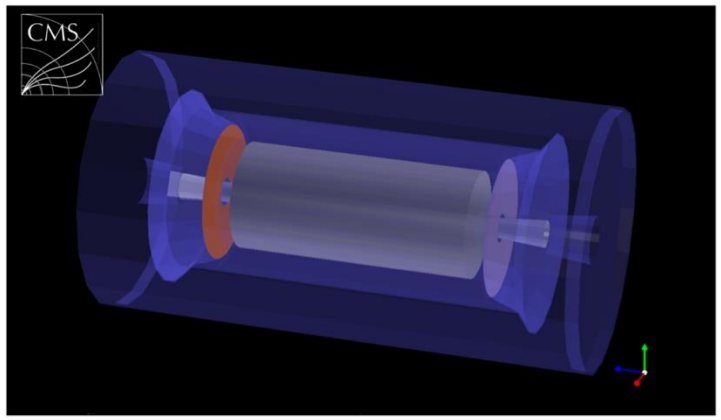

Figure 1.5: A simplified GEANT geometry of the timing layer implemented in CMSSW for simulation studies comprises a LYSO barrel (grey cylinder), at the interface between the Tracker and the ECAL, and two silicon endcap (orange discs) timing layers in front of the CE calorimeter.

either option.

1.3 Elements of the CMS timing upgrade

Precision timing can be provided by the front section of the upgraded endcap calorimeter (CE) [1] and by the barrel electromagnetic calorimeter (ECAL) with a specific upgrade of the readout electronics [11]. However, neither the CE nor the ECAL detectors will provide efficient precision timing information for minimum ionizing particles (MIPs). Therefore, global event timing with the ability to reconstruct the vertex time and exploit time information in charged particle reconstruction requires a dedicated MIP Timing Detector (MTD) covering the barrel and endcap regions. The scale of the time resolution needed in each of these detectors is primarily determined by the spread in time of the luminous region at the HL-LHC. This spread amounts to about 180 ps RMS and sets the time resolution required to achieve an effective line density of vertices comparable to LHC (0.3 mm^{-1}) to around 30 ps. This required time resolution does not depend on the HL-LHC luminosity leveling options. Rather, the timing upgrade of CMS will provide an extra measure of robustness against any possible future beam-crossing scenarios that may maximize or otherwise alter the luminosity production capabilities of the HL-LHC.

- Cost effective design over a large area: Performance studies motivate the need of a hermetic coverage, with time resolution of order 30–40 ps for charged tracks throughout the detector lifetime.
- Integration constraints: A single layer device between the Tracker and calorimeters, covering up to $|\eta| \sim 3$, is imposed by space and integration constraints.
- Granularity: A channel area of order 1 cm^2 in the barrel, and varying in the endcaps down to 3 mm^2 at $|\eta| \sim 3$, yields a good compromise between low time response spread within a channel, low occupancy and low channel count. The channel occupancy is limited to a few percent, ensuring both a small probability of double hits, needed for unambiguous time assignment, and a manageable data volume.

Region	η	R (cm)	z (cm)	Fluence (cm^{-2})	Dose (kGy)
barrel	0.0	117	0	1.7×10^{14}	16
barrel	1.15	117	170	1.9×10^{14}	21
barrel	1.45	117	240	2.0×10^{14}	25
endcap	1.6	127	304	1.1×10^{14}	25
endcap	2.0	84	304	2.4×10^{14}	75
endcap	2.5	50	304	6.6×10^{14}	260
endcap	3.0	30	304	1.7×10^{15}	690

CMS timing layer

- Calorimeter upgrades can already provide precision timing for high energy photons in the central region, moderate energy photons, and higher energy hadrons in the forward region
- **Additional capabilities: MIP timing to cover large fraction of charged particles in the event**
- **Targeting $\sigma_t = 30$ ps**
- **Extension to Phase-II Upgrade: MIP timing layer**
- Concept for central region: Thin **LYSO + SiPM** layer built into tracker barrel support tube (in between tracker and ECal Barrel)

  $\rightarrow$ precision timing for charged particles and converted photons

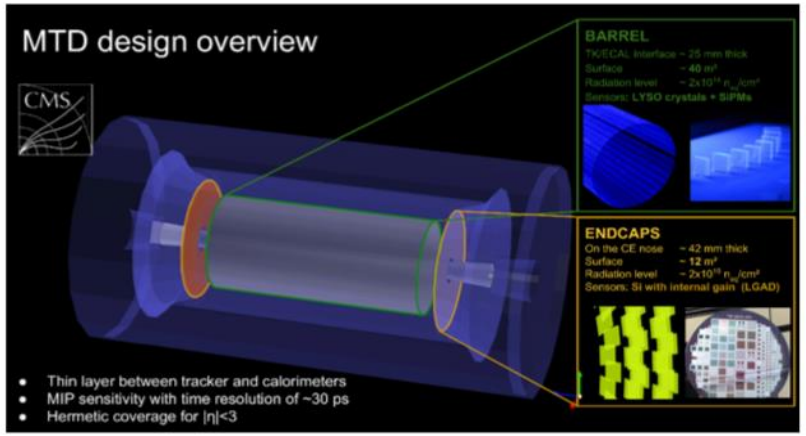

- Concept for forward region (more stringent radiation hardness requirements): **LGAD** (Silicon with Gain), single layer between tracker and HGCal (on HGCal nose)

Properties	BGO	LYSO
Density ($g \cdot cm^{-3}$)	7.13	7.3
Melting point (°C)	1050	2047
Index of refraction	2.15	1.82
Radiation length (cm)	1.10	1.16
Attenuation (cm^{-1})	0.96	0.87
Decay constant (ns)	300	50
Light yield (%) NaI (Nl)	25	75

Comparison of the properties of BGO and LYSO crystals...

Barrel Layout

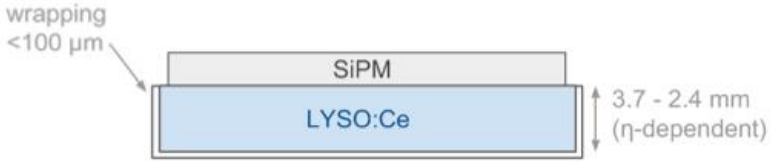

11x11 mm tile, 4x4 mm SiPM active area, $\sim$ 250k channels

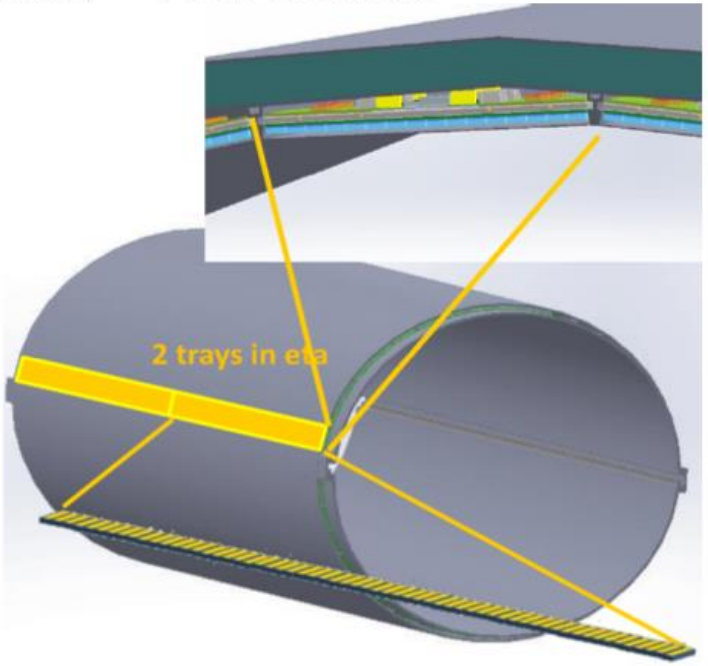

25 mm of available space within tracker support tube

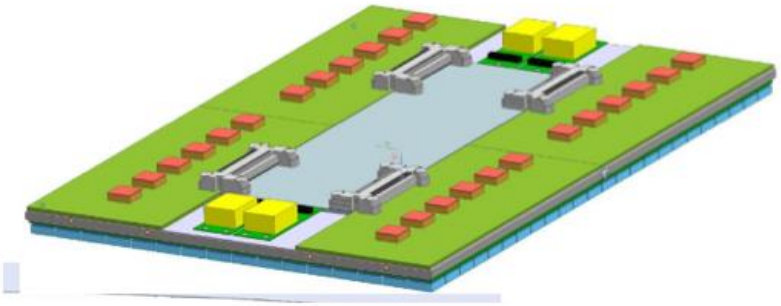

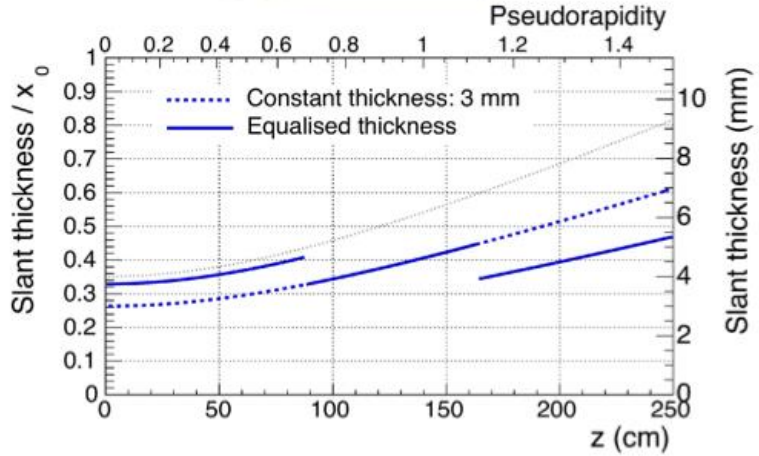

Variable thickness to maintain more uniform material budget and signal-to-noise

LYSO crystals+SiPMs

Figure 2.4: Top left: Set of $11 \times 11 \times 3$ mm^3 LYSO:Ce crystals with depolished lateral faces, before and after Teflon wrapping. Bottom left: 6×6 mm^2 HPK SiPMs glued on LYSO crystals. Right: Crystal+SiPM sensors plugged on the NINO board used for test beam studies.

LYSO+SiPM time resolution

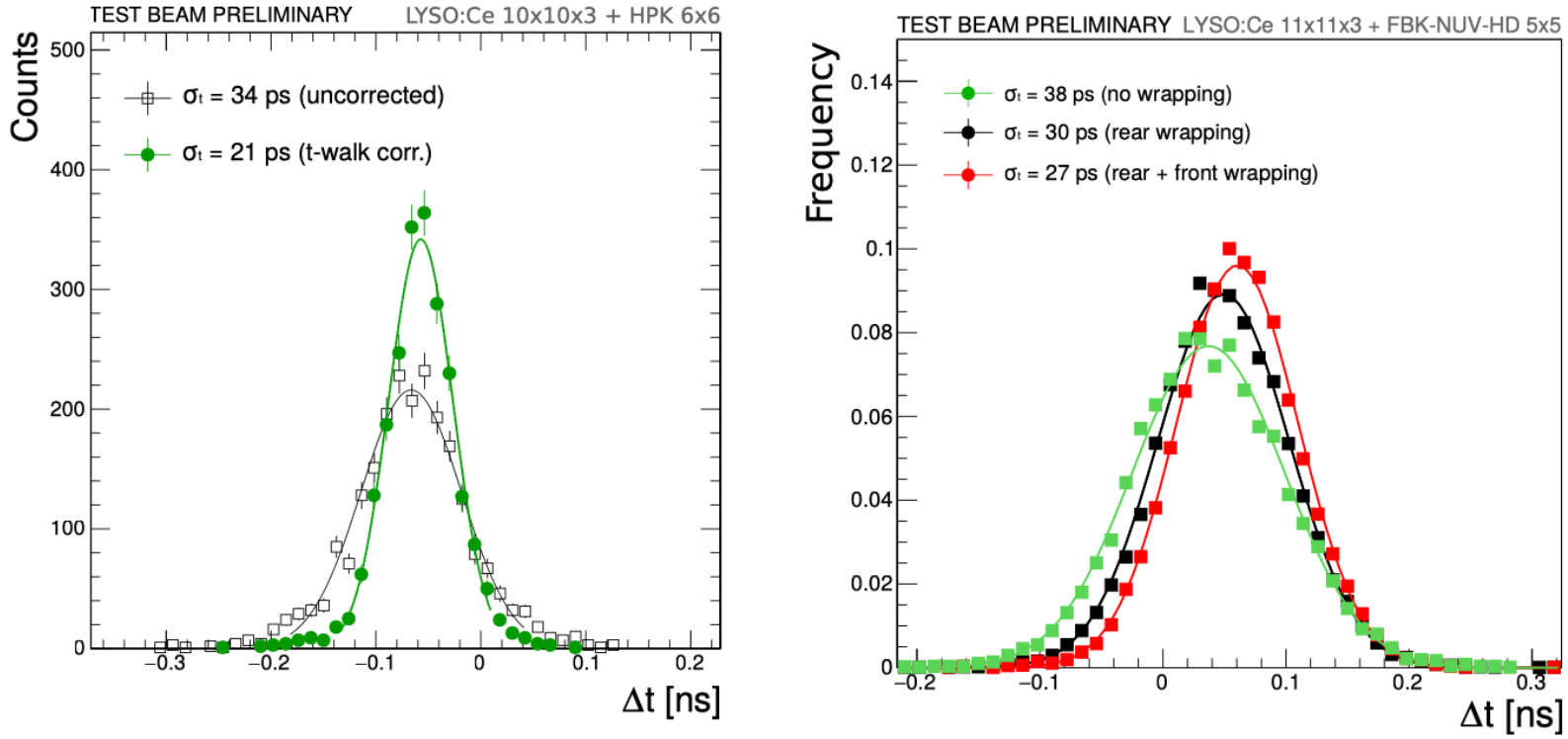

Figure 2.5: Distribution of the time difference in a pair of LYSO:Ce tiles exposed to a 3 mm wide beam of MIPs hitting the centre of the tiles. Left: Results before and after time walk correction for $10 \times 10 \times 3$ mm^3 crystals read out with 6×6 mm^2 HPK SiPMs. Right: Results for $11 \times 11 \times 3$ mm^3 crystals read out with 5×5 mm^2 FBK SiPMs under different wrapping configurations.

Timing with silicon sensors

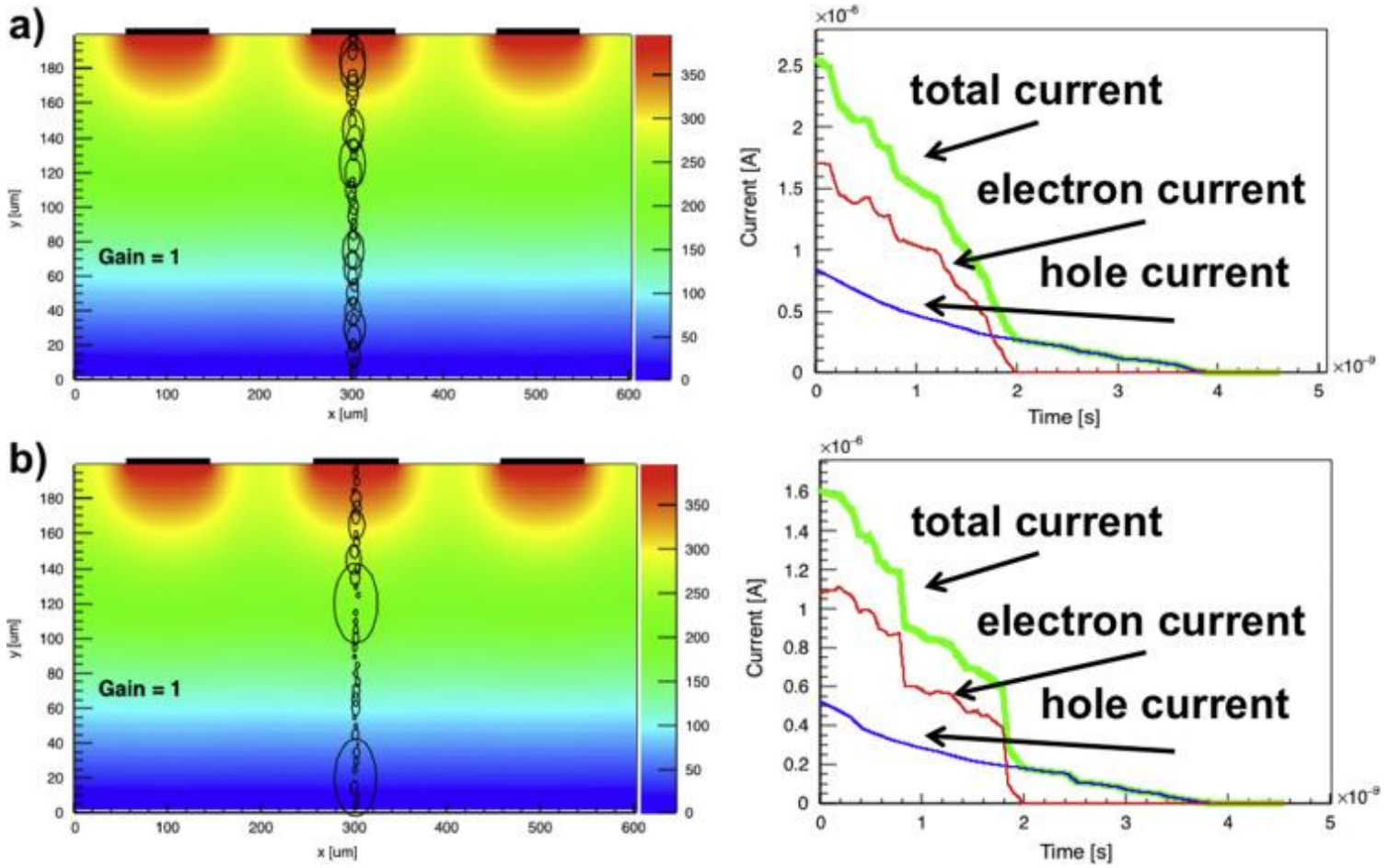

Nuclear Instruments and Methods in Physics Research Section A: Accelerators, Spectrometers, Detectors and Associated Equipment
Volume 845, 11 February 2017, Pages 47-51

Tracking in 4 dimensions

N. Cartiglia [a], R. Arcidiacono [a, g], B. Baldassarri [a, c], M. Boscardin [b, d], F. Cenna [a, e], G. Dellacasa [a, e], G.-F. Dalla Betta [b, f], M. Ferrero [a, e], V. Fadeyev [h], Z. Galloway [h], S. Garbolino [a, e], H. Grabas [h], V. Monaco [a, e], M. Obertino [a, e], L. Pancheri [b, f], G. Paternoster [b, d], A. Rivetti [a], M. Rolo [a] ... A. Zatserklyaniy [h]

After the primary particle has deposited the charge, the movements of the charge ‘instantly’ induces a current on the readout electrode.

If one could apply a threshold directly to this signal, time resolution would be ‘infinite’.

Every realistic amplifier has ‘finite’ bandwidth, i.e. the signal has finite risetime.

Together with the inevitable electronics noise this leads to finite time resolution.

For a silicon sensor without gain, the signal to noise ratio is most of the time actually the dominant contribution to time resolution.

→ Gain

Low Gain Avalanche Detectors (LGADs)

The LGAD sensors, as proposed and manufactured by CNM

(National Center for Micro-electronics, Barcelona):

High field obtained by adding an extra doping layer

E ~ 300 kV/cm, closed to breakdown voltage

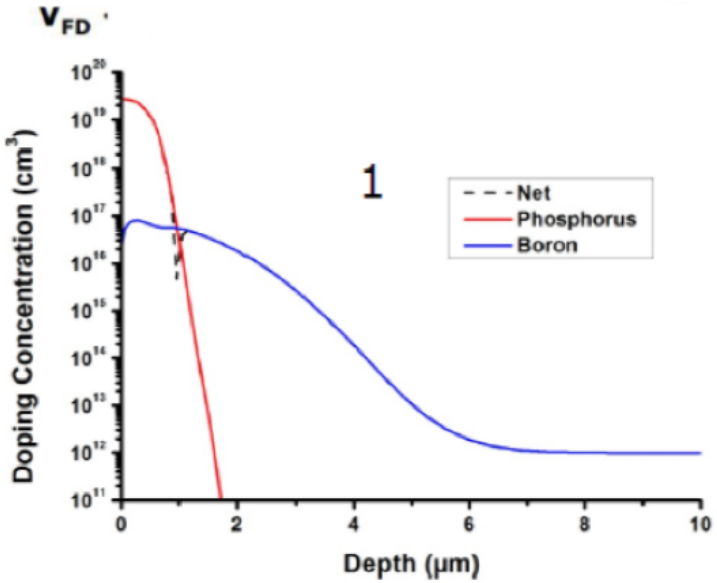

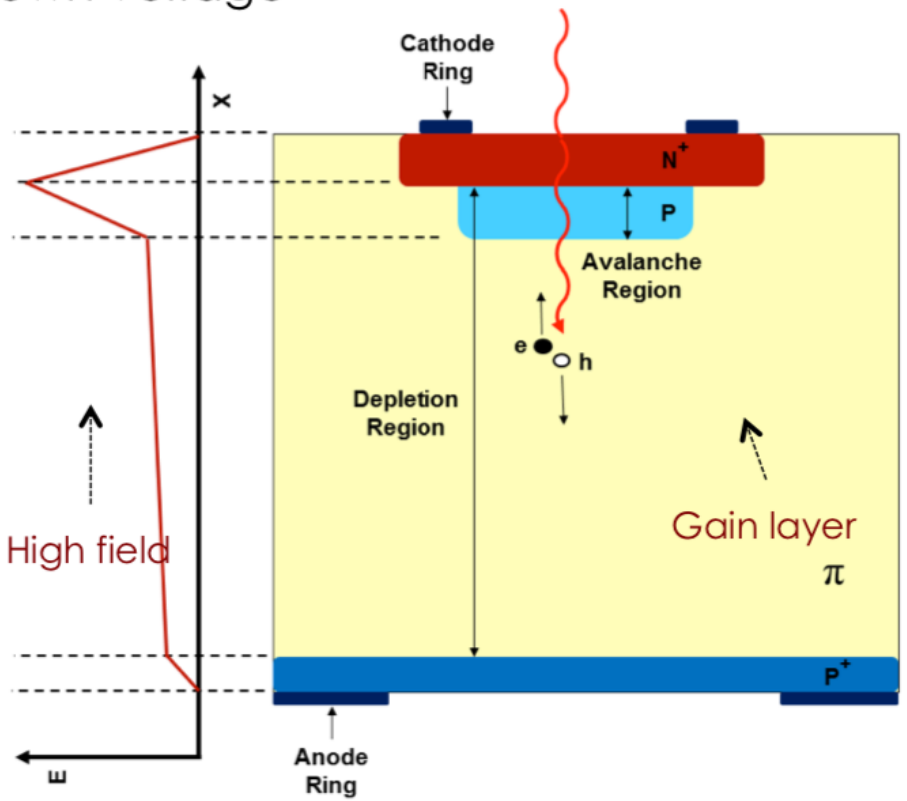

How gain shapes the signal

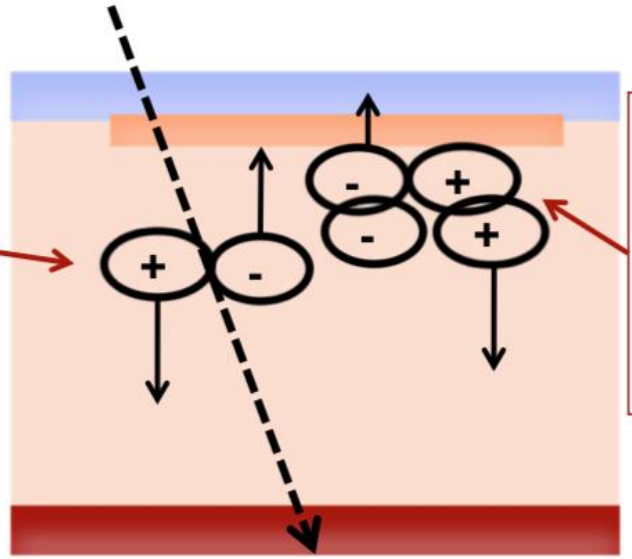

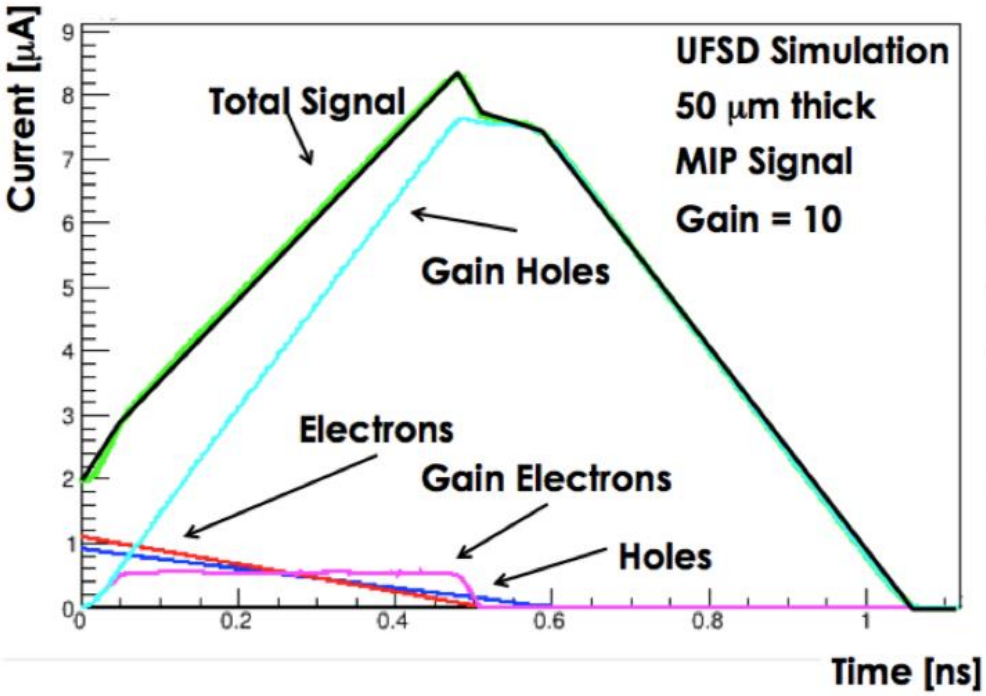

Electrons multiply and produce additional electrons and holes.

- **Gain electrons have almost no effect**
- **Gain holes dominate the signal**

➔ **No holes multiplications**

LGAD Test Beam Results

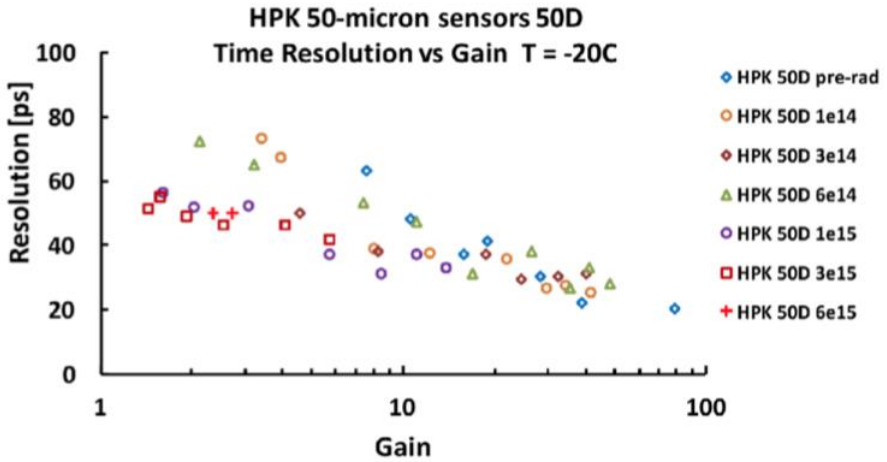

Region	η	R (cm)	z (cm)	Fluence (cm^{-2})	Dose (kGy)
barrel	0.0	117	0	1.7×10^{14}	16
barrel	1.15	117	170	1.9×10^{14}	21
barrel	1.45	117	240	2.0×10^{14}	25
endcap	1.6	127	304	1.1×10^{14}	25
endcap	2.0	84	304	2.4×10^{14}	75
endcap	2.5	50	304	6.6×10^{14}	260
endcap	3.0	30	304	1.7×10^{15}	690

- 30 ps resolution achievable with existing sensors up to 1e15 neq/cm^2
- <40 ps resolution across whole detector up to 2e15
- Ongoing R& D (doping, sensor thickness) to further improve radiation hardness and fill factor

Some basic considerations on time resolution of silicon sensors

JINST

PUBLISHED BY IOP PUBLISHING FOR SISSA MEDIALAB

RECEIVED: *June 23, 2017*
ACCEPTED: *October 21, 2017*
PUBLISHED: *November 21, 2017*

Time resolution of silicon pixel sensors

W. Riegler[1] **and G. Aglieri Rinella**

CERN EP,
CH-1211 Geneve 23, Switzerland

E-mail: werner.riegler@cern.ch

ABSTRACT: We derive expressions for the time resolution of silicon detectors, using the Landau theory and a PAI model for describing the charge deposit of high energy particles. First we use the centroid time of the induced signal and derive analytic expressions for the three components contributing to the time resolution, namely charge deposit fluctuations, noise and fluctuations of the signal shape due to weighting field variations. Then we derive expressions for the time resolution using leading edge discrimination of the signal for various electronics shaping times. Time resolution of silicon detectors with internal gain is discussed as well.

KEYWORDS: Charge transport and multiplication in solid media; Detector modelling and simulations II (electric fields, charge transport, multiplication and induction, pulse formation, electron emission, etc); Solid state detectors; Timing detectors

Approximate formula for LGAD time resolution

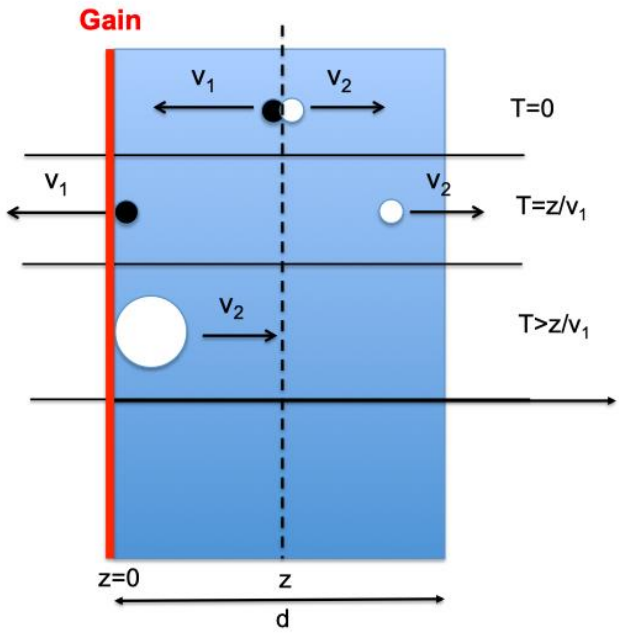

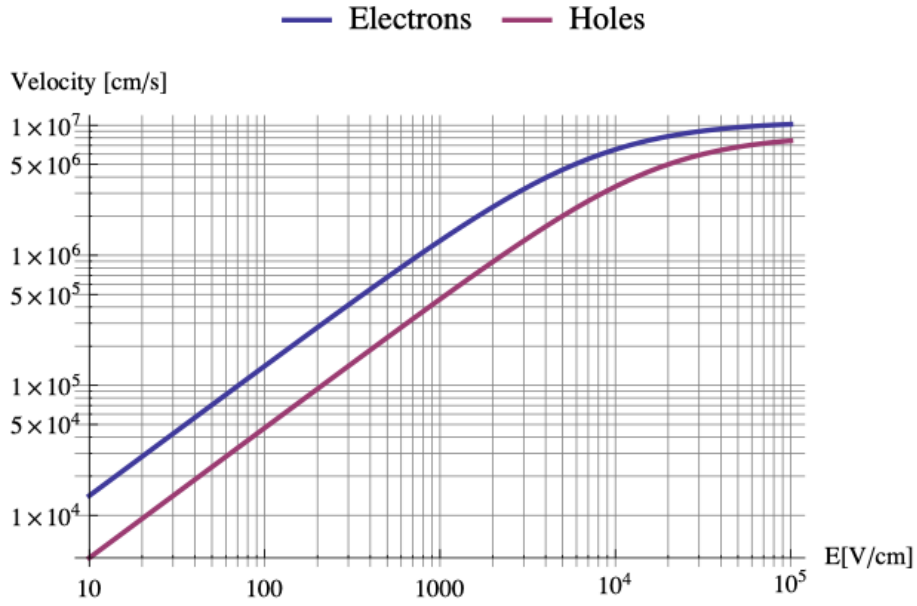

Time for electrons and holes to cross a silicon sensor of a given thickness

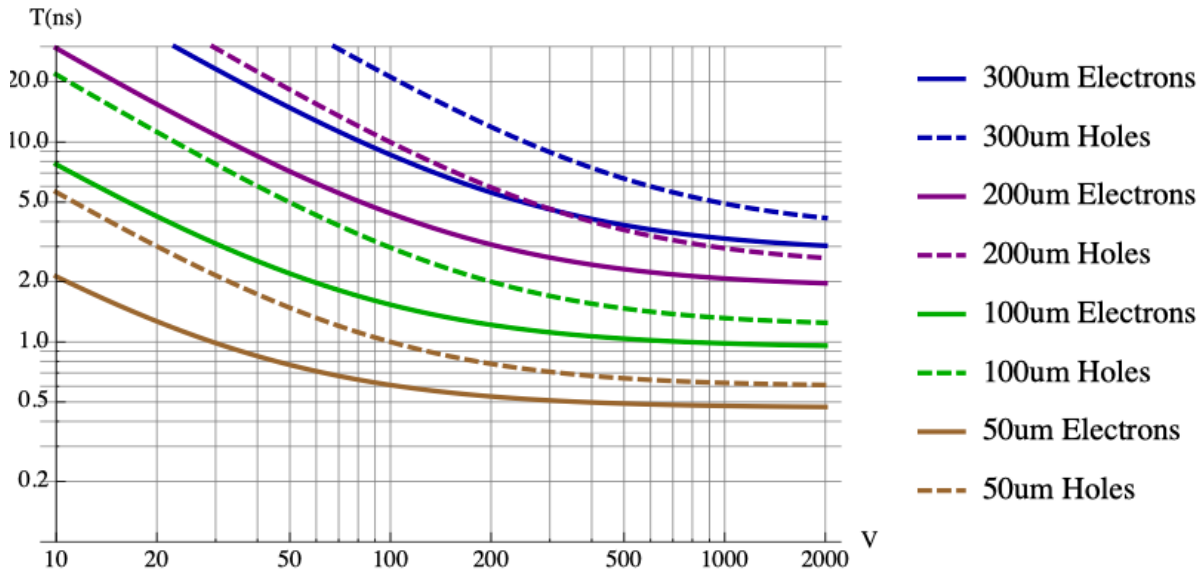

Approximate formula for LGAD time reolsution

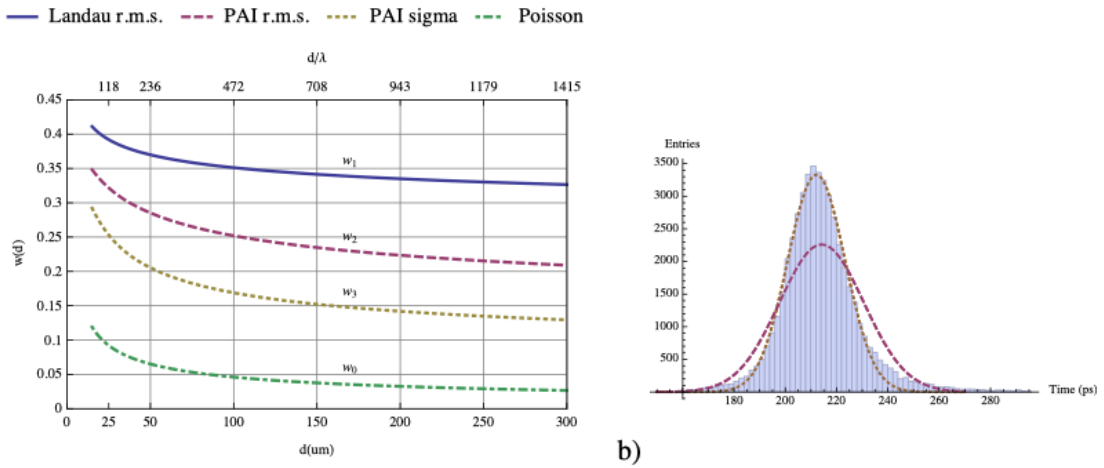

$$\Delta_\tau = w(d)\,\frac{d}{\sqrt{12}v_1}$$

Figure 4. a) The function $w(d)$ for different values of silicon thickness. w_1 represents the Landau theory, w_2 represents the PAI model and w_3 applies for the PAI model if we use a Gaussian fit instead of the r.m.s. as a measure of the time resolution. b) Centroid time distribution for $d = 50\,\mu$m and $V = 220$ V for the PAI model. The dashed curve represents a Gaussian with a $\sigma = \Delta_\tau$ (w_2) and the dotted curve is a Gaussian fit to the histogram (w_3).

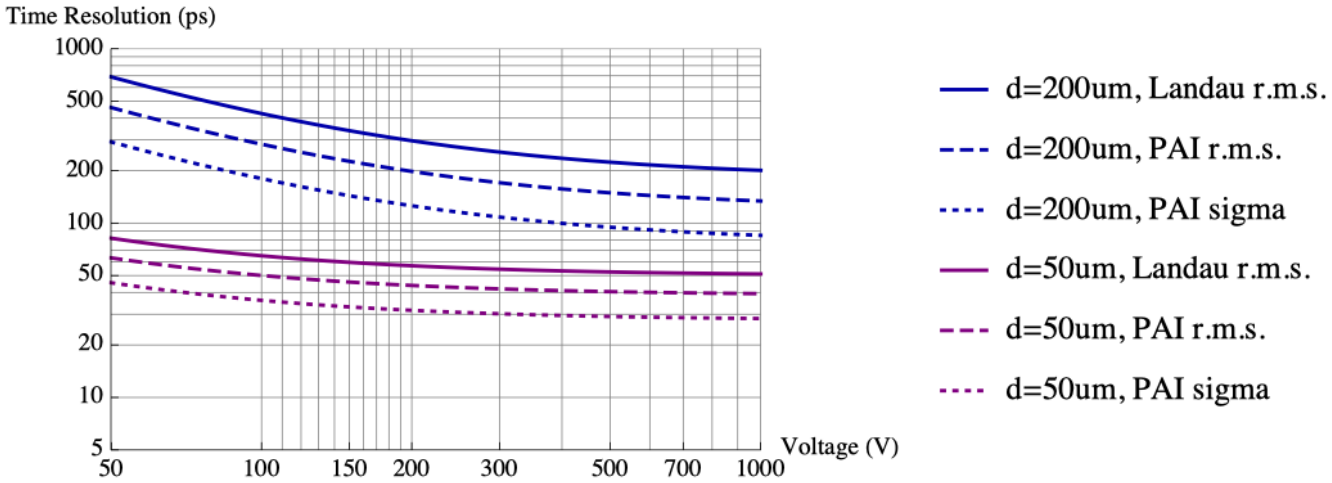

The CMS Experiment Upgrade

CMS design for
10 yrs operation
at $1x10^{34}cm^{-2}s^{-1}$

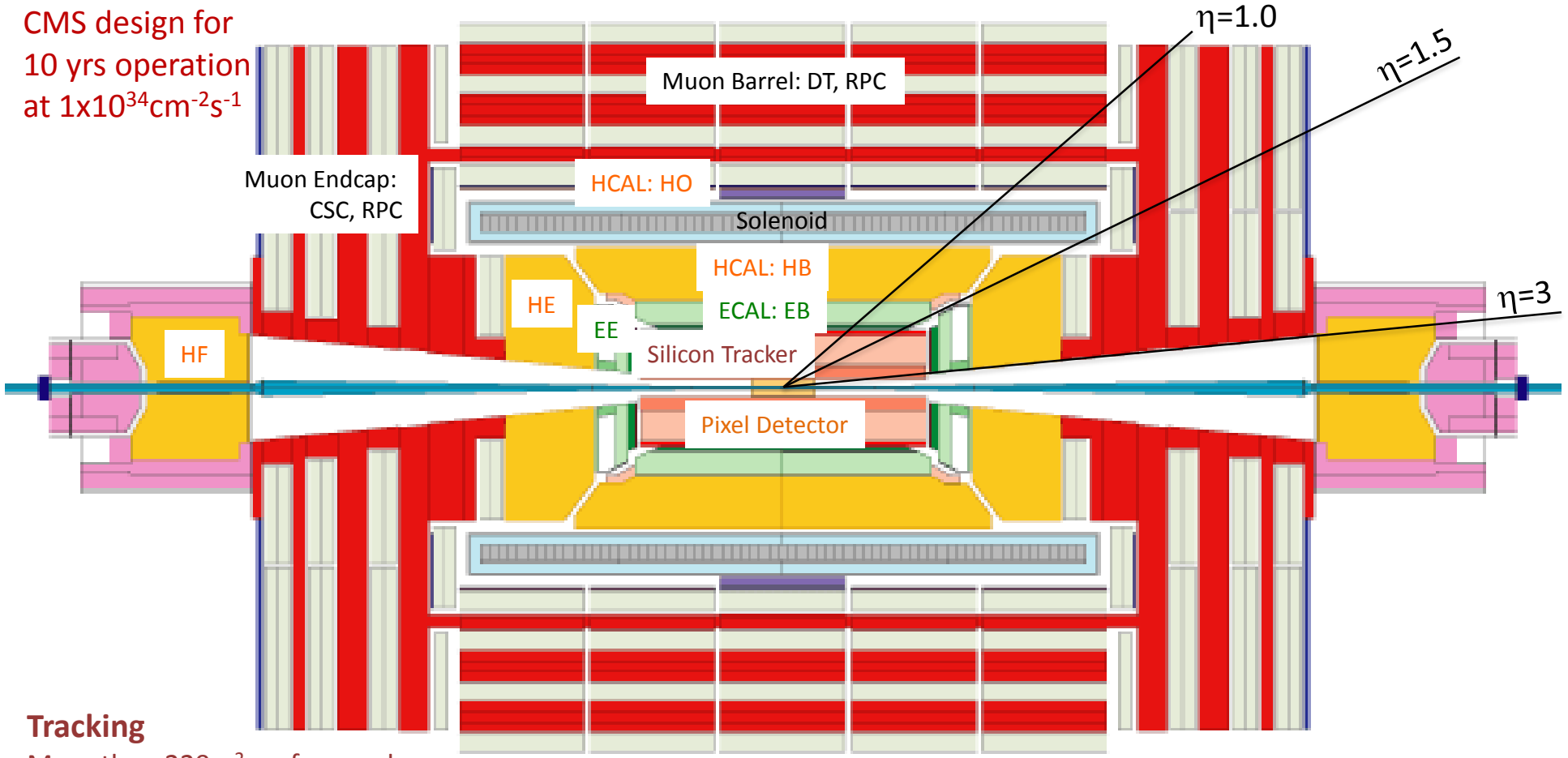

Tracking

More than $220m^2$ surface and
76M channels (pixels & strips)
6m long, ~2.2m diameter
Tracking to $|\eta|<2.4$

ECAL

Lead Tungstate ($PbWO_4$)
EB: 61K crystals, EE: 15K crystals

HCAL

HB and HE: Brass/Plastic scintillator
Sampling calorimeter. Tiles and WLS fiber
HF: Steel/Quartz fiber Cerenkov calo.
HO: Plastic scintillator "tail catcher"

Muon System

Muon tracking in the return field
Barrel: Drift Tube & Resistive Plate Chambers
Endcap: Cathode Strip Chambers & RPCs

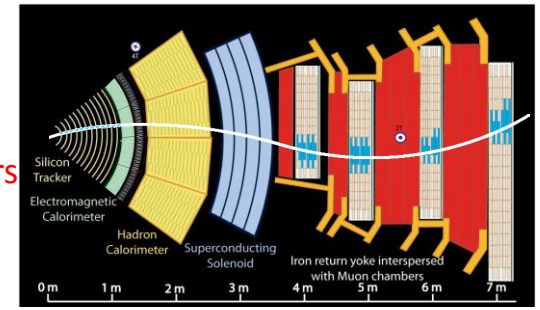

Trigger

Level 1 in hardware, 3.2μs latency ,100 kHz
ECAL+HCAL+Muon
HLT Processor Farm,1 kHz: Tracking , Full reco

CMS

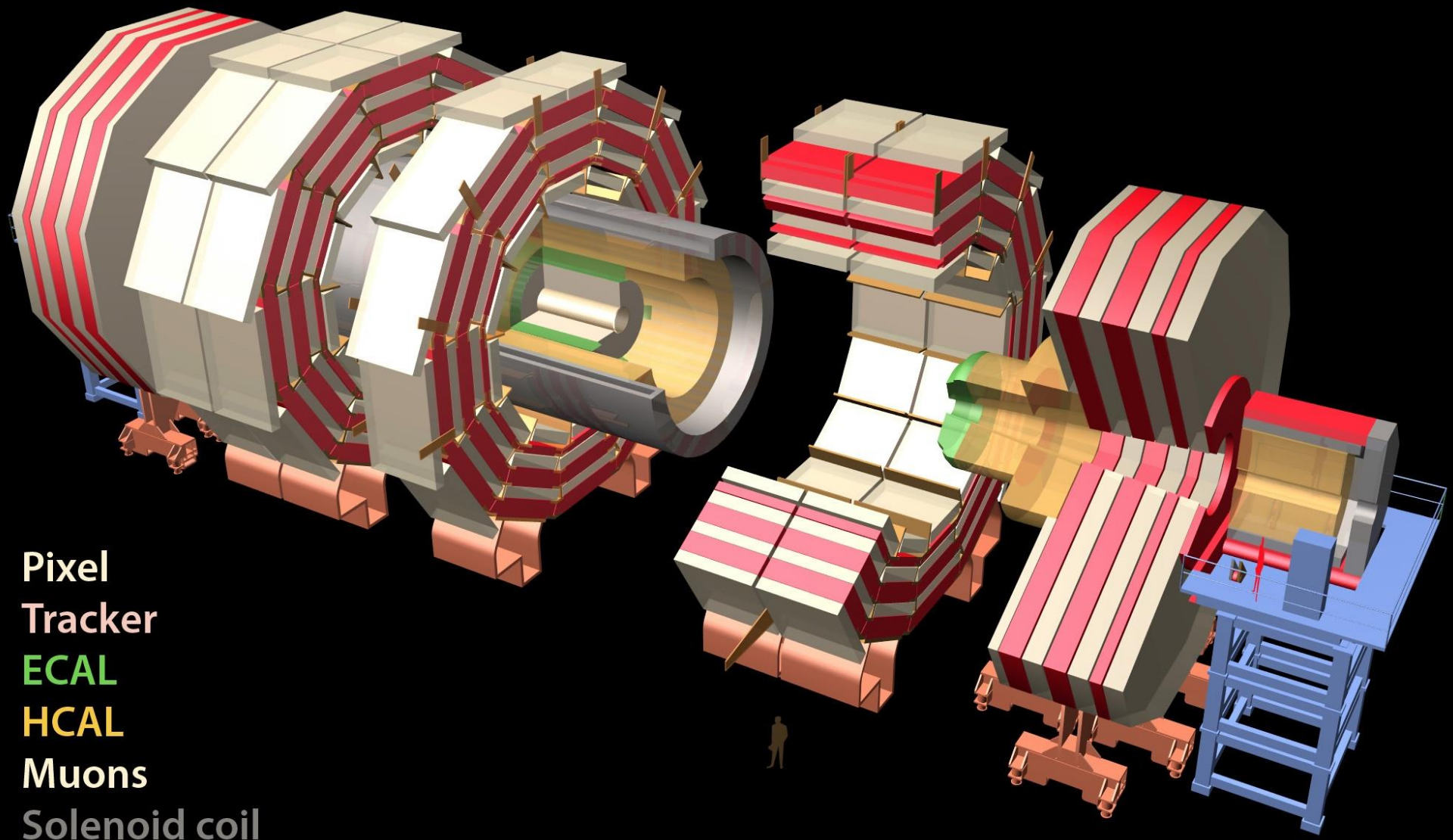

Phase 1 Upgrades – Pixel Detector

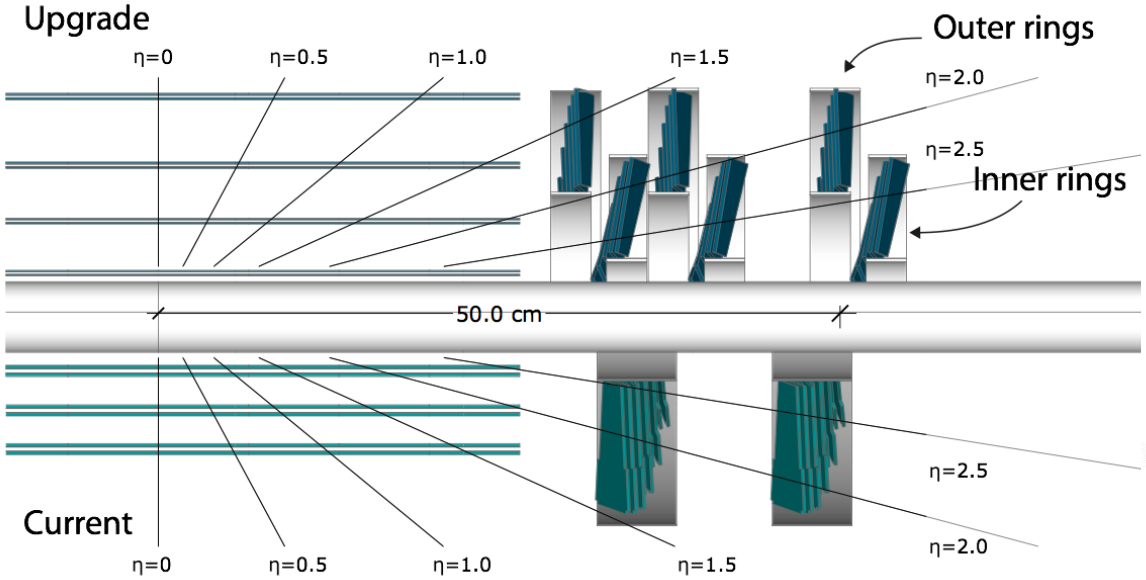

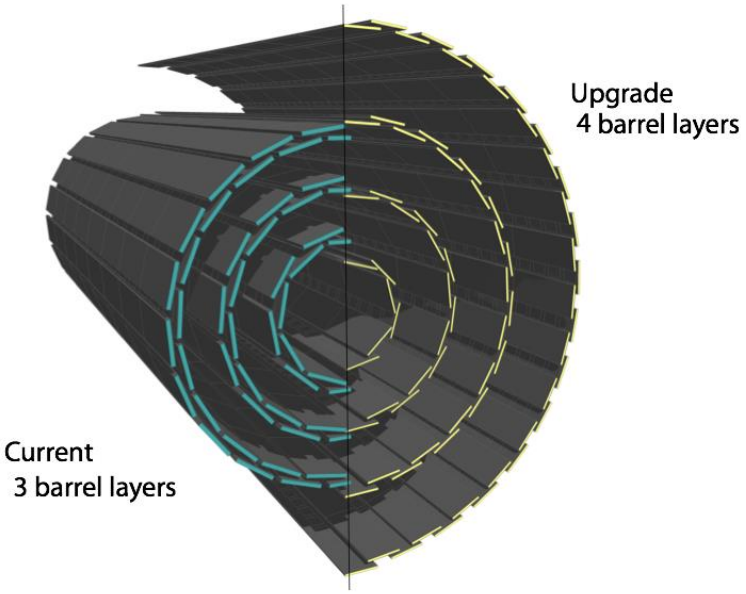

- 4 layers / 3 disks
  - 1 more space point, 3 cm inner radius
  - Improved track resolution and efficiency
- New readout chip
  - Recovers inefficiency at high rate and PU
- Less material
  - CO2 cooling, new cabling and powering scheme (DC-DC)
- Longevity
  - Tolerate up to 100 PU and survive to 500 fb^{-1}, with exchange of innermost layer

Pilot blade (partial disk) in LS1

Phase 1 Upgrades – HCAL

- Backend electronics upgrade to μTCA
- New readout chip (QIE10) with TDC

} HF BE upgrade in LS1, FE at end of 2015

  - Timing: improved rejection of beam-related backgrounds, particularly HF

- Replace HPDs in HB and HE with SiPMs

HB/HE FE upgrade in LS2

  - Small radiation tolerant package, stable in magnetic field
  - PDE improved x3, lower noise
  - Allows depth segmentation for improved measurement of hadronic clusters,

backgrounds, and re-weighting for radiation damage

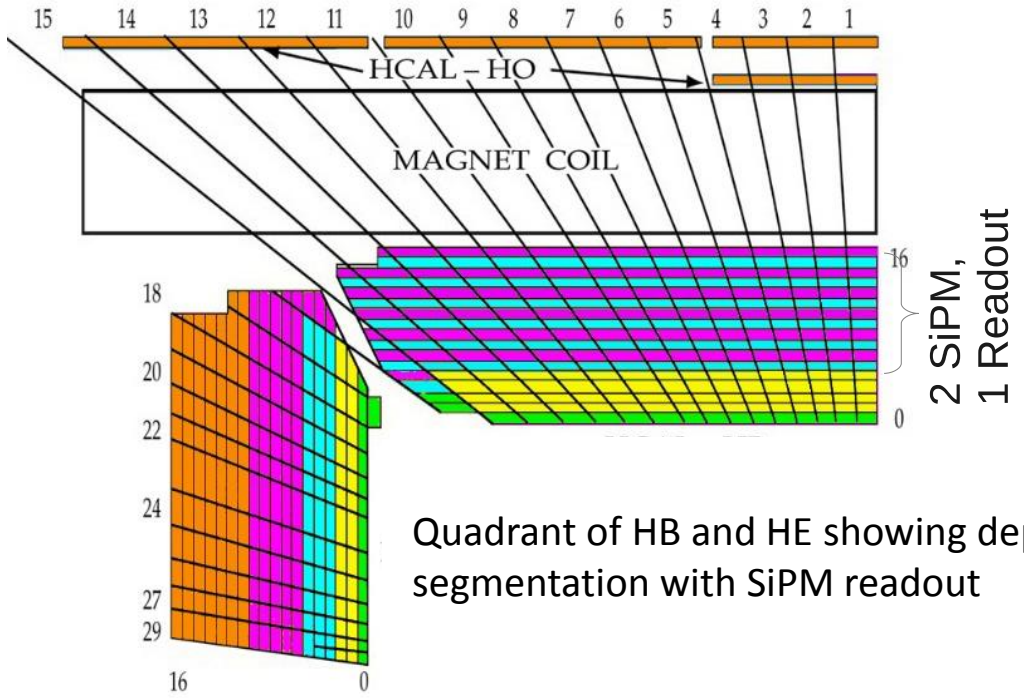

Quadrant of HB and HE showing depth segmentation with SiPM readout

SiPMs: successful R&D program

- Tested to 3000 fb-1
- Neutron sensitivity low

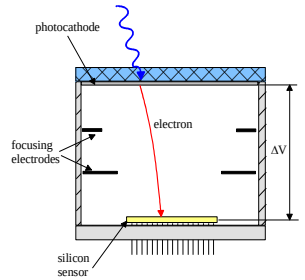

Driving Considerations for the Phase 2 Upgrade

- By LS3 the integrated luminosity will exceed 300 fb^{-1} and may approach 500 fb^{-1} (use 500 for detector studies)
- CMS looks forward to over 5x more data beyond that, at significantly higher PU (and steady throughout the fill) and radiation
- HL-LHC with lumi-leveling at $5x10^{34}cm^{-2}s^{-1}$ will deliver 250 fb^{-1} per year

- Driving considerations in defining the scope for Phase 2
  - Performance longevity of the Phase 1 detector
  - Physics requirements for the HL-LHC program and beam conditions
  - Development of cost effective technical solutions and designs
  - Logistics and scope of work during LS3

- The performance longevity is extensively studied and modeled, and the radiation damage models are included in full simulation

- While the barrel calorimeters, forward calorimeter (HF) and muon chambers – will perform to 3000 fb^{-1}, it is clear that the tracking system and endcap calorimeters must be upgraded in LS3

Electromagnetic Endcap Calorimeter ($PbWO_4$ Crystals), light output will become too small due to radiation damage

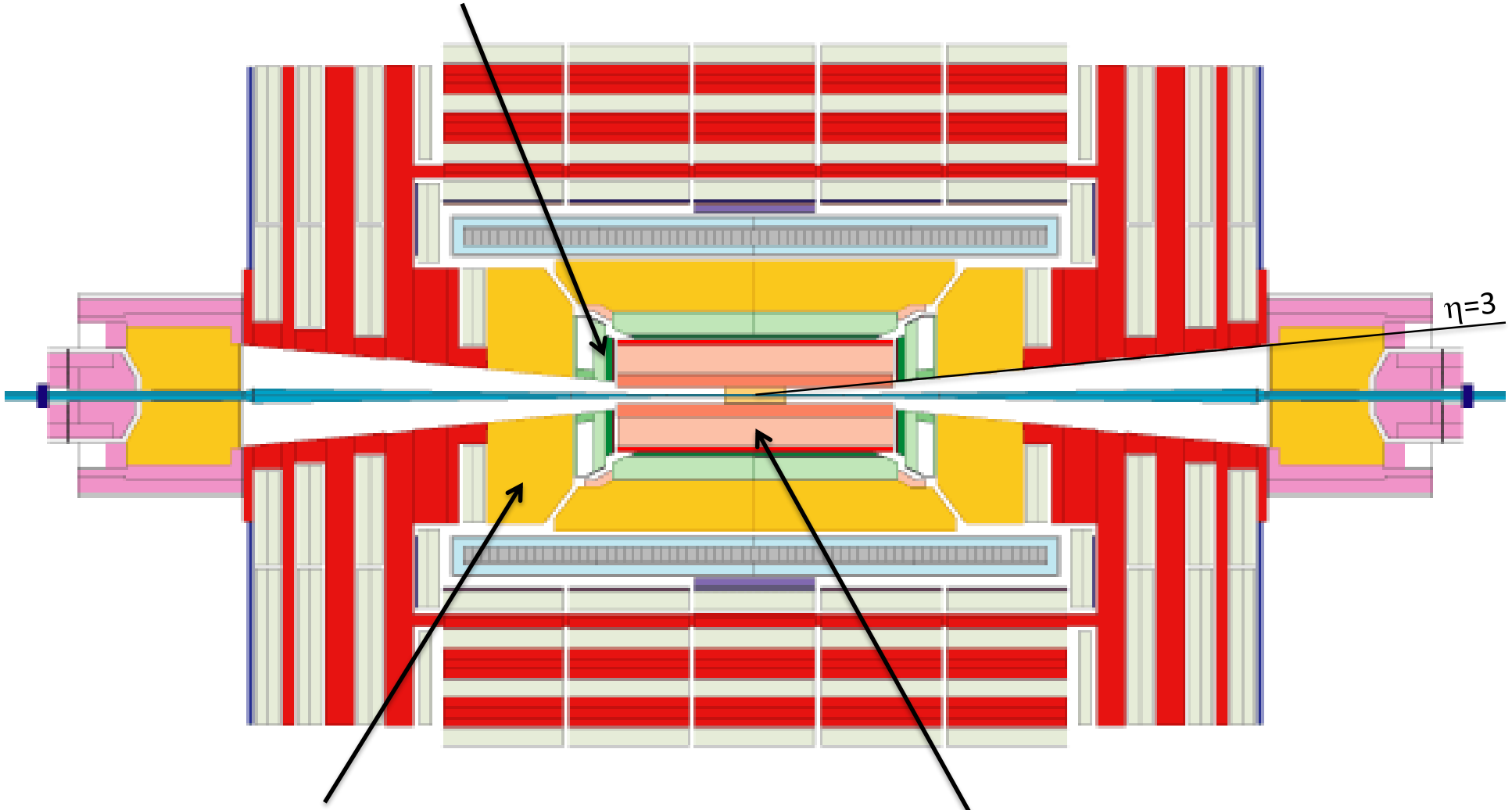

Hadron Endcap Calorimeter (Brass Scintillator) has to be replaced. Crytals, Plastic Scintillators and WLS fibers will broken by radiation.

Entire silicon Tracker has to be replaced → radiation hardness and readout (track triggering)

Performance Considerations

- Mitigation of the effects of high PU relies on particle flow reconstruction and excellent tracking performance.
  - The Phase 2 tracker design must maintain good performance at very high PU
  - We propose to extend the tracker coverage to higher η - the region of VBF jets
  - We are investigating precision timing in association with the calorimeters as a means to mitigate PU for neutral particles

- Endcap coverage
  - The present transition between the endcap and HF, at $|\eta| = 3$, is at the peak of the distribution of jets from VBF. We are studying the feasibility of extending the endcap coverage, and integrating a muon tagging station.
  - This has the potential for a significant improvement for VBF channels, but will have implications for radiation and background levels. Studies are ongoing.
  - Physics studies ongoing to optimize the requirements in resolution & granularity.

Vector Boson Fusion (VBF) -Jets

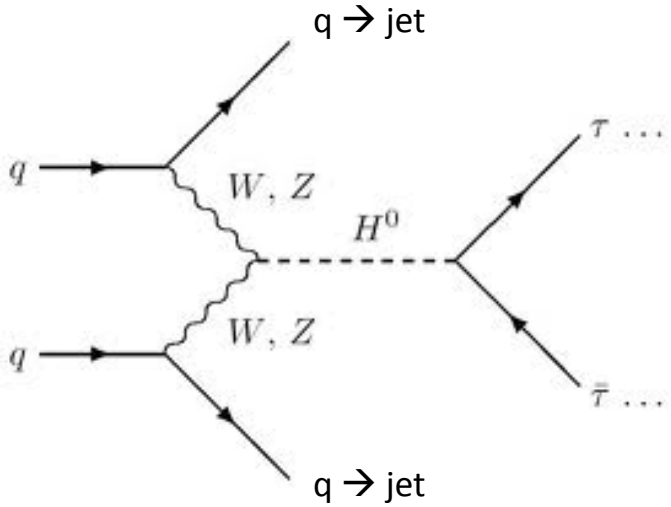

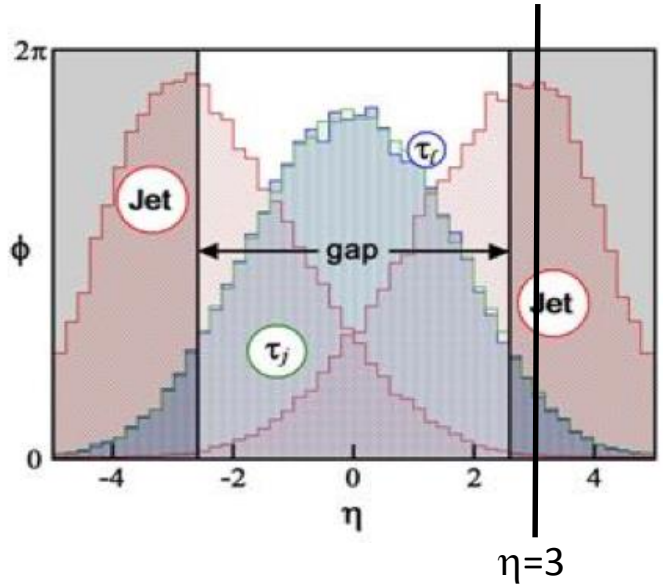

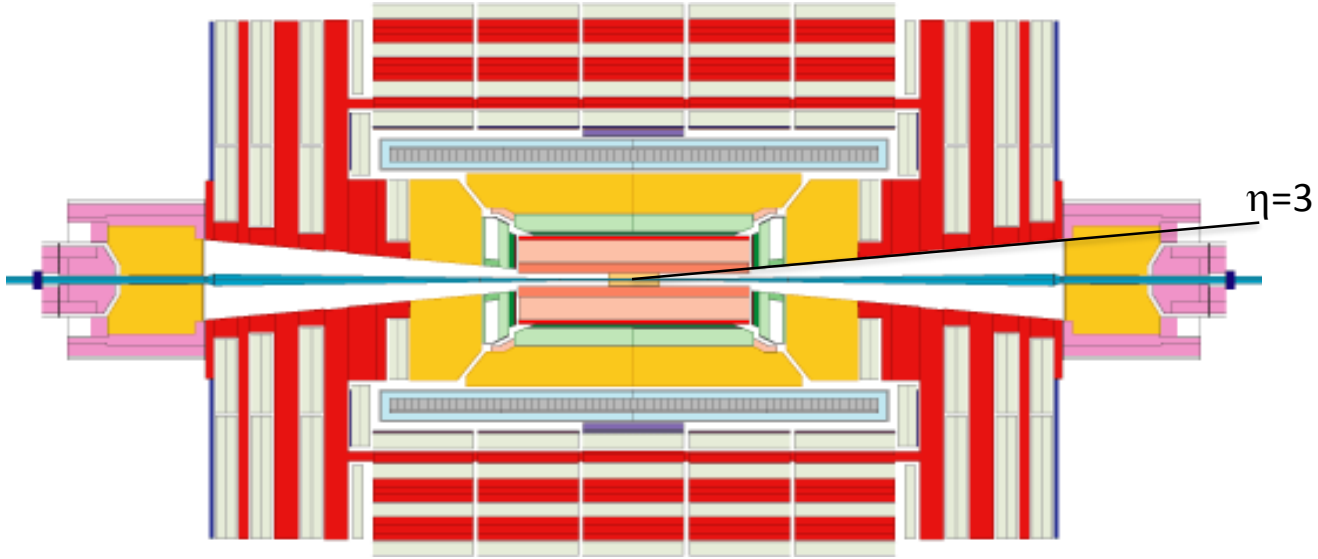

Very important channel to measure.

Quarks do not interact through color exchange i.e. the jets are peaked in forward direction at η=3.

Signature: high jet activity in forward region, little hadronic activity in the barrel.

η = 3 is exactly in the transition region of the endcap calorimeters !

Phase 2 Tracker: conceptual design

- Outer tracker
  - High granularity for efficient track reconstruction beyond 140 PU
  - Two sensor “Pt-modules” to provide trigger information at 40 MHz for tracks with Pt≥2GeV
  - Improved material budget
- Pixel detector
  - Similar configuration as Phase 1 with 4 layers and 10 disks to cover up to |η|= 4
  - Thin sensors 100 µm; smaller pixels 30 x 100 µm
- R&D activities
  - In progress for all components - prototyping of 2S modules ongoing
  - BE track-trigger with Associative Memories

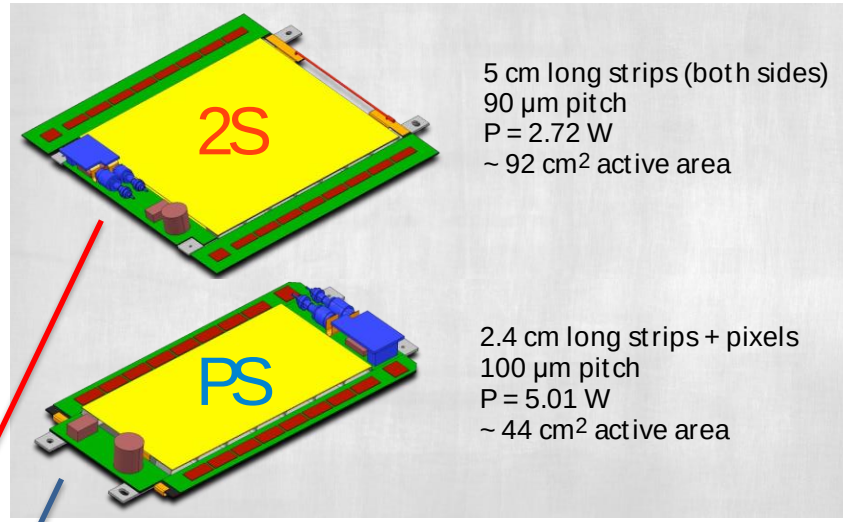

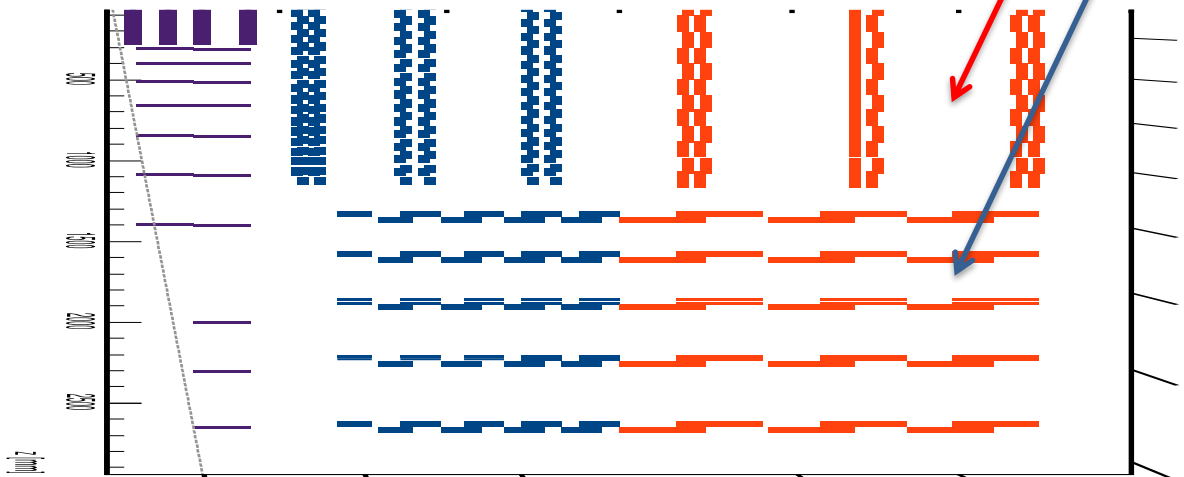

Trigger track selection in FE

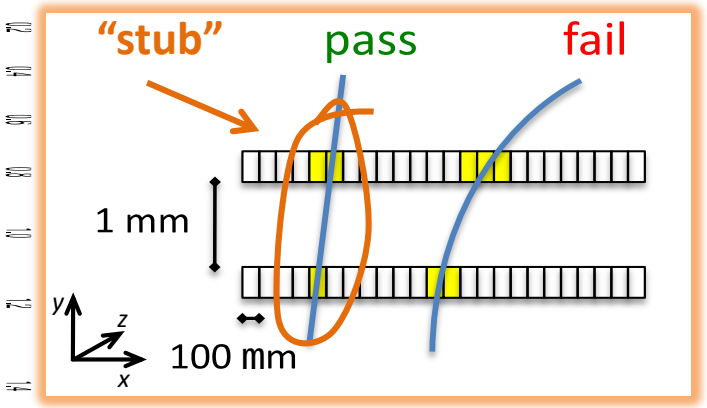

CMS crystal calorimeter performance for HL-LHC radiation

16th International Conference on Calorimetry in High Energy Physics (CALOR 2014) IOP Publishing
Journal of Physics: Conference Series **587** (2015) 012014 doi:10.1088/1742-6596/587/1/012014

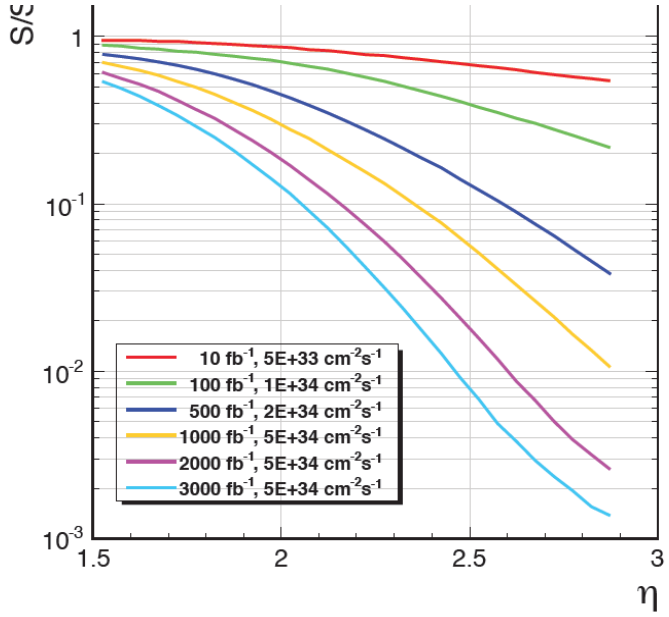

gure 2. Simulated fraction of ECAL response to 50 GeV electrons under different operating nditions as a function of pseudorapidity.

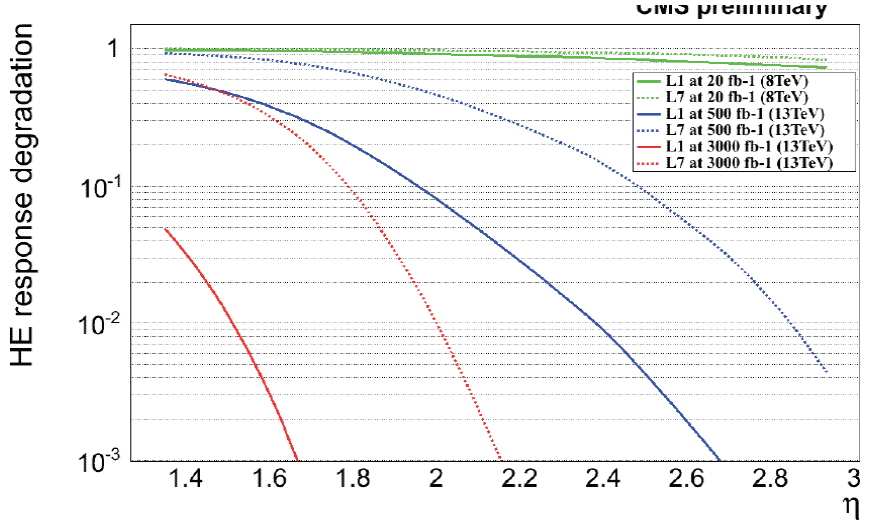

'igure 3. Response degradation of the Hadron Endcap calorimeters at different operating points fo wo different longitudinal segmentations in the calorimeter and as a function of pseudorapidity.

CMS endcap calorimeter upgrade

TP Calorimeter Design

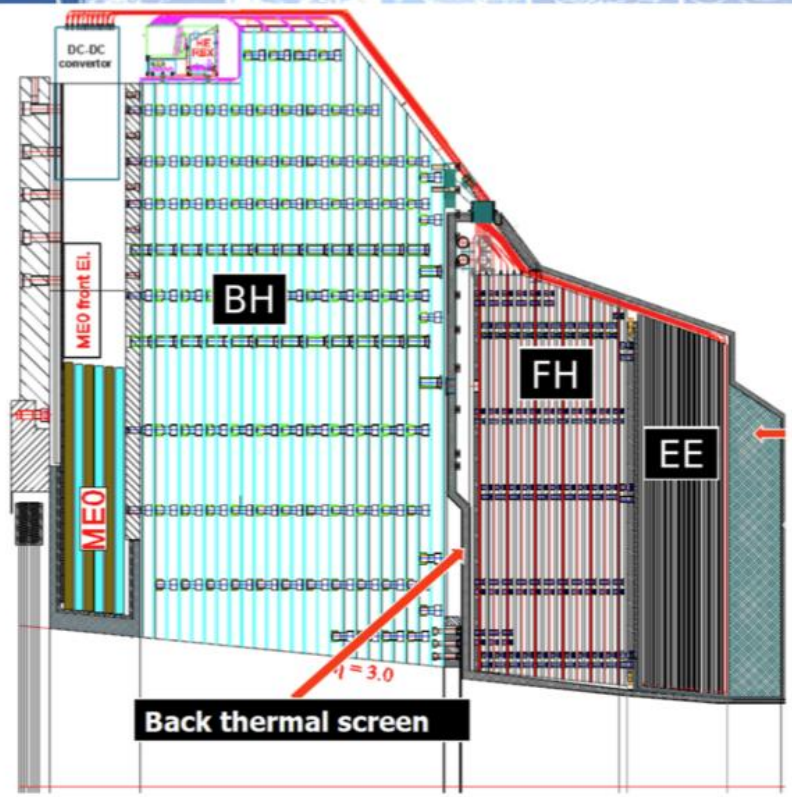

Construction:

- *Hexagonal Si-sensors built into modules.*
- *Modules with a W/Cu backing plate and PCB readout board.*
- *Modules mounted on copper cooling plates to make wedge-shaped cassettes.*
- *Cassettes inserted into absorber structures at integration site (CERN)*

Key parameters:

- *593 m^2 of silicon*
- *6M ch, 0.5 or 1 cm^2 cell-size*
- *21,660 modules (8" or 2x6" sensors)*
- *92,000 front-end ASICS.*
- *Power at end of life 115 kW.*

System Divided into three separate parts:

EE – Silicon with tungsten absorber – 28 sampling layers – 25 X_o (~1.3 λ)
FH – Silicon with brass (now stainless steel) absorber – 12 sampling layers – 3.5 λ
BH – Scintillator with brass absorber – 11 layers – 5.5 λ

EE and FH are maintained at – 30°C. BH is at room temperature.

Electro Magnetic Calorimetry

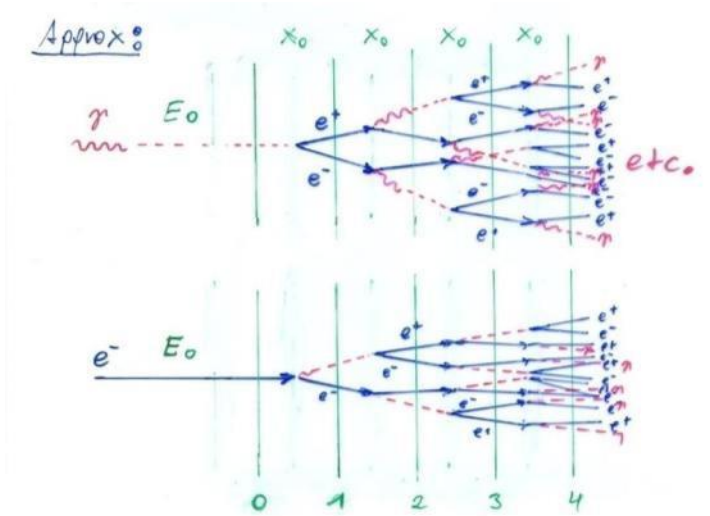

Electromagnetic Shower → EM Calorimeter

$N(n) = 2^n$ .... Number of particles ($e^\pm, \gamma$) after $n X_0$

$E(n) = \frac{E_0}{2^n}$ .... Average Energy of particles after $n X_0$

Shower stops if $E(n) = E_{critical}$

$n_{max} = \frac{1}{\ln 2} \ln \frac{E_0}{E_c}$ → Shower length rises with $\ln E_0$

Critical Energy E_c = electron energy where energy loss due to Bremsstrahlung equals energy loss due to ionization.

$$X_0 = \frac{A}{4\alpha N_A \rho Z^2 \left(\frac{1}{4\pi\varepsilon_0}\frac{e^2}{mc^2}\right)^2 \ln 183 Z^{-\frac{1}{3}}}$$

$$E_c \sim \frac{610}{Z+1.24}\ \text{MeV} \sim \frac{610}{Z}\ \text{MeV}$$

For Pb (Z=82) and 1000GeV electrons n_{max}=17

Simulated EM Shower Profiles in $PbWO_4$

Simulation of longitudinal shower profile **Simulation of transverse shower profile**

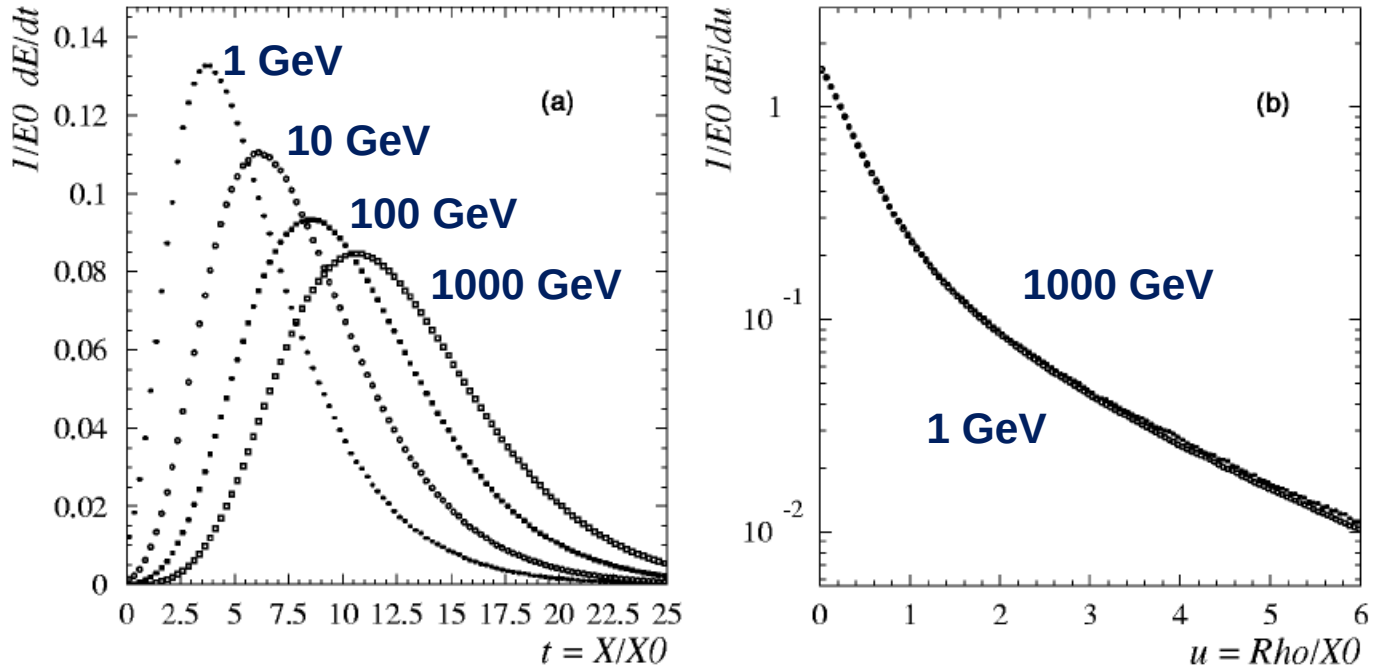

FIG. 2. (a) Simulated shower longitudinal profiles in $PbWO_4$, as a function of the material thickness (expressed in radiation lengths), for incident electrons of energy (from left to right) 1 GeV, 10 GeV, 100 GeV, 1 TeV. (b) Simulated radial shower profiles in $PbWO_4$, as a function of the radial distance from the shower axis (expressed in radiation lengths), for 1 GeV (closed circles) and 1 TeV (open circles) incident electrons. From Maire (2001).

In calorimeters with thickness ~ 25 X_0, the shower leakage beyond the end of the active detector is much less than 1% up to incident electron energies of ~ 300 GeV (LHC energies).

X_0 of Pb = 0.56 cm → $25X_0$=14cm **X_0 of $PbWO_4$ = 0.89cm → $25X_0$=22.5cm**

Crystals for Homogeneous EM Calorimetry

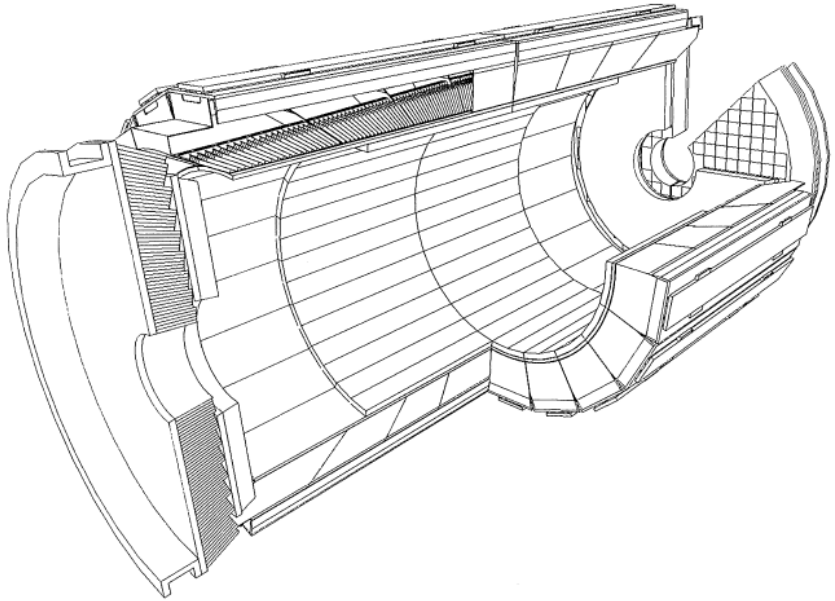

Length of Crystal = 23cm

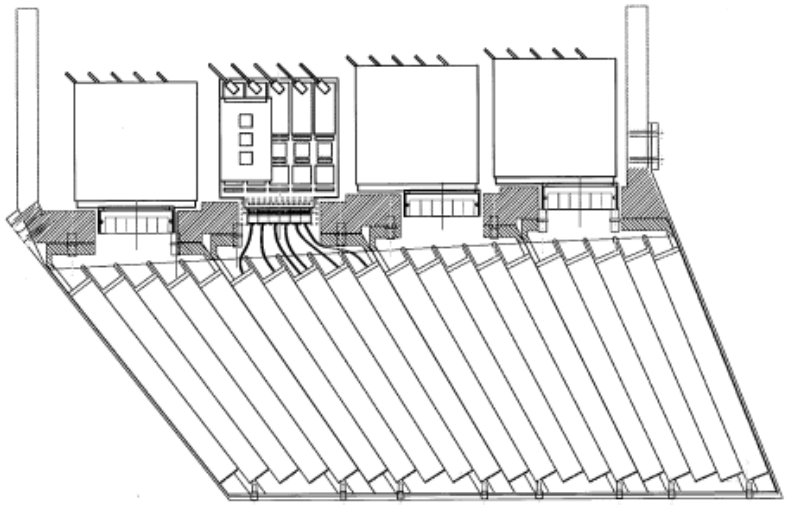

Fig. 2. Longitudinal drawing of module 2, showing the structure and the front-end electronics layout.

Hadronic Calorimetry

In hadronic cascades the longitudinal shower is given by the absorption length λ_a $\quad I \sim e^{-\frac{x}{\lambda_a}}$

In typical detector materials λ_a is much larger than X_0

$$\lambda \sim \frac{1}{\rho} \cdot 35\, A^{\frac{1}{3}}$$

	ρ	X_0	λ
Fe	7.87	1.76 cm	~17 cm
Pb	11.35	0.56 cm	~17 cm

To absorb a hadron shower one typically needs 10-11 interaction lengths.

The interaction length is not such a strong function of the material, it should just be very HEAVY ! Cu, Fe, Pb

10 lambda = 170cm of iron.

CMS uses a Cu/Zn mixture with lambda = 16.4cm and a total of 6 interaction lengths + detector = 120cm in order to keep the coil radius small.

To arrive at >10 lambda in total, a 'tail catcher' is added outside the coil.

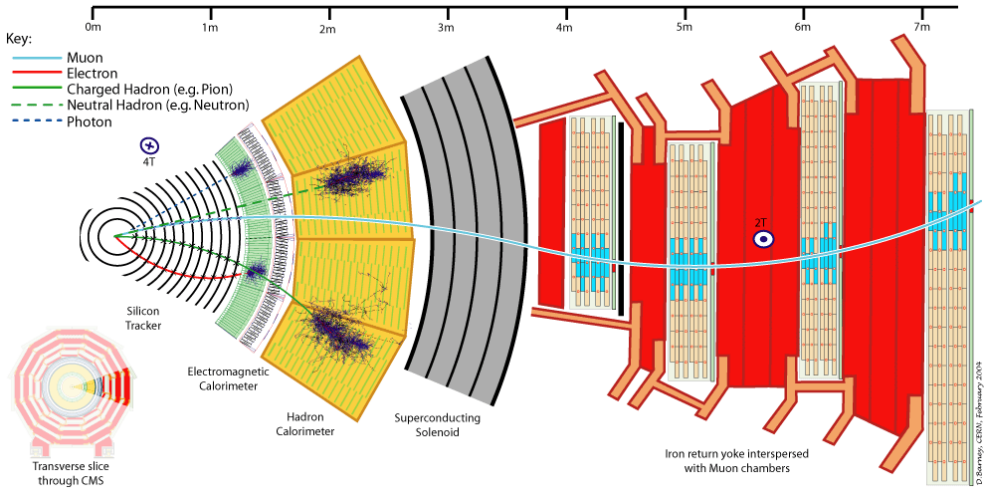

Density of elements

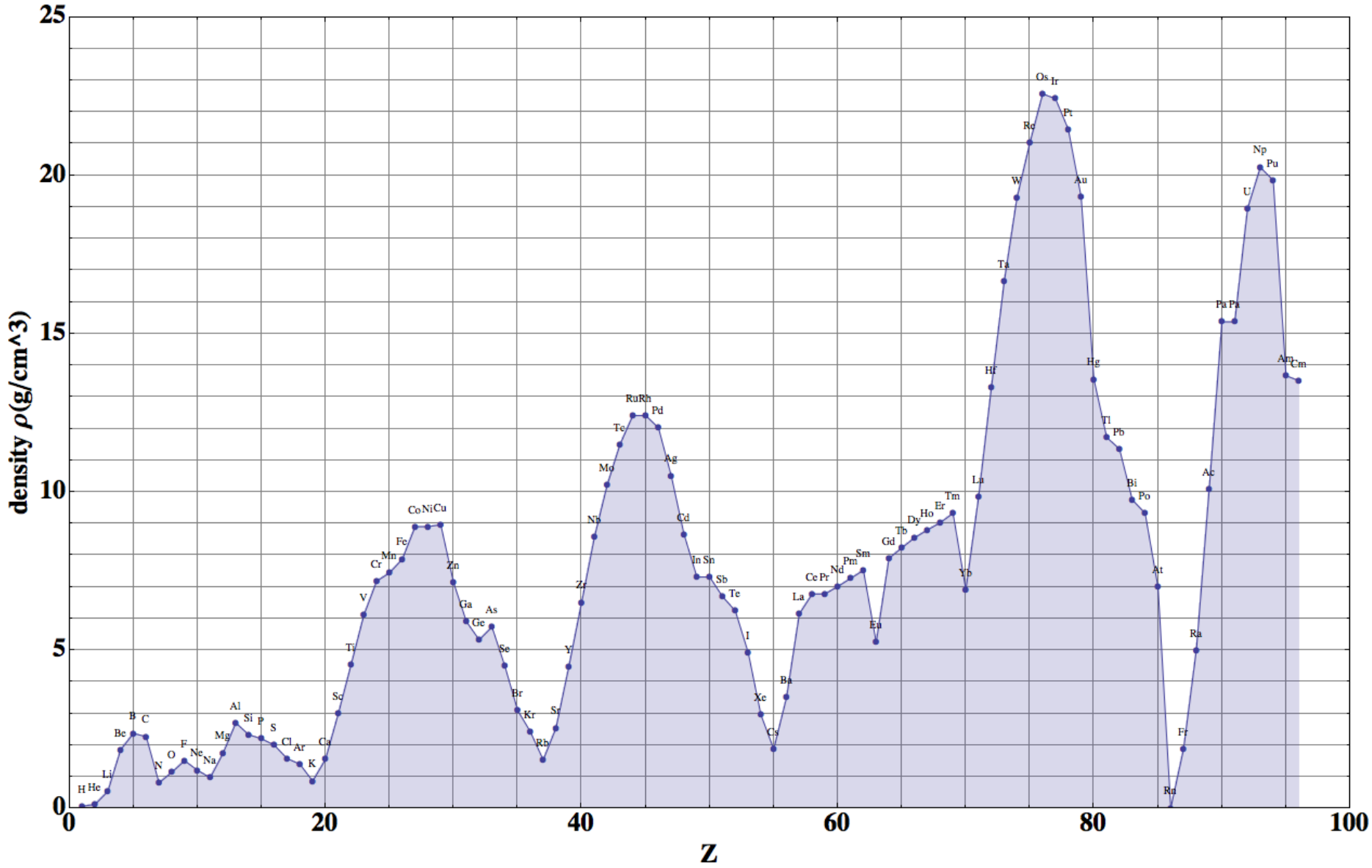

Radiation length of elements

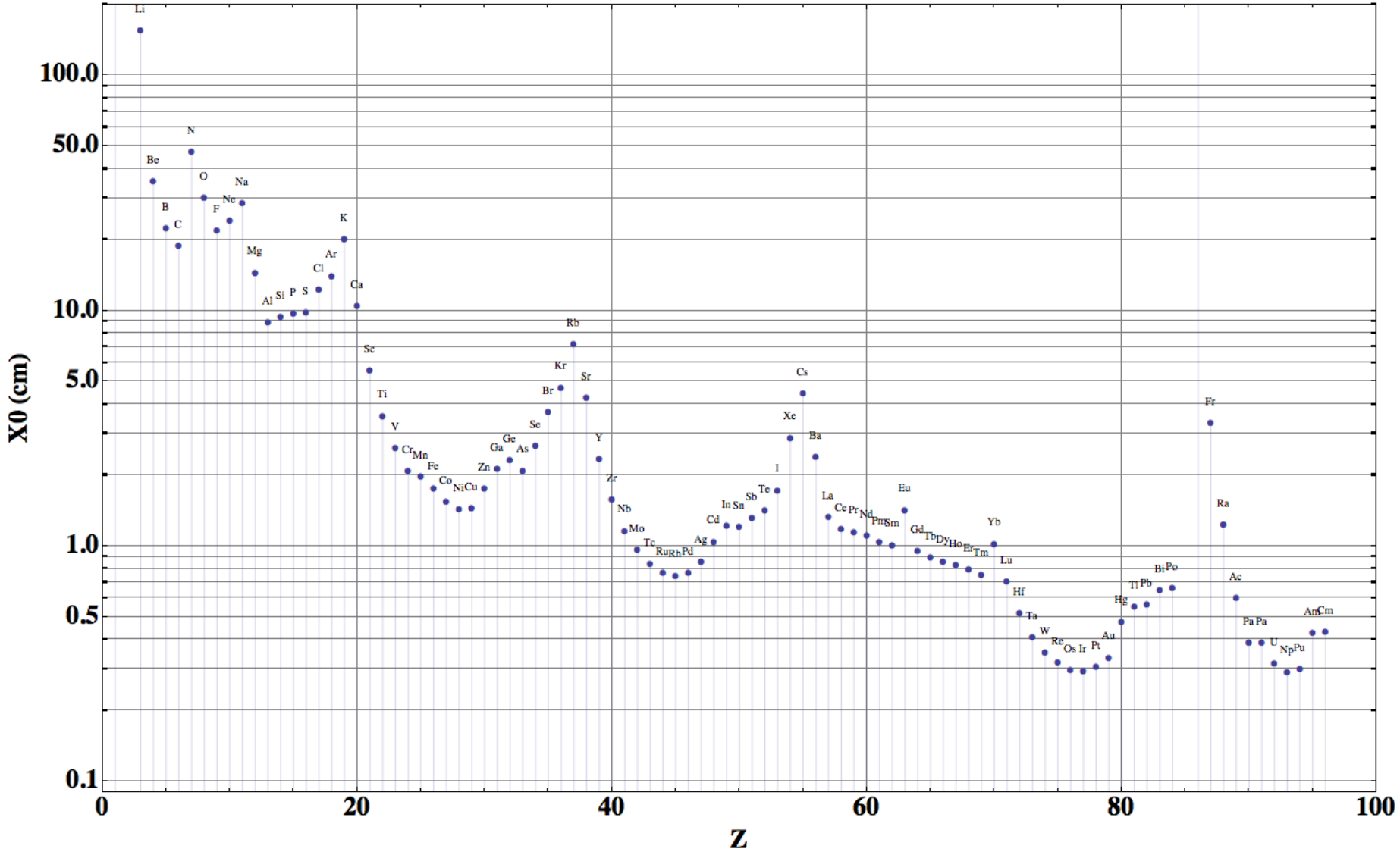

Radiation length of elements

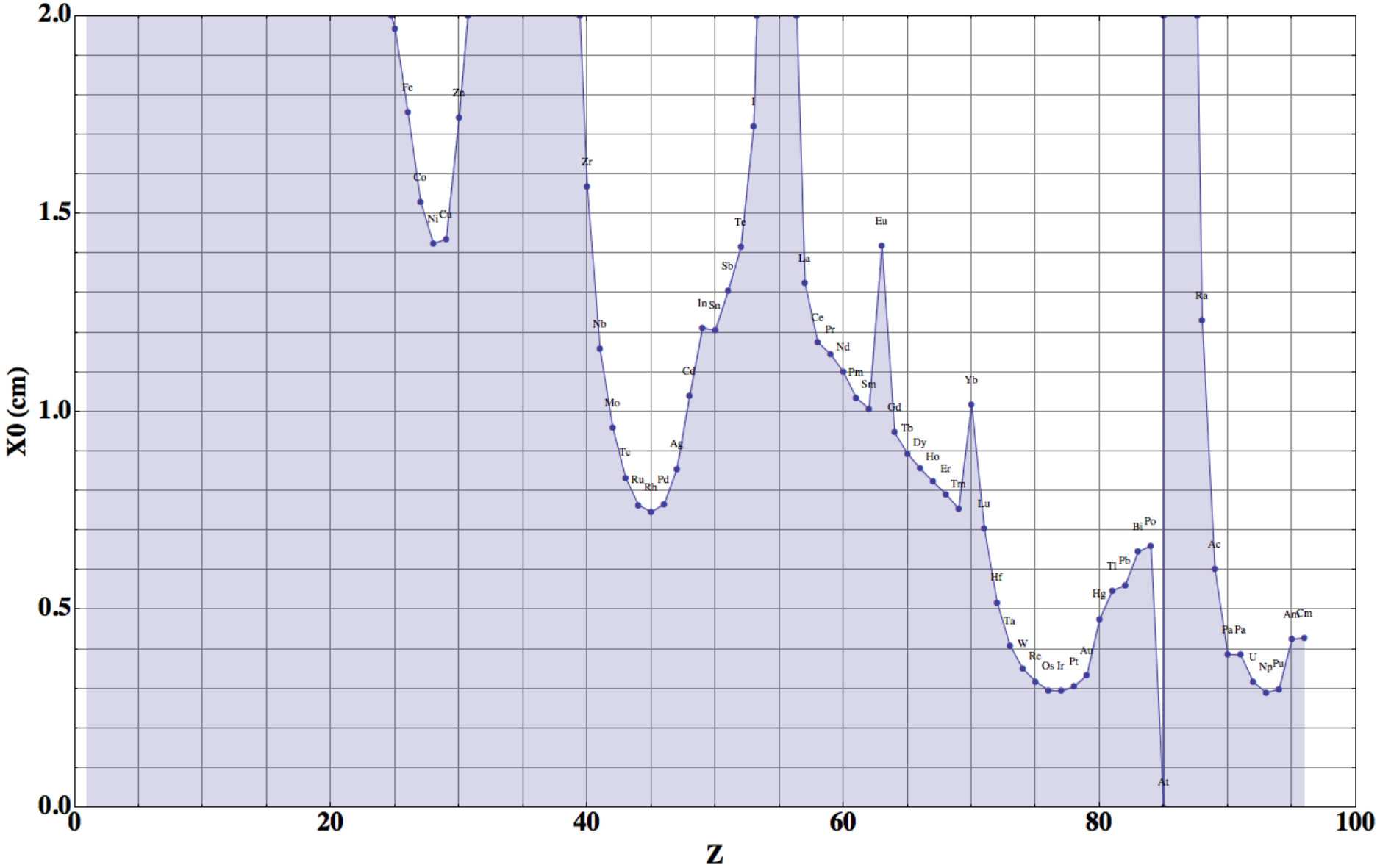

Moliere radius

To limit the overlap of events in the calorimeter it is important to keep the transverse shower size to a minimum.

→ Moliere radius

The transverse Shower Dimension is mainly related to the Multiple scattering of the low Energy Electrons.

$$\theta_0 \sim \frac{21\,[\mathrm{MeV}]}{\beta p\left[\frac{\mathrm{MeV}}{c}\right]} z_1 \cdot \sqrt{\frac{x}{X_0}}$$

Electrons E_c , $E \sim p \cdot c$

$$\theta_0 \sim \frac{21\,[\mathrm{MeV}]}{\beta E_c[\mathrm{MeV}]} \cdot z_1 \cdot \sqrt{\frac{x}{X_0}} \qquad z_1 = 1\,,\ \beta = 1$$

$$E_c \sim \frac{610}{Z+1.24}\ \mathrm{MeV} \sim \frac{610}{Z}\ \mathrm{MeV}$$

$$\theta_0 = 0.0344 \cdot Z \cdot \sqrt{\frac{x}{X_0}}$$

Moliere Radius ρ_m = Lateral Shower Radius after $1 X_0$:

$$\rho_m \approx 0.0344 \cdot Z \cdot X_0$$

95% of Energy are in a Cylinder of $2\rho_m$ Radius.

Moliere radius of elements

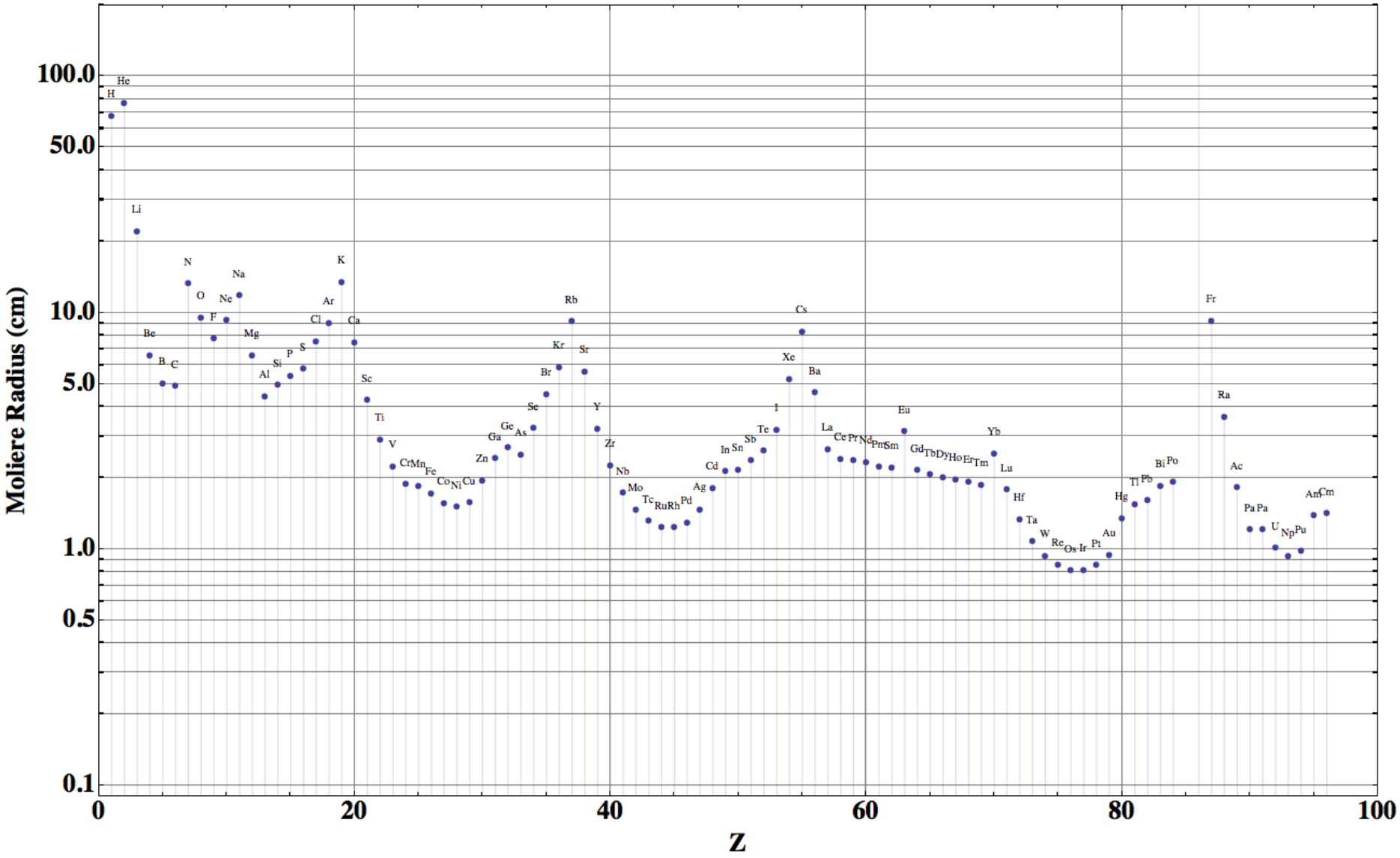

Transverse shower size

Moliere radius of elements

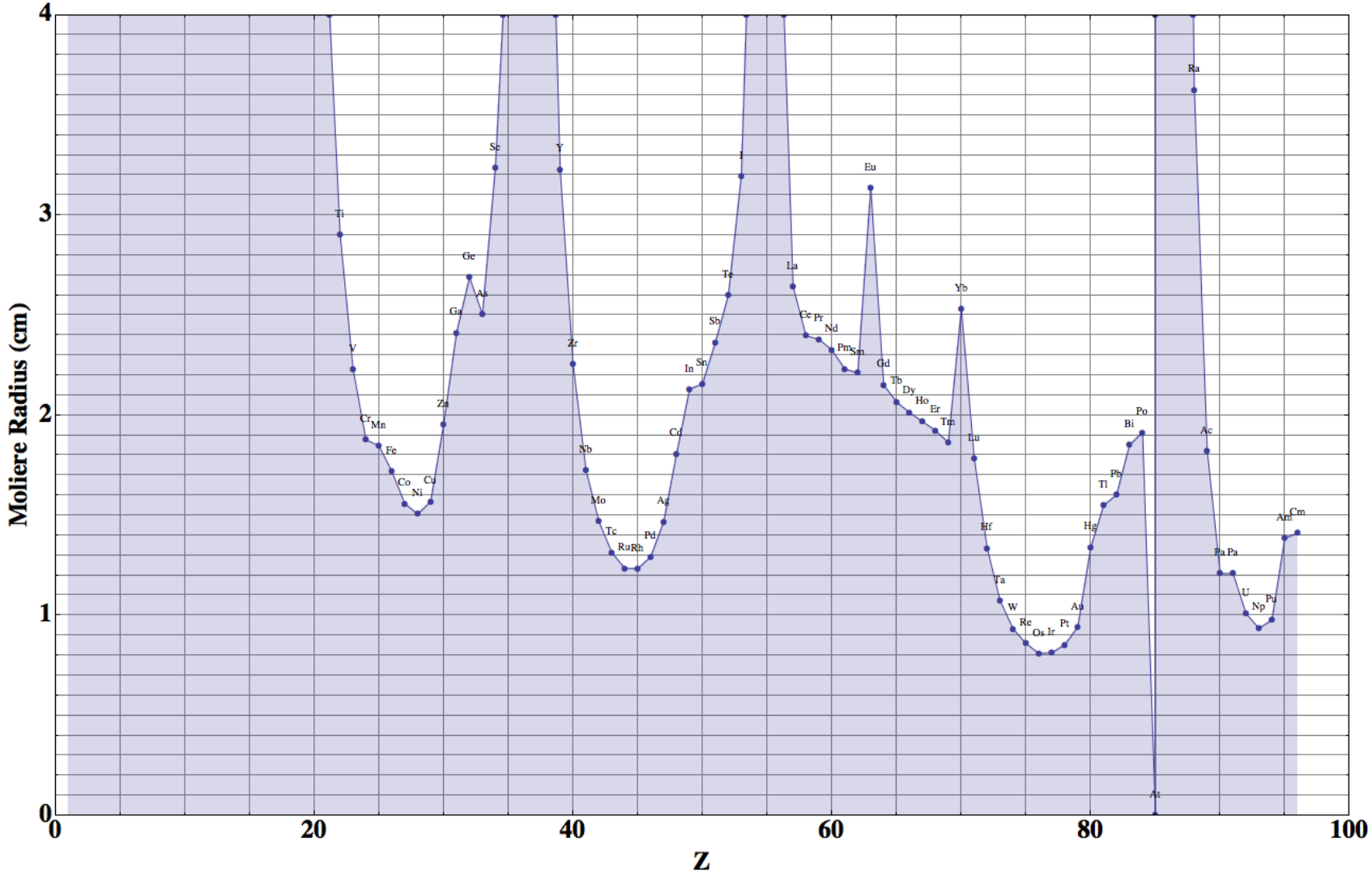

Transverse shower size: W 0.93cm , Pb 1.6cm

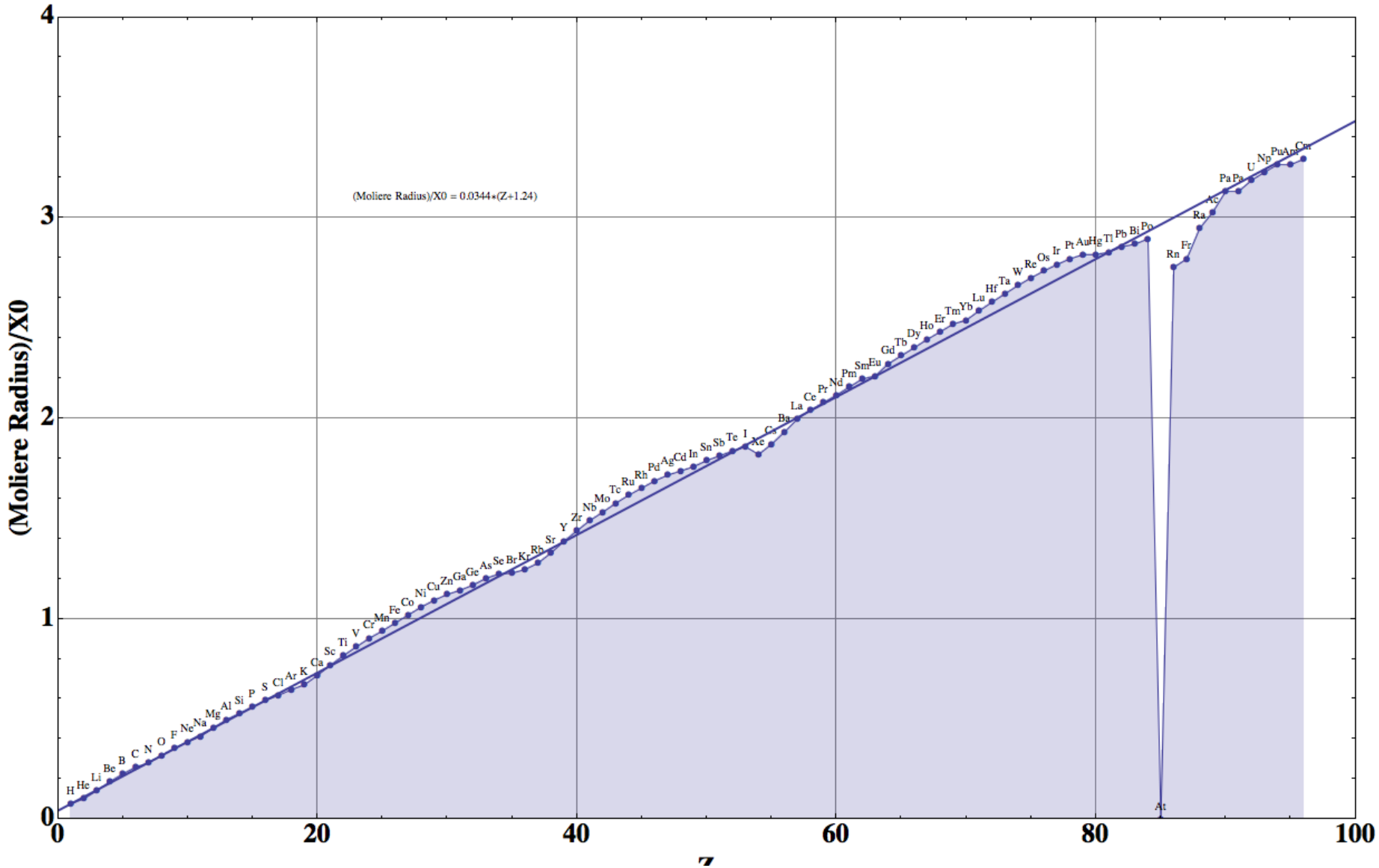
(Moliere Radius)/X0 = 0.0344*(Z+1.24)
(Moliere Radius)/X0
Z
0
1
2
3
4
0
20
40
60
80
100
H He Li Be B C N O F Ne Na Mg Al Si P S Cl Ar K Ca Sc Ti V Cr Mn Fe Co Ni Cu Zn Ga Ge As Se Br Kr Rb Sr Y Zr Nb Mo Tc Ru Rh Pd Ag Cd In Sn Sb Te I Xe Cs Ba La Ce Pr Nd Pm Sm Eu Gd Tb Dy Ho Er Tm Yb Lu Hf Ta W Re Os Ir Pt Au Hg Tl Pb Bi Po At Rn Fr Ra Ac Pa Pa U Np Pu Am Cm

Nuclear interaction lengths of elements

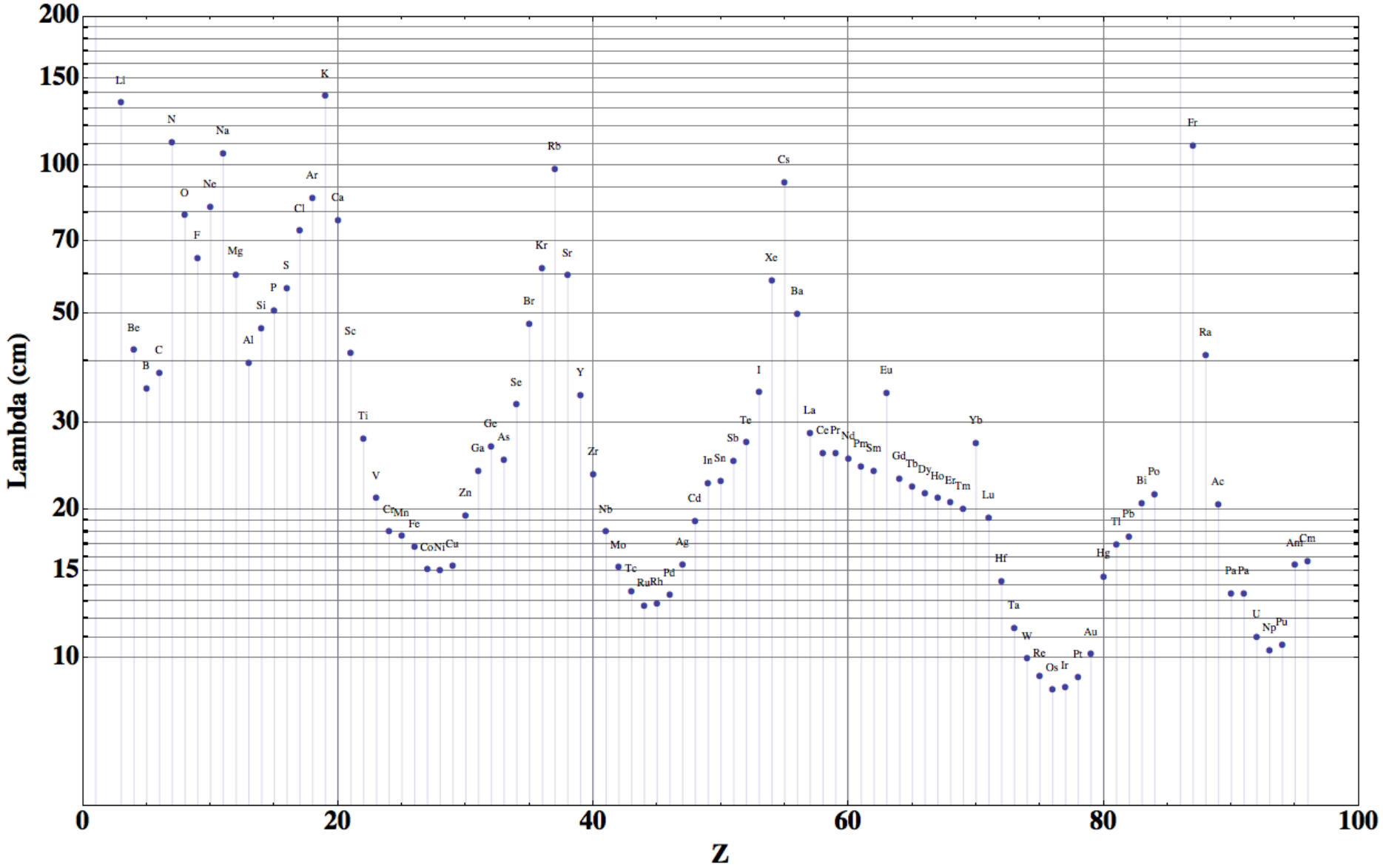

Nuclear interaction lengthsof elements

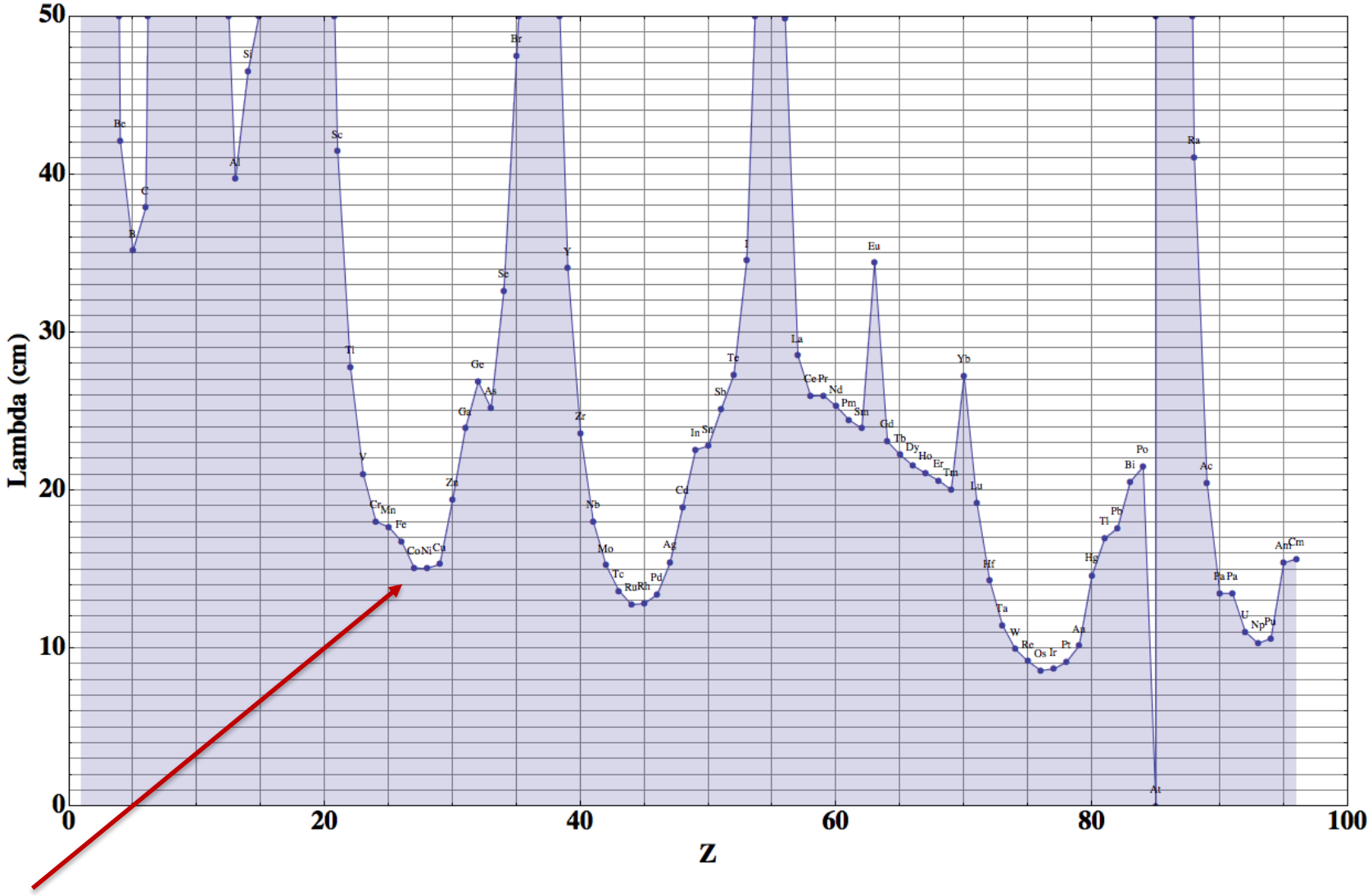

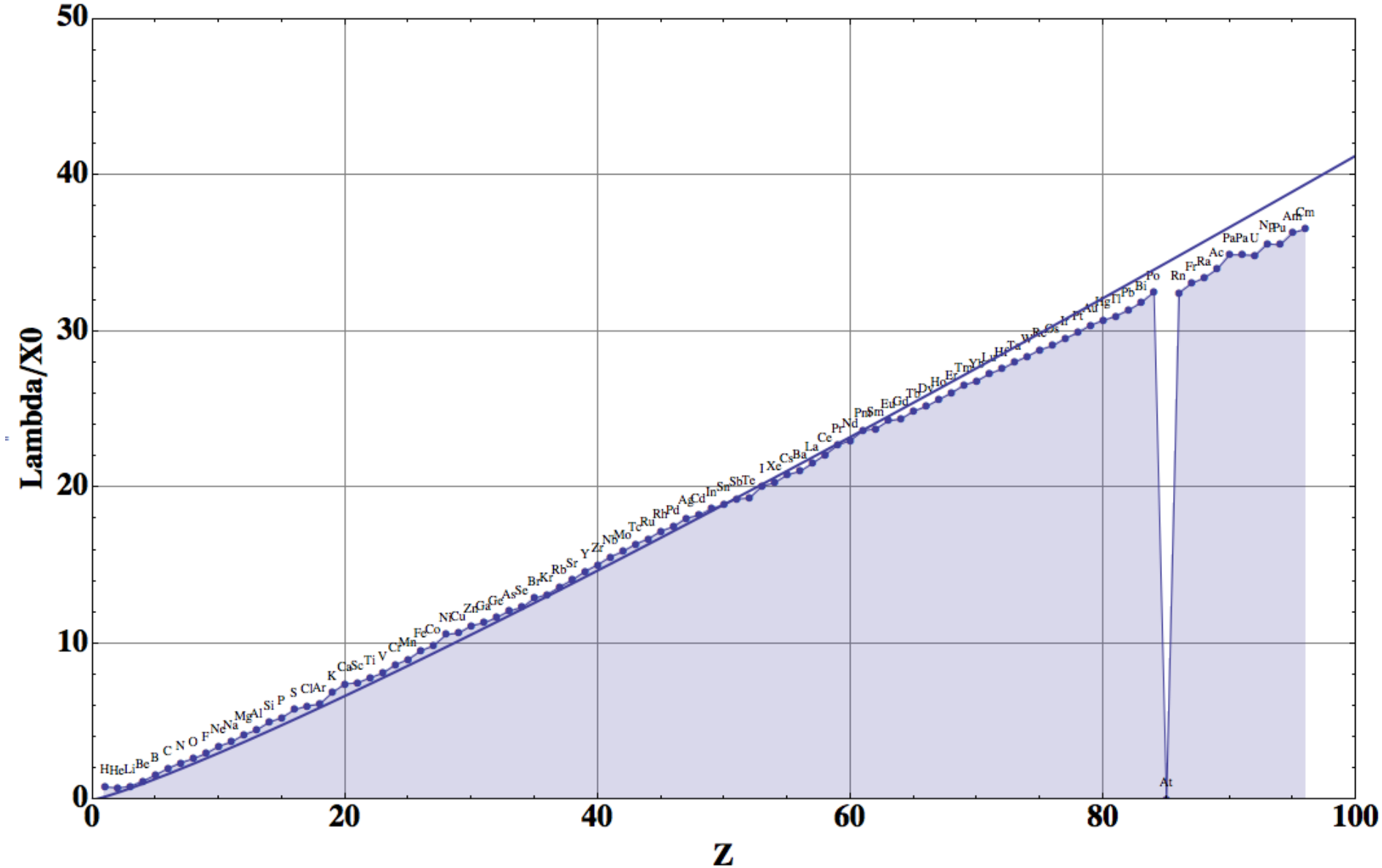
Lambda/X0
Z
0
10
20
30
40
50
0
20
40
60
80
100
H He Li Be B C N O F Ne Na Mg Al Si P S Cl Ar K Ca Sc Ti V Cr Mn Fe Co Ni Cu Zn Ga Ge As Se Br Kr Rb Sr Y Zr Nb Mo Tc Ru Rh Pd Ag Cd In Sn Sb Te I Xe Cs Ba La Ce Pr Nd Pm Sm Eu Gd Tb Dy Ho Er Tm Yb Lu Hf Ta W Re Os Ir Pt Au Hg Tl Pb Bi Po At Rn Fr Ra Ac Pa Th U Np Pu Am Cm

The ALICE Experiment upgrade

ALICE Upgrade

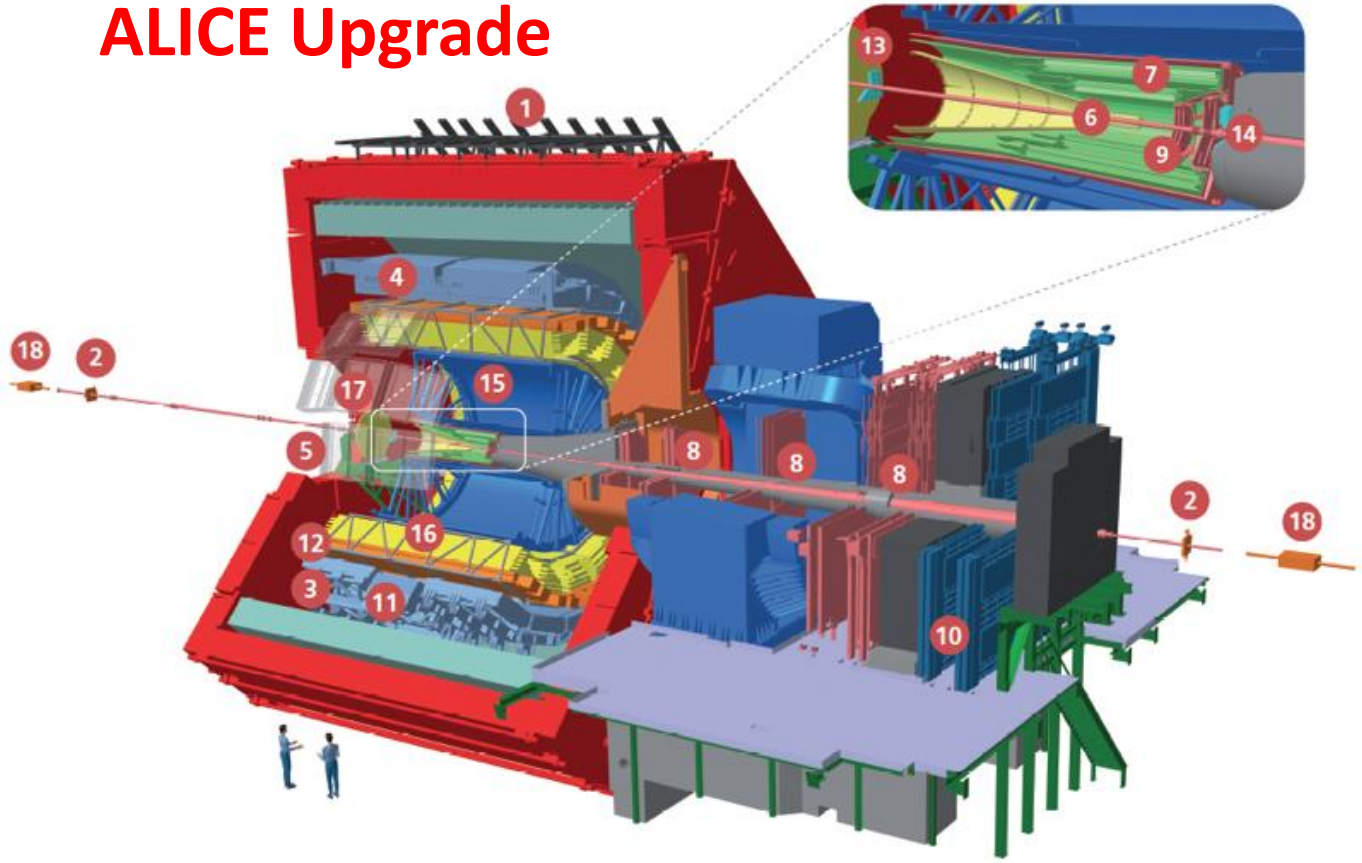

1. **ACORDE** | ALICE Cosmic Rays Detector
2. **AD** | ALICE Diffractive Detector
3. **DCal** | Di-jet Calorimeter
4. **EMCal** | Electromagnetic Calorimeter
5. **HMPID** | High Momentum Particle Identification Detector
6. **ITS-IB** | Inner Tracking System - Inner Barrel
7. **ITS-OB** | Inner Tracking System - Outer Barrel
8. **MCH** | Muon Tracking Chambers
9. **MFT** | Muon Forward Tracker
10. **MID** | Muon Identifier
11. **PHOS / CPV** | Photon Spectrometer
12. **TOF** | Time Of Flight
13. **T0+A** | Tzero + A
14. **T0+C** | Tzero + C
15. **TPC** | Time Projection Chamber
16. **TRD** | Transition Radiation Detector
17. **V0+** | Vzero + Detector
18. **ZDC** | Zero Degree Calorimeter

Time Projection Chamber (TPC)

- New readout chambers using GEM technology
- New electronics for continuous readout (SAMPA)

MUON ARM

- New electronics for Muon Chambers (SAMPA)
- New electronics for Muon Trigger

Online Offline (O2) system

- new computing facility
- on line tracking & data compression
- 50kHz PbPb event rate

New Trigger Detectors (FIT)
New Central Trigger Processor (CTP)
TOF, TRD new readout electronics
PHOS, EMCAL, CPV, HMPID
improvement of readout rate with existing electronics

Common Projects:
Common Readout Unit (CRU) for all detectors (PCI card)
SAMPA common FE chip for TPC and Muon arm

Time Projection Chamber (TPC):

Gas volume with parallel E and B Field.
B for momentum measurement. Positive effect: Diffusion is strongly reduced by E//B (up to a factor 5).

Drift Fields 100-400V/cm. Drift times 10-100 μs.
Distance up to 2.5m !

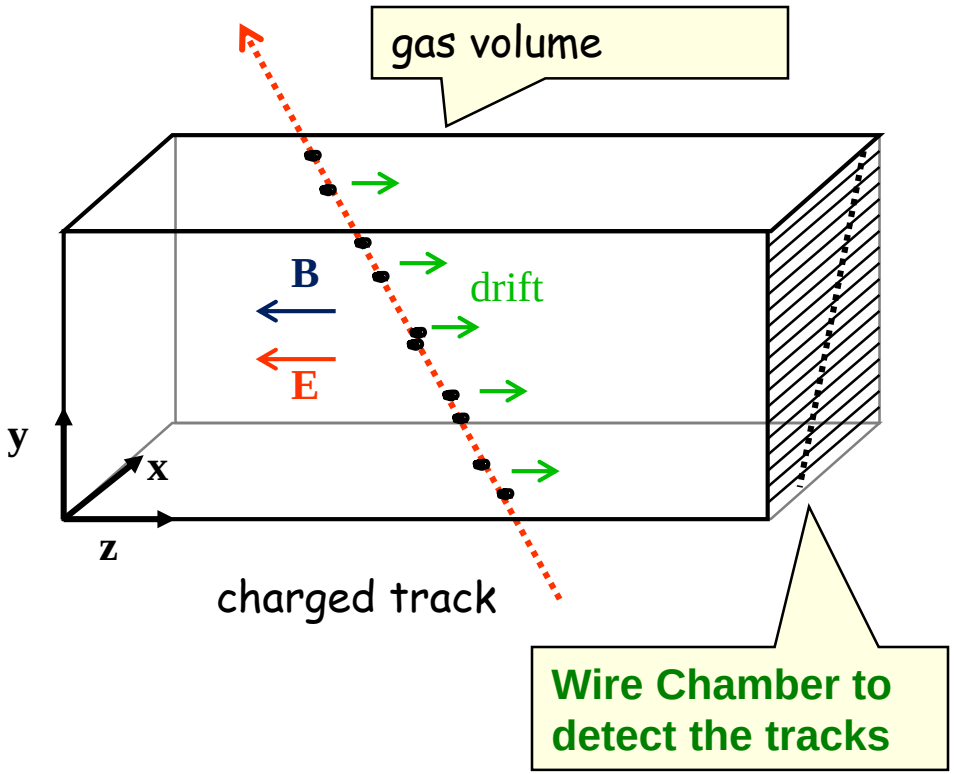

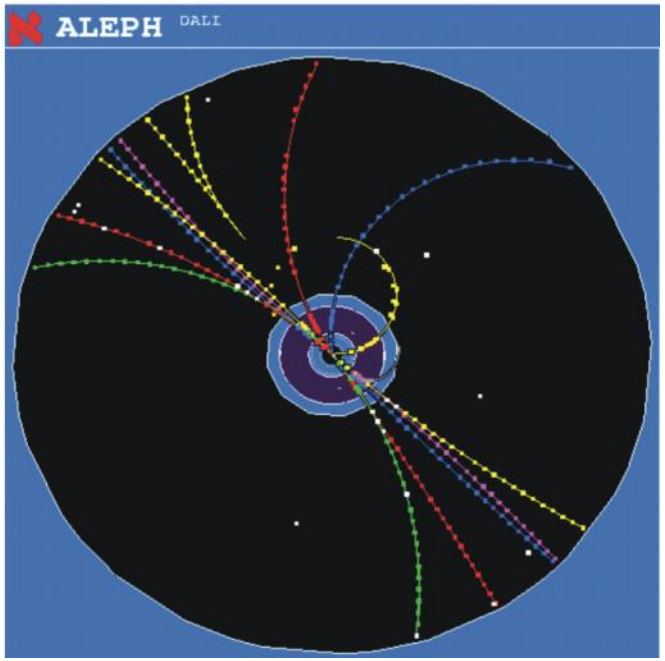

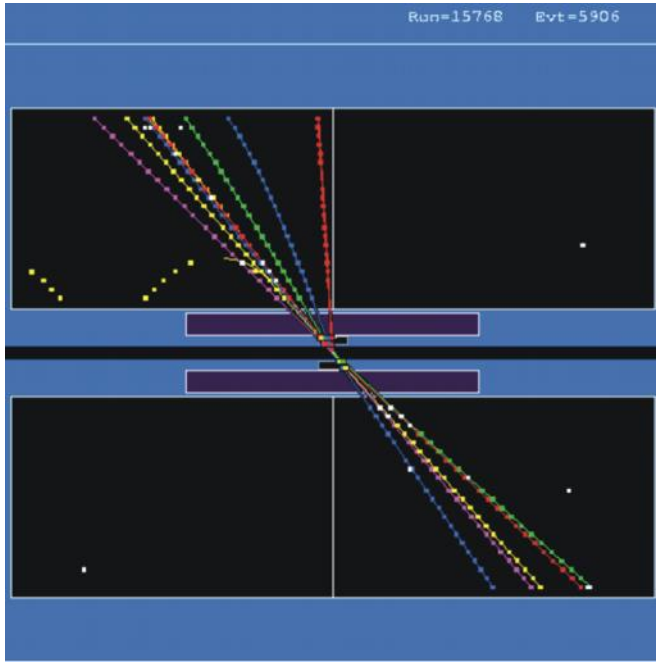

STAR TPC (BNL)

Event display of a Au Au collision at CM energy of 130 GeV/n.

Typically around 200 tracks per event.

Great advantage of a TPC: The only material that is in the way of the particles is gas → very low multiple scattering → very good momentum resolution down to low momenta !

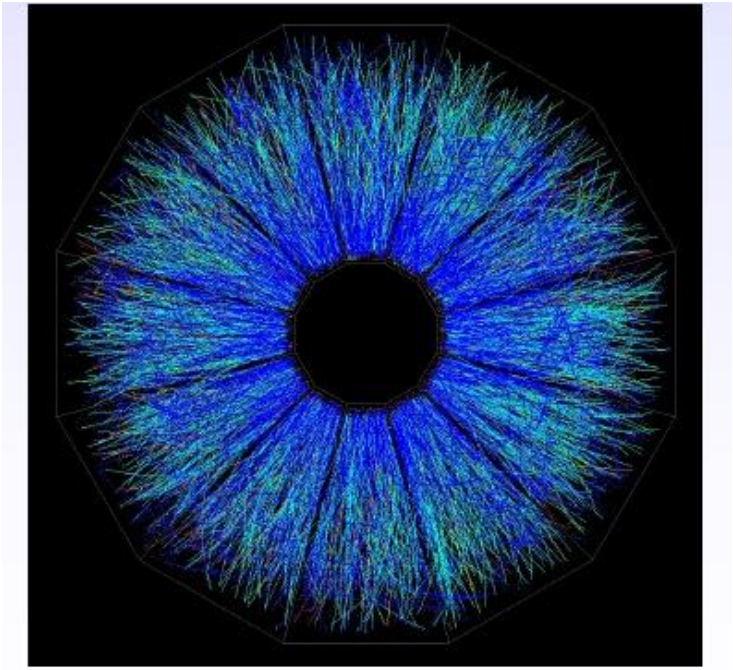

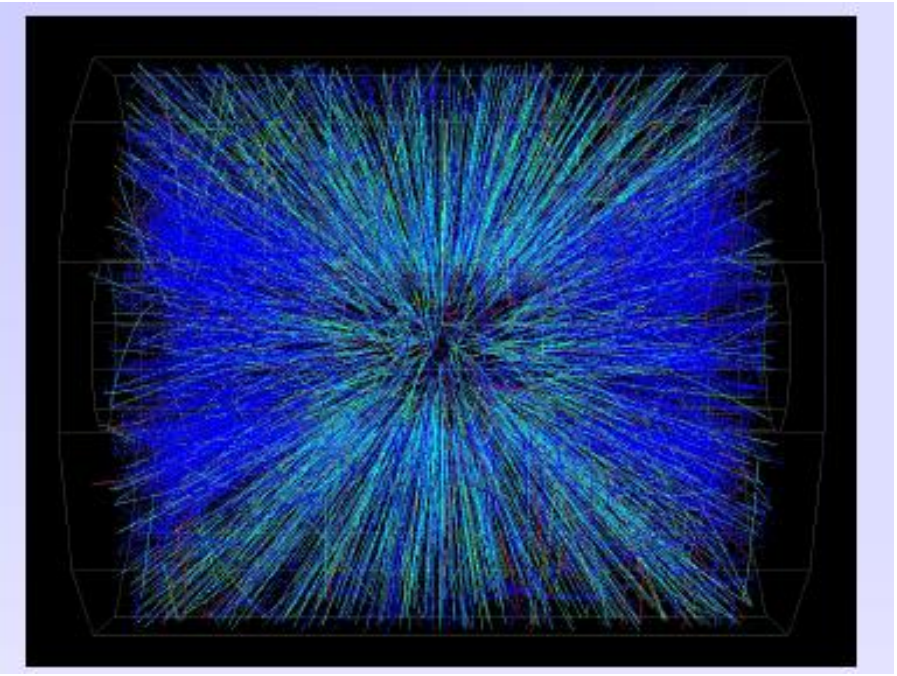

ALICE TPC: Detector Parameters

- Gas Ne/ CO_2 90/10%
- Field 400V/cm
- Gas gain >10^4
- Position resolution σ= 0.25mm
- Diffusion: σ_t= 250μm $\sqrt{cm}$
- Pads inside: 4x7.5mm
- Pads outside: 6x15mm
- B-field: 0.5T

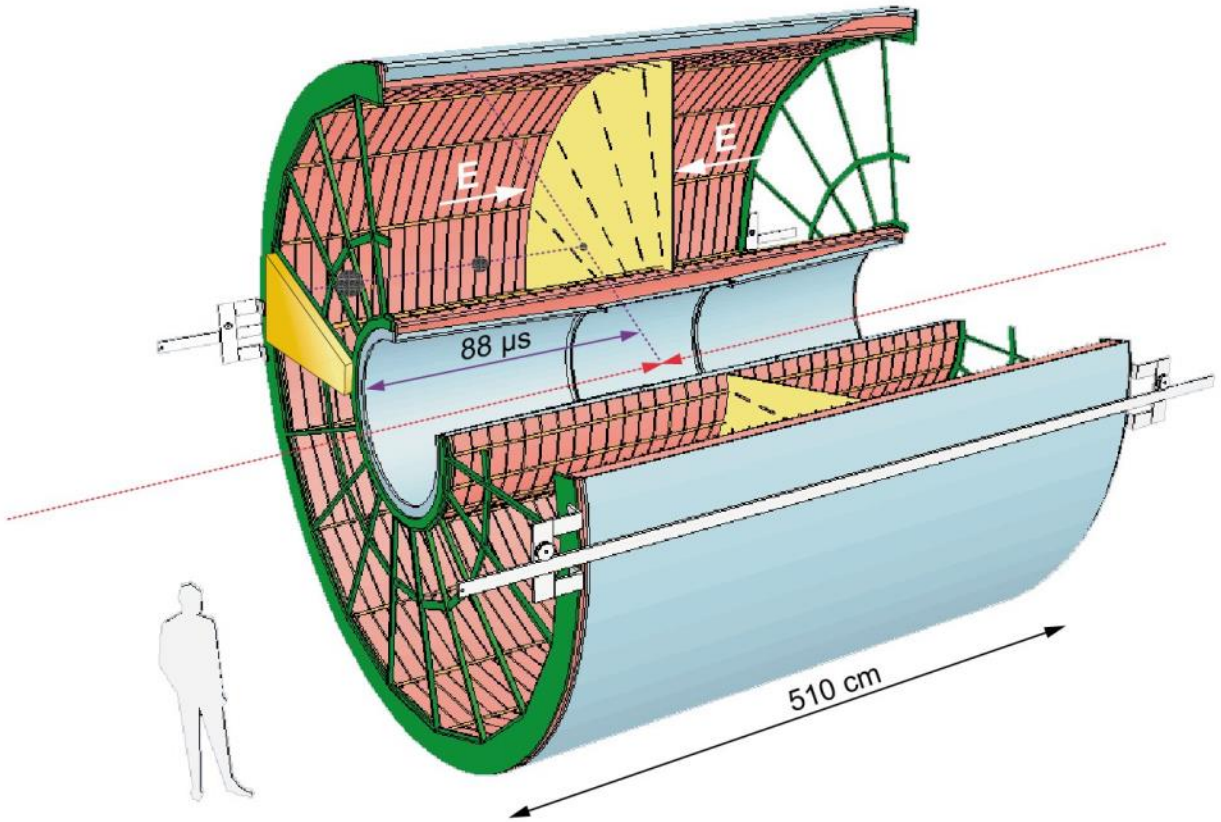

ALICE TPC: Construction Parameters

- Largest TPC:
  - Length 5m
  - Diameter 5m
  - Volume 88m^3
  - Detector area 32m^2
  - Channels ~570 000
- High Voltage:
  - Cathode -100kV
- Material X_0
  - Cylinder from composite materials from airplane industry (X_0= ~3%)

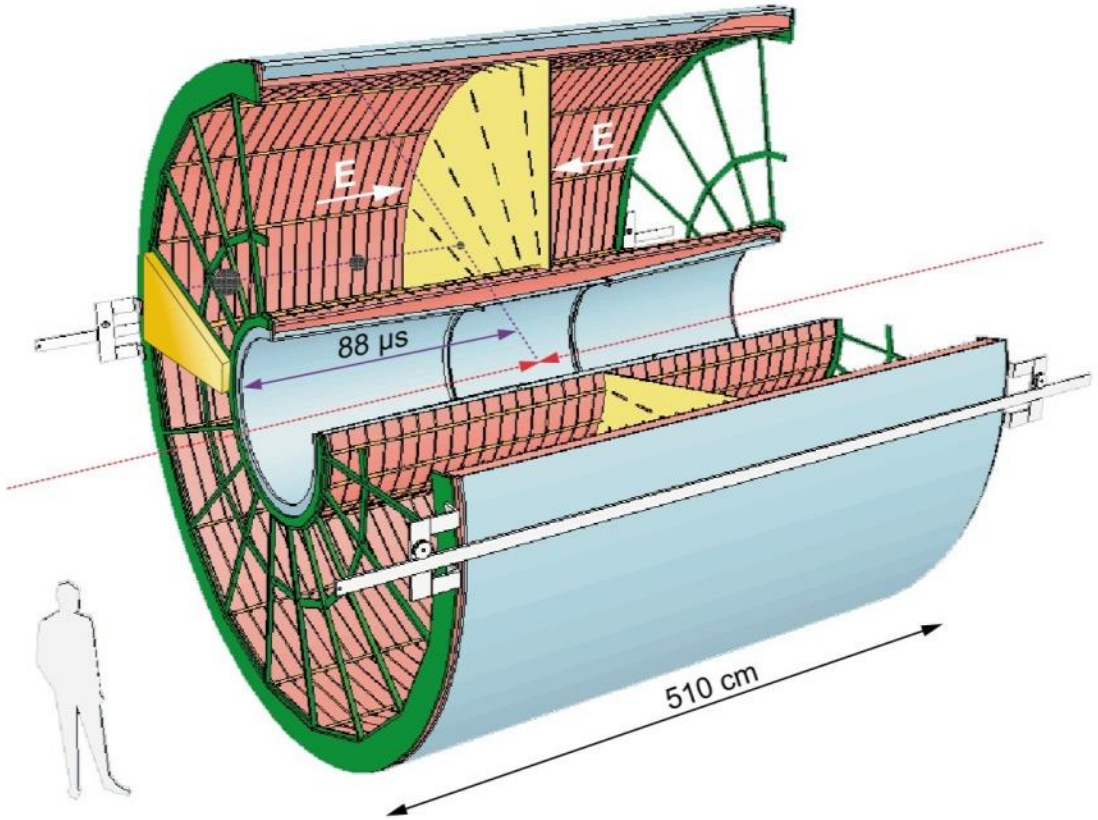

ALICE TPC: Pictures of the Construction

Precision in z: 250μm

End plates 250μm

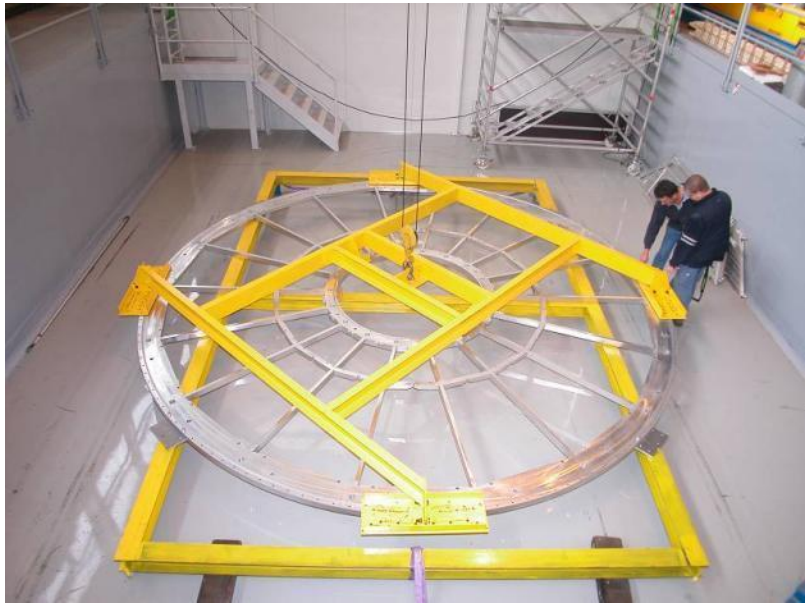

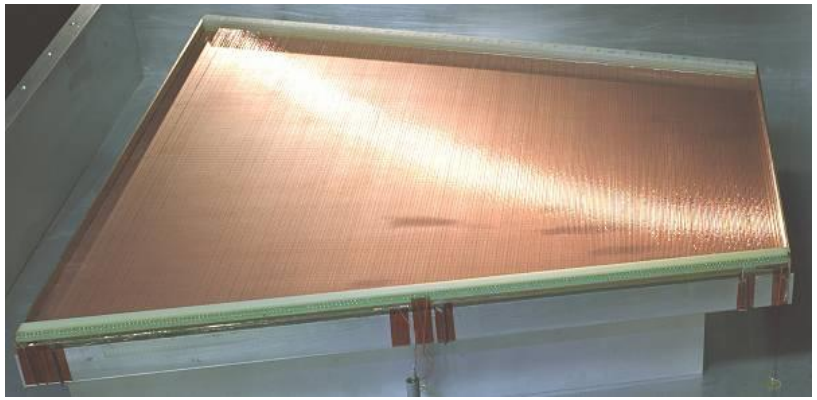

Wire chamber: 40μm

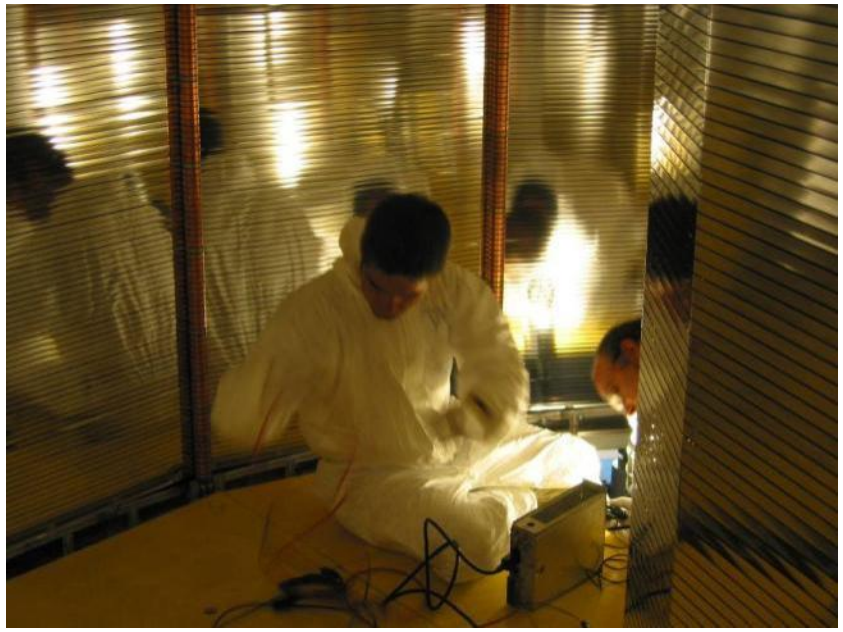

ALICE TPC Construction

My personal contribution:

A visit inside the TPC.

TPC installed in the ALICE Experiment

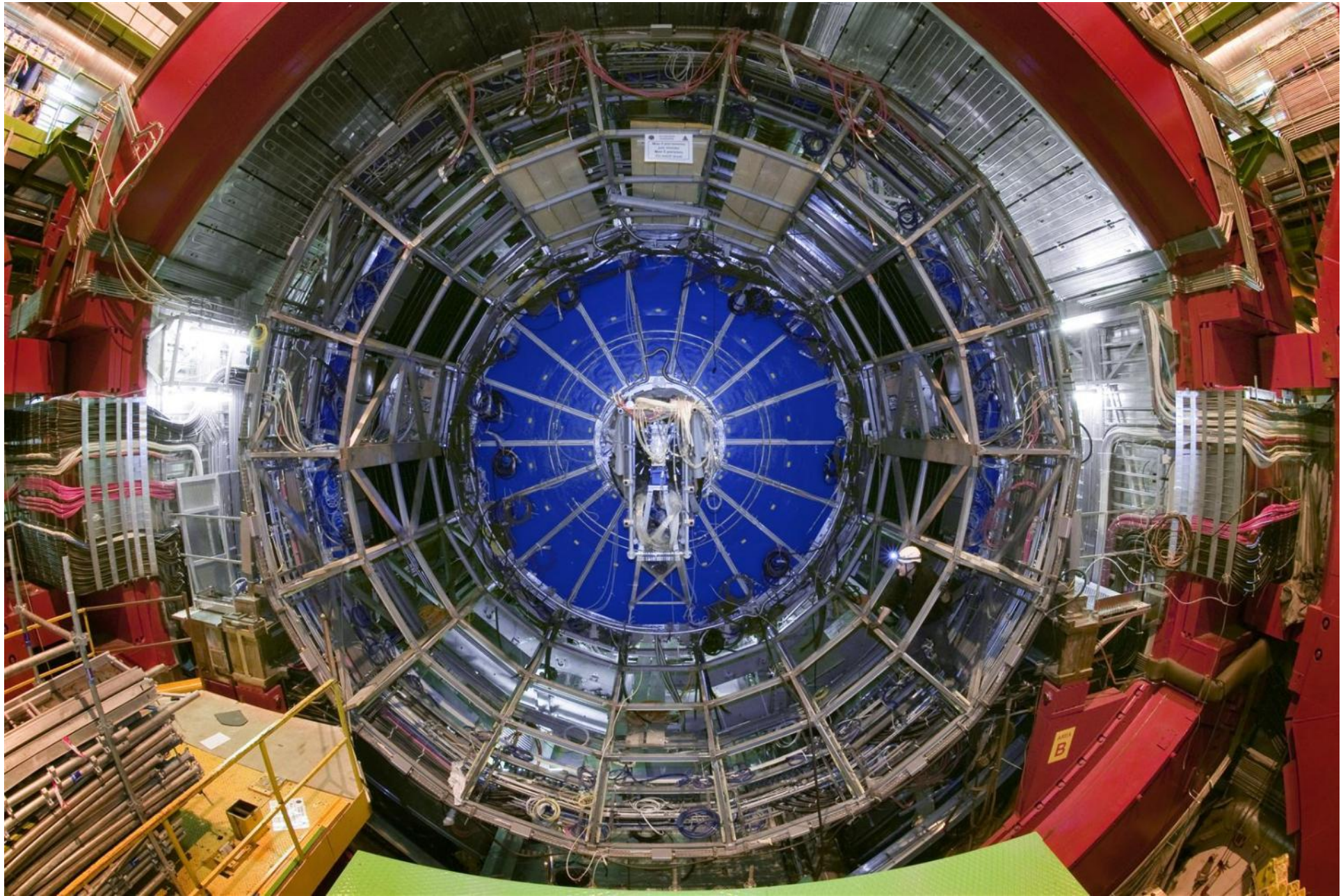

First 7 TeV p-p Collisions in the ALICE TPC in March 2010 !

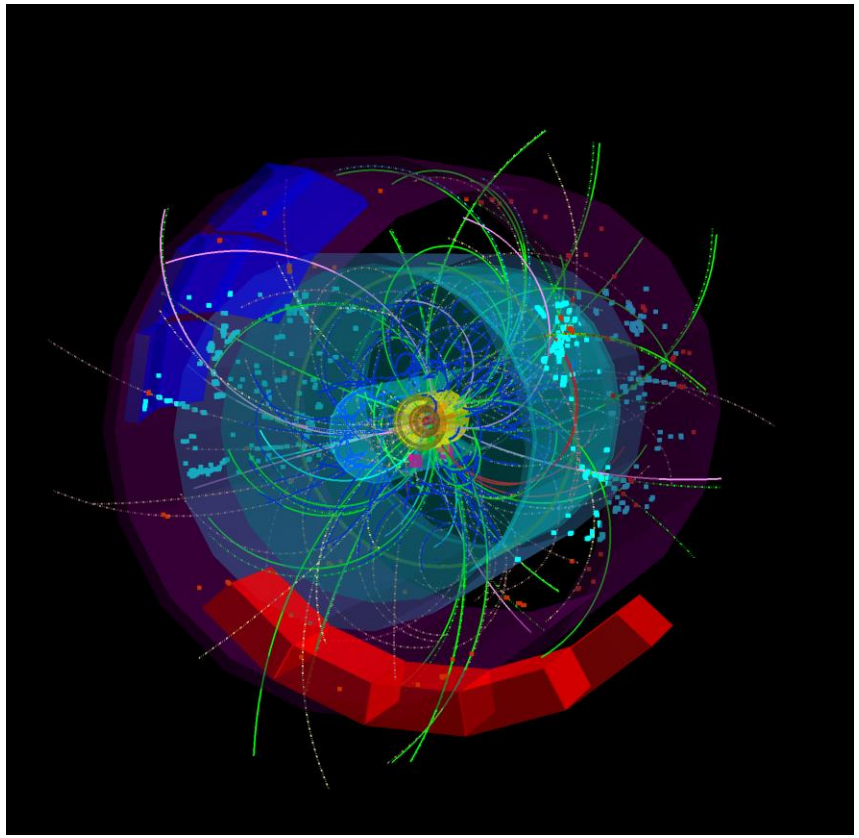

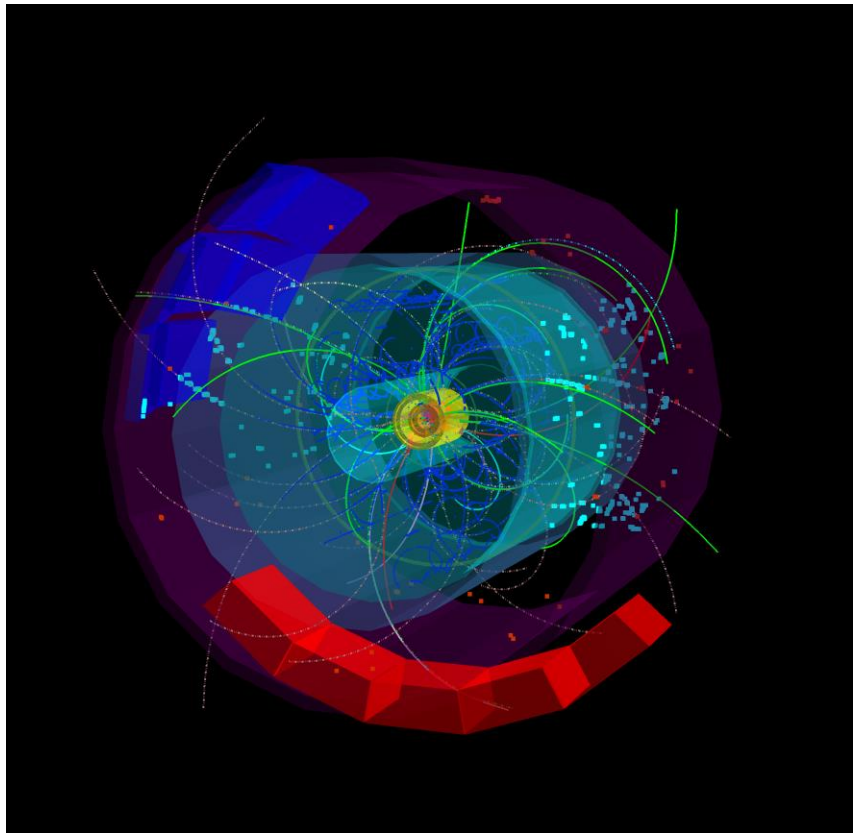

First Pb Pb Collisions in the ALICE TPC in Nov 2010 !

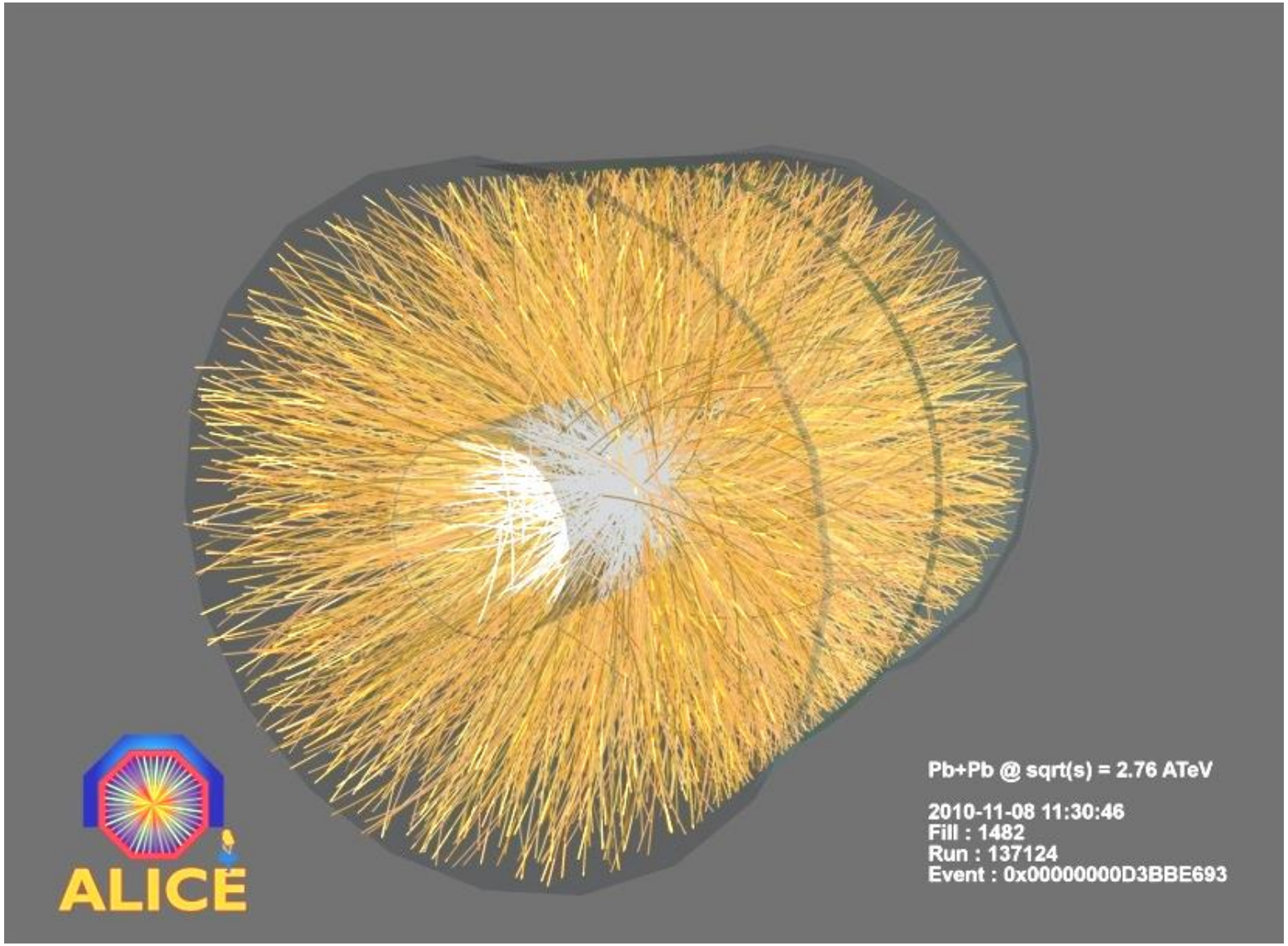

Move TPC to the surface for upgrade (1 Mar 2019)

TPC Upgrade with GEMs

Replace wire chambers
With quadruple-GEM chambers

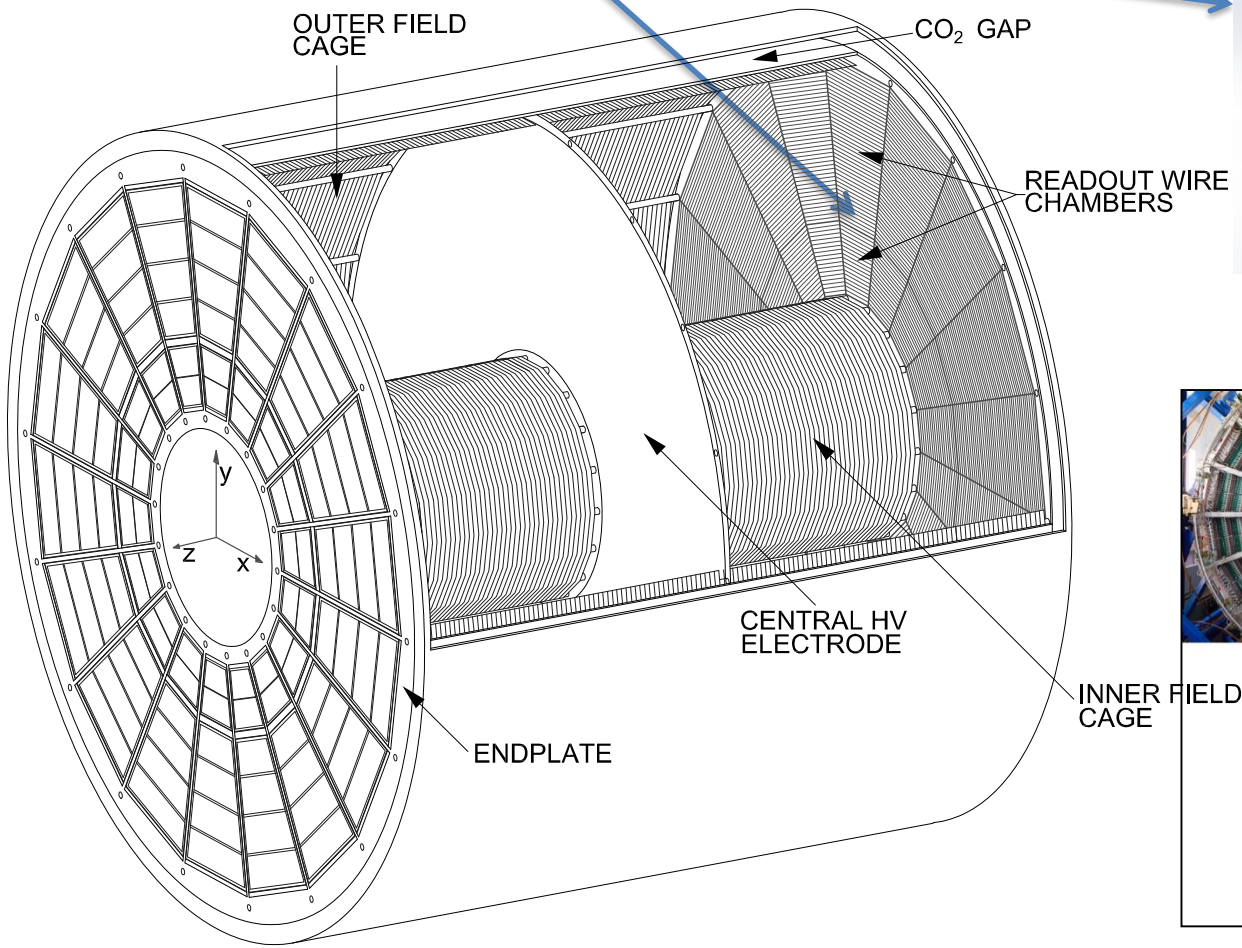

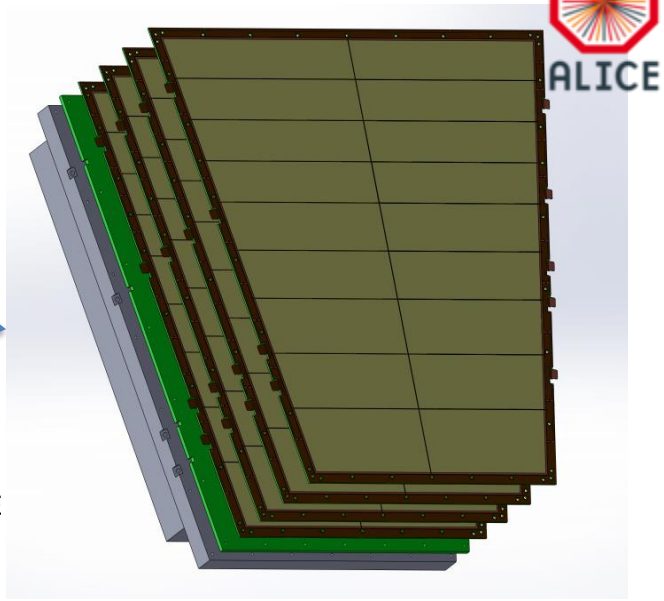

Exploded view of a GEM IROC

TPC upgrade – Why?

ROC ion feedback (λ_{int} and $\lambda_{readout}$ dependent)

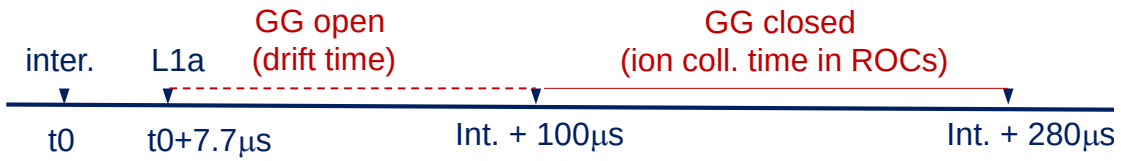

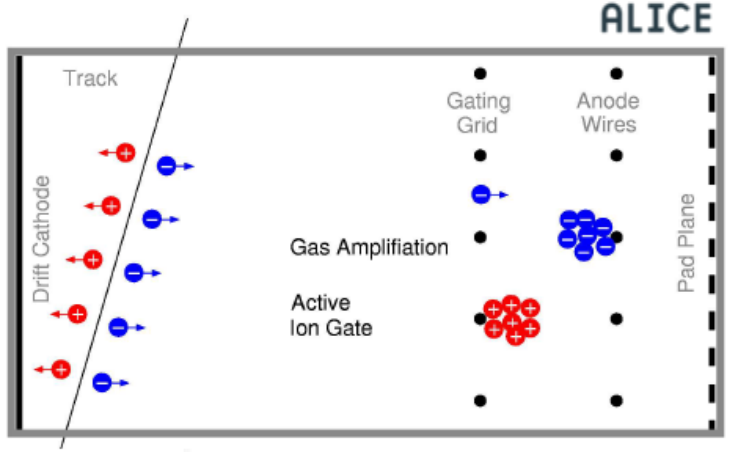

- Space charge (no ion feedback from triggering interaction)
  - GG open [t0, t0+100us], t0 ≡ interaction that triggers TPC
  - GG closed [t0+100us, t0+280us]
  - Effective dead time ~ 280us ➡ max readout rate ~3.5 kHz
  - Maximum distortions for λ_{int} =50kHz and L1=3.5kHz: Δr ~1.2mm (STAR TPC distorsions ~1cm)
- Space charge for continuous readout (GG always open)
  - gain ~6×10^3
  - 20% ion feedback if GG always open ➡ ion feedback ~10^3 x ions generated in drift volume
  - Max distortions for 50kHz ~100cm

MWPC not compatible with 50 kHZ operation

Triple-GEM principle of operation

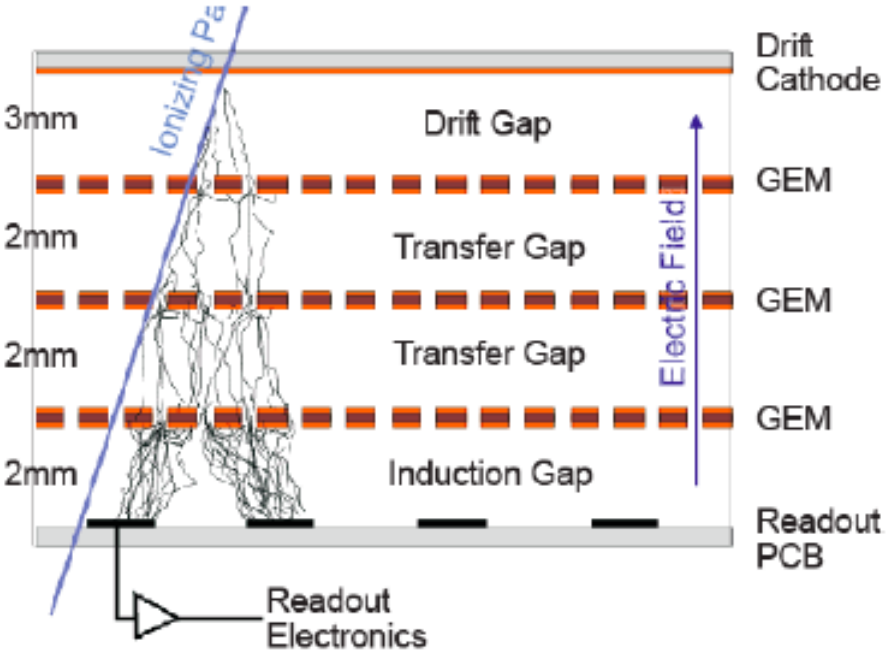

GEMs are made of a copper-kapton-copper sandwich, with holes etched into it

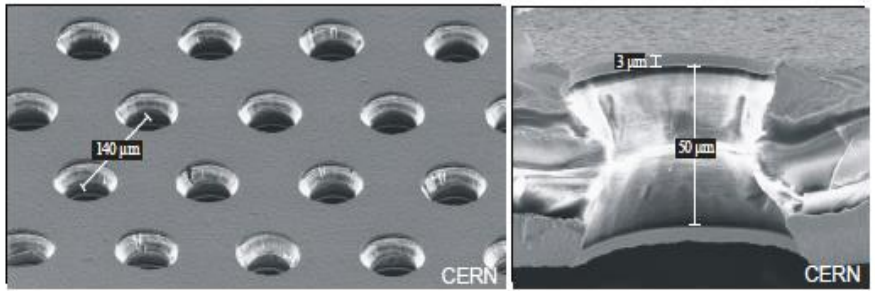

Electron microscope photograph of a GEM foil

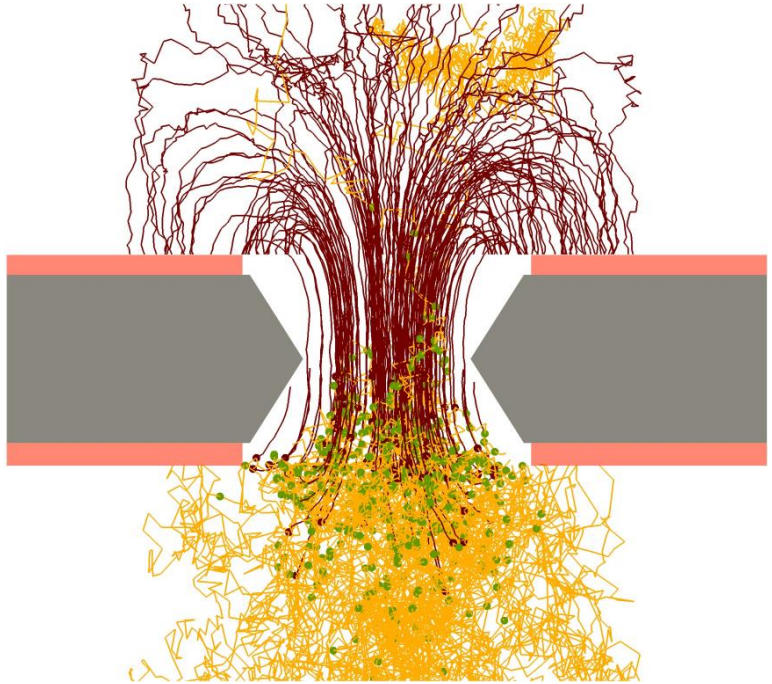

- Fast electron signal (polarity!)
- no “ion tail”
- No “coupling to other electrods”

➔ Gas gain about a factor 3 lower than in MWPC

TPC upgrade – Why?

R&D status with quadruple GEMs

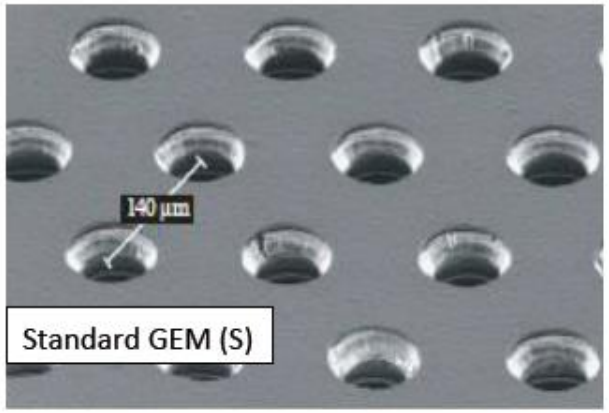

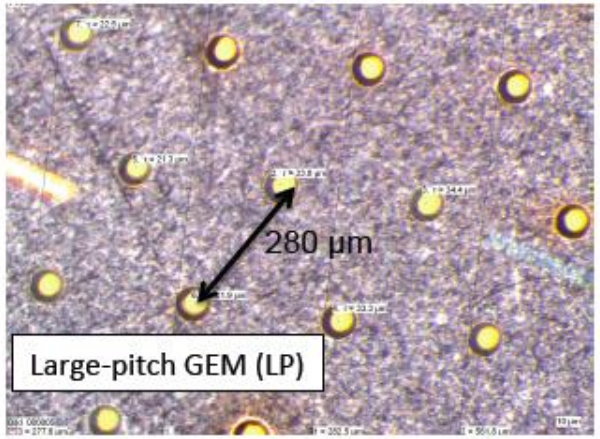

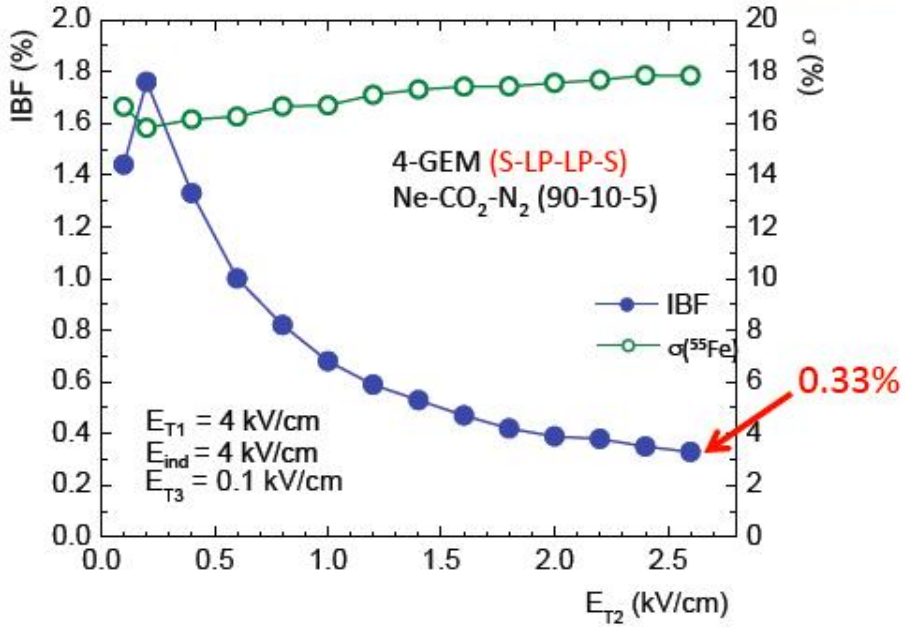

- further reduction of IBF in 4-GEM system with large-pitch GEMs (S-LP-LP-S)
- consideration of energy resolution is important: d*E*/d*x* performance requires $\sigma(^{55}Fe) \leq 12\%$

further optimization: IBF vs. energy resolution

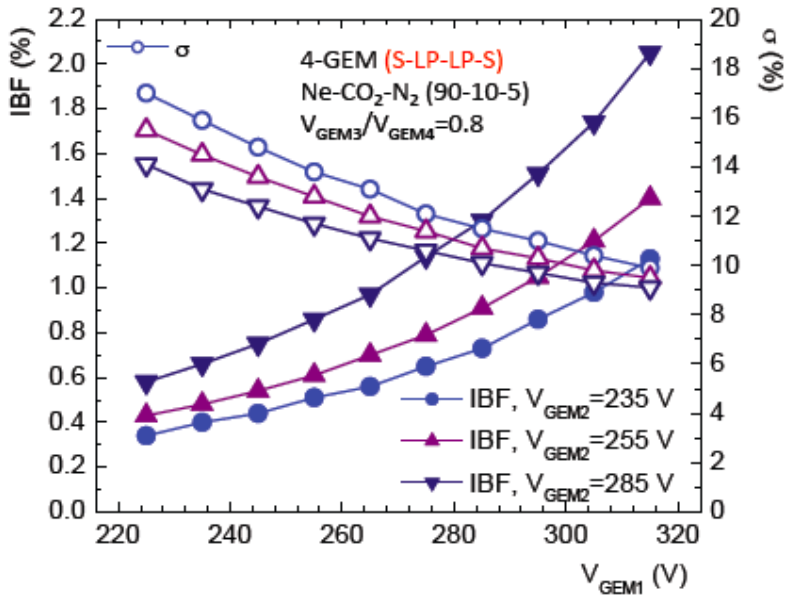

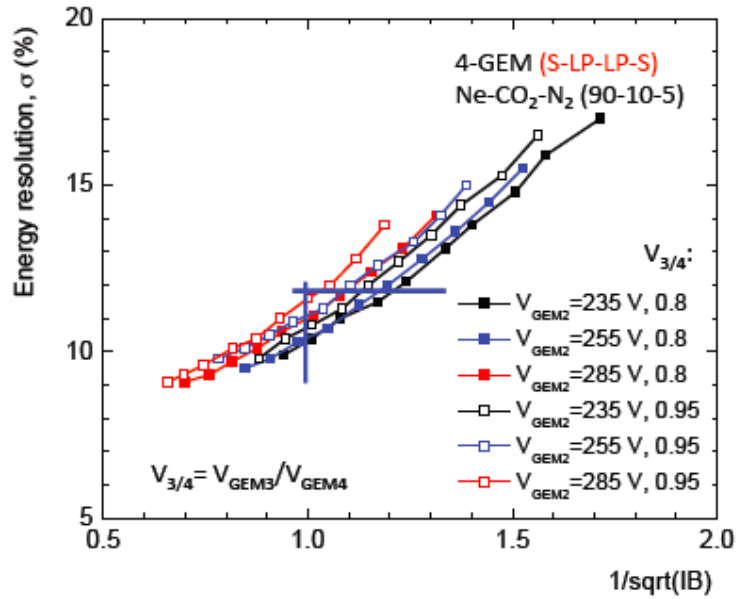

- Comprehensive voltage scan establishes operational point with IBF < 1% and energy resolution σ(^{55}Fe) < 12%

→ All performance studies are for IBF = 1% at gain = 2000, i.e. ε = 20

ALICE TPC upgrade

simulation: IBF in 4-GEM systems

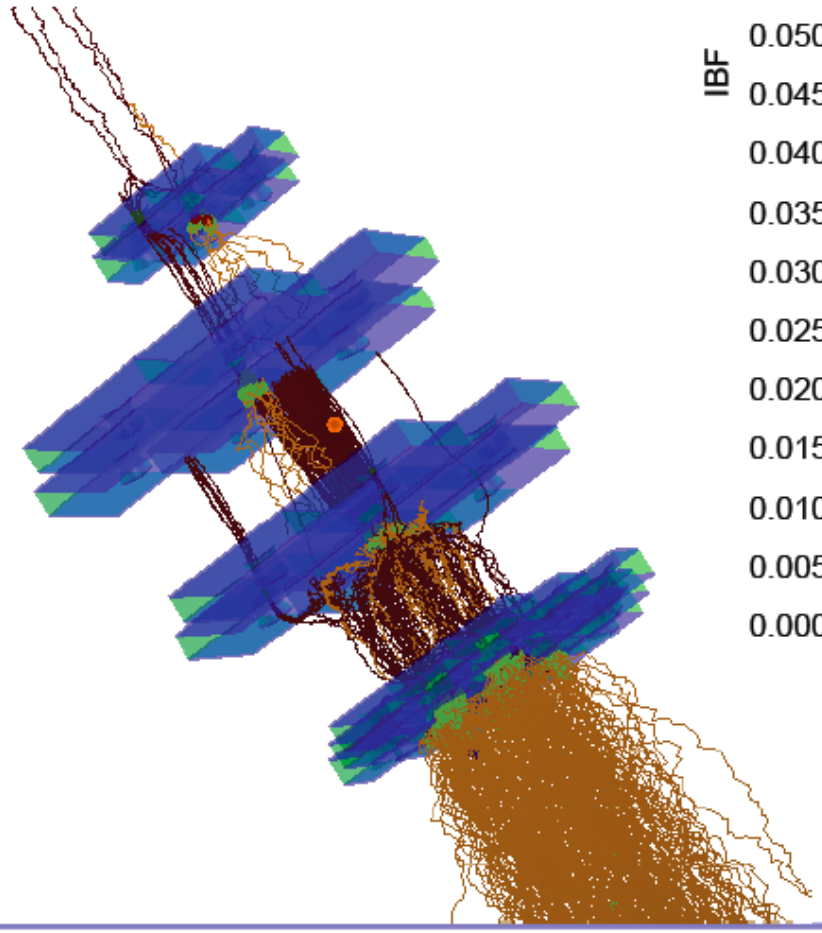

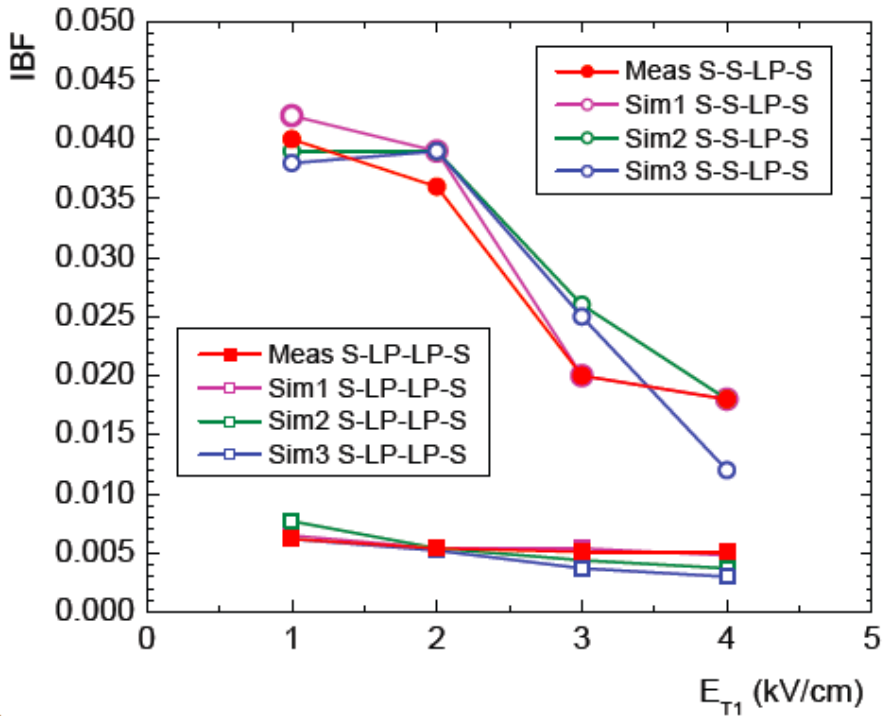

- IBF quantitatively well described by simulation based on Garfield++

ALICE TPC upgrade

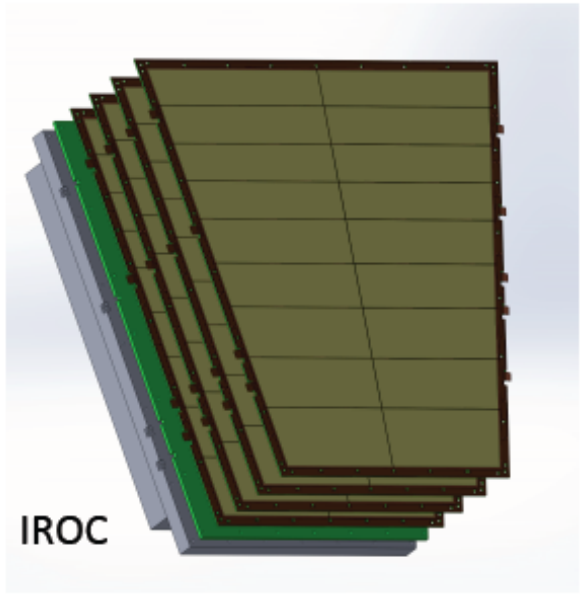

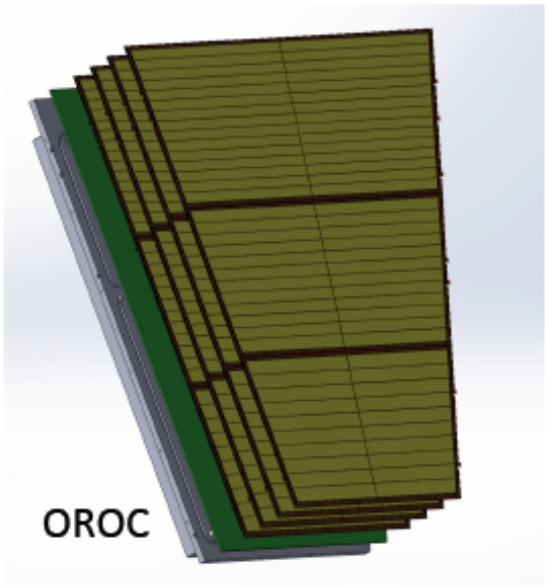

- large-size single-mask GEM foils
- one (three) per layer in IROC (OROC)

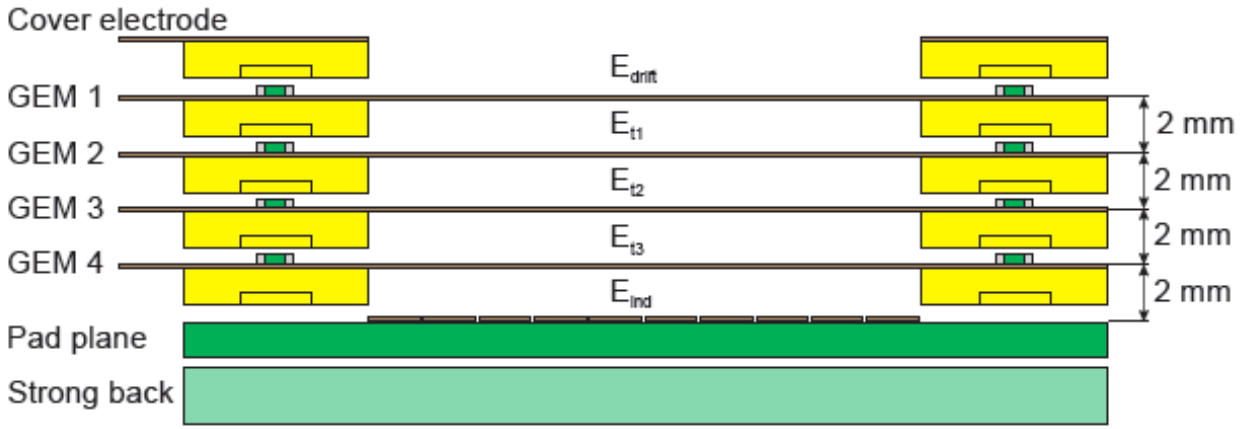

ALICE TPC upgrade

Wire chambers

GEM detectors

ALICE

BEFORE

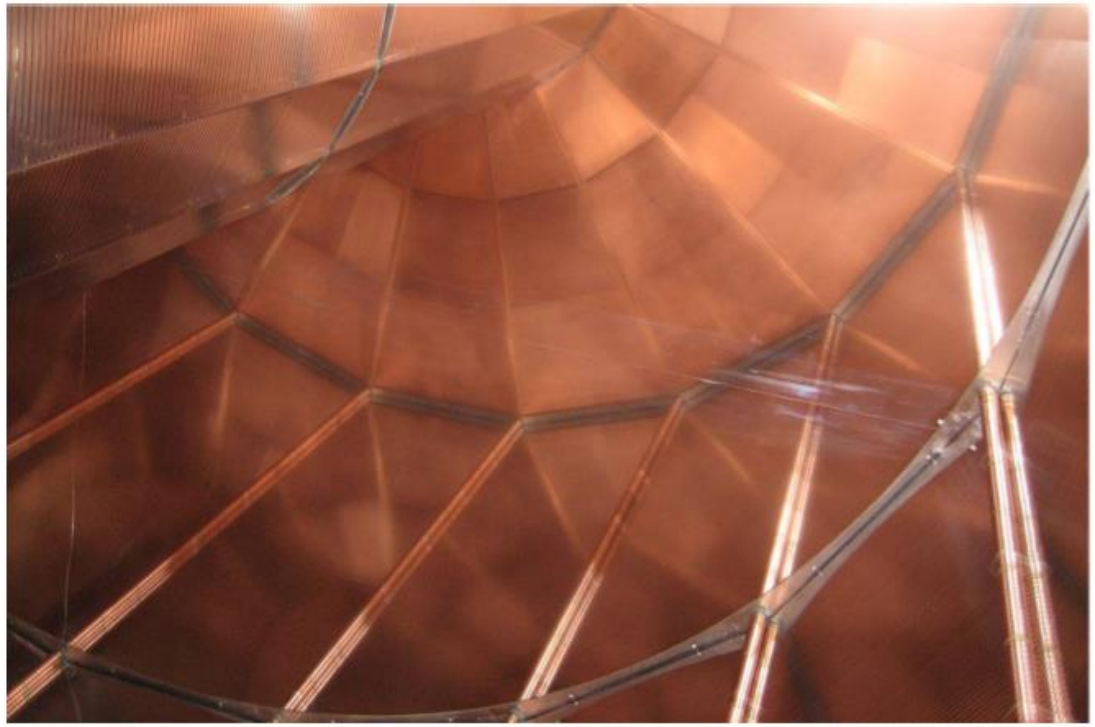

AFTER

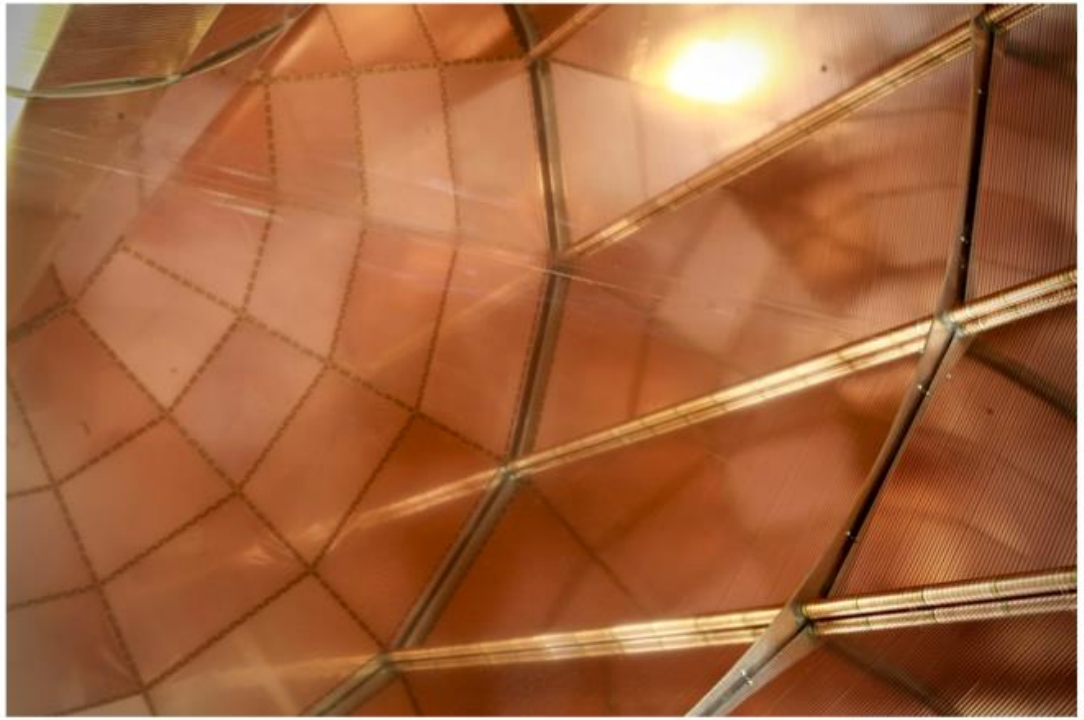

Find $\mathcal{O}(10^9)$ differences between two pictures

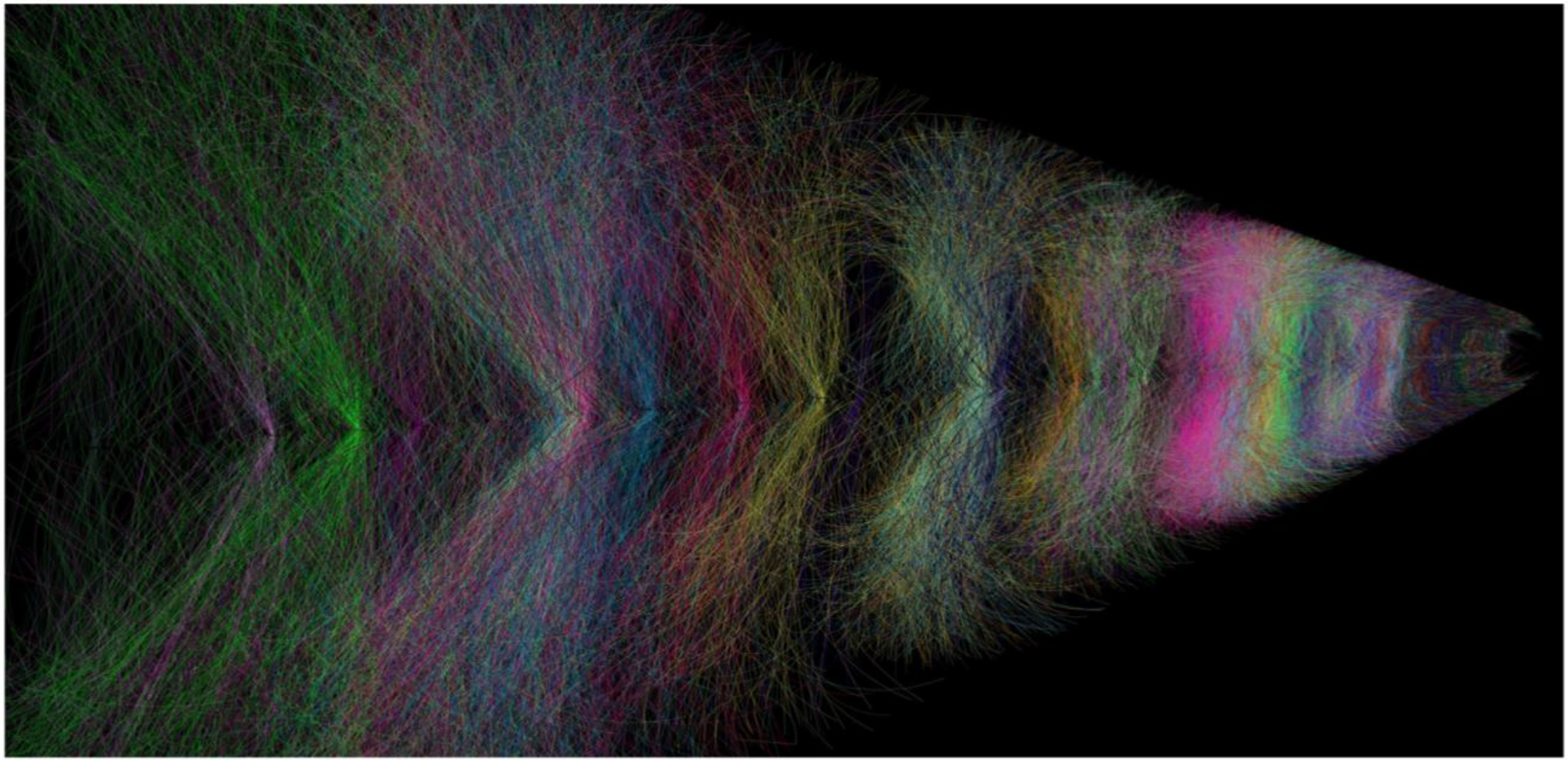

Summary

… a random walk through detector principles, recent technologies and LHC experiment upgrade ideas …

Since the original construction of the LHC detectors, many developments have taken place that are being implemented in the LHC detector upgrades.

New radiation hard silicon sensor with n-in-p technology will be used for the Phase-I and Phase-II upgrades.

Major progress on monolithic silicon sensors allows large scale application in areas with already significant radiation loads. The technology develops very fast.

Silicon photomultipliers are being used on a large scale for calorimetry, fiber tracking and precision timing.

LGAD sensors for precision timing are implemented in the HL-LHC upgrades on a large scale.

Availability of 40MHz sampling ADCs and high rate radiation hard optical links allow to read out of the entire calorimeter and muon system information as well as coarse tracking information at the full bunch crossing rate for sophisticated high level triggering.

The significant increase in available computing power allows sophisticated selection algorithms and data compression in the HLTs.